UNIVERSITA' VITA-SALUTE SAN RAFFAELE

CORSO DI DOTTORATO DI RICERCA INTERNAZIONALE IN MEDICINA MOLECOLARE

CURRICULUM IN CELL AND GENE THERAPY

Vascularized Islet Organ: An Extracorporeal Model Evolving from In Vitro to In Vivo Application in Diabetes

DoS: Dr. Antonio Citro

Second Supervisor: Prof. Cristina Nostro

Tesi di Dottorato di Ricerca di Alessia Neroni

matr. 019215

Ciclo di dottorato XXXVII

SSD MED/13

Anno Accademico 2023/2024

CONSULTAZIONE TESI DI DOTTORATO DI RICERCA

I Alessia Neroni

Registration number 019215

Born at Roma

On 15/09/1993

Author of the PhD Thesis titled: Human Vascularized Islet Organ (hVIO) as an extracorporeal model for the study of physiopathology and drug screening in diabetes

☐ AUTHORIZES *the public release of the thesis*

X DOES NOT AUTHORIZE the public release of the thesis for 12 months from the PhD thesis date, specifically

From 26/11/2024 To 26/11/2025

Because:

☐ The whole project or part of it might be subject to patentability;

X Parts of the thesis have been or are being submitted to a publisher or are in press;

☐ The thesis project is financed by external bodies that have rights over it and on its publication.

Copyright the contents of the thesis in whole or in part is forbidden

Date 28/10/2024 Firma /Signature Alessia Neroni

DECLARATION

This thesis has been:

- composed by myself and has not been used in any previous application for a degree. Throughout the text I use both 'I' and 'We' interchangeably.
- has been written according to the editing guidelines approved by the University.

Permission to use images and other material covered by copyright has been sought and obtained. Figures 1 to 6 belong to an "open access" publication.

The *in vivo* data, results, figures (Fig.9, Fig.22, Fig.23, Fig.24, and Fig.25), figure legends, and material and methods of this work are included in a previous publication (Citro et al., 2024), where I am the second author. I contributed to the project by handling the experimental work and the manuscript drafting.
Also, parts of the introduction of this work are included in a previous publication (Pignatelli et al.,2022), where I am the third author, as well as in a chapter of the book "Pluripotent Stem Cell Therapy for Diabetes" (Piemonti et al., 2023), where I am the co-first author.

All the results presented here were obtained by myself, except for:

1) All the slices of lung and pancreatic islets were processed by Dr. Amleto Fiocchi, Animal Histopathology Facility, San Raffaele Scientific Institute, Milan, Italy.

2) Spatial Transcriptomic Results and Bioinformatics analysis (Results, chapter 5.4.1, figure 15,16) were performed in collaboration with Kasper Thorsen, Sara R. N. Jensen, and Thomas Damm Als of the MOMA Single-Cell Core Centre, Aarhus University Hospital, Aarhus, Denmark.

3) Heatmaps were generated in collaboration with Dr. Ilaria Marzinotto, Ph.D., Diabetes Research Institute, San Raffaele Scientific Institute, Milan, Italy.

4) *In vivo* transplantation experiments (Results, chapter 5.7.2, figure 24) were performed by Dr. Antonio Citro, Project leader at the Pancreas Bioengineering unit, Diabetes Research Institute, San Raffaele Scientific Institute, Milan, Italy.

5) Results from the *in vivo* part of the thesis were performed by collaboration among some members of our lab (Cataldo Pignatelli, Ph.D, Dr. Francesco Campo, PhD student, and Dr. Matteo Monieri, Lab Technician from Diabetes Research Institute, San Raffaele Scientific Institute, Milan, Italy).

All sources of information are acknowledged by means of reference.

ABSTRACT

BACKGROUND: As of now, one of the major needs in the field of tissue engineering and diabetes is the lack of a dual-purpose technology that may resemble a perfusable and functional endocrine niche *ex vivo* that may serve: i) as a model to study the endocrine function and ii) to efficiently restore *in vivo* the normoglycemia in a preclinical model of diabetes. Recent evidence in pancreas bioengineering showed that a reliable *ex vivo* model should be composed of i) native organ ECM to sustain endocrine cues, ii) an organized vascularization to connect pancreatic islets, and iii) a reliable source of endocrine cells.

The present project focuses on advancing diabetes bioengineering by developing the first version of a vascularized islet organ that may composed of clinically relevant cell sources for both *in vitro* and *in vivo* validation. As first milestone we will validate the generation of the technology and its function over a long-term *in vitro* culture. Once certified, the *in vitro* assembly in short (7 days) and long-term (14 days) culture, we challenge the *in vitro* technology in the context of a relevant inflammatory pathway in the field of diabetes. Recent evidence showed that IL-8-CXCR1/2 inflammatory pathway's impact on islet survival and function, particularly in the context of islet transplantation. Inhibiting this pathway is suggested to improve islet outcomes post-transplantation. Here, we will evaluate the plasticity of our technology in the presence of an inflammatory insult mediated by IL-8 pathway investigating its role in hVIO platform. Once validated, we will move hVIO in a step forward applying the technology in the β-cell replacement field. To bypass the scarcity of human islet we adapted hVIO in the presence of neonatal pig islet (NPIs), as alternative, unlimited and editable endocrine cells generating a new concept device namely VEP (Vascularized Endocrine Pancreas). Finally, in line with the engineering of a dual-purpose technology, we investigate if the VEP platform may serve an *ex vivo* model to predict xeno-reaction on leucocyte trafficking before moving the technology to a more complex *in vivo* humanized mouse model.

MATERIALS & METHODS: hVIOs and VEPs were created by repopulating the decellularized rat lung left lobe with human pancreatic islets (HIs)/NPIs and endothelial cells (BOEC) through the trachea, pulmonary artery, and vein. This allowed us to recreate the endocrine functional unit in a complex 3D vascularized structure like the alveolus-islet niche. Customized bioreactors enabled dynamic perfusion for 14 days (in hVIO), with the first 7 days dedicated to device assembly (Maturation Phase_MP- in both hVIO and VEP) and the subsequent 7 days (Testing

Phase TP) for testing endocrine and vascular function under different stimuli, exclusively in hVIO. MiR-375, a surrogate marker of β cell death, was used to gauge β cell mass in both the MP and TP. Insulin secretion tests, fluorangiography assays, IF, and spatial transcriptomic analyses were employed to evaluate endocrine and vascular compartments during both phases. Additionally, the matured VEPs were then i) subcutaneously transplanted into diabetic NSG and compared with matched NPIs transplanted in different implantation sites (kidney capsule, deviceless, and liver); ii) used for the *ex vivo* experiment for leukocyte trafficking to monitor and track immune rejection of the graft.

RESULTS: We successfully engineer functional VEP and hVIO within 7 and 14 days of culture. During the MP, hVIOs showed complete revascularization with integrated pancreatic islets. The absence of miR-375 confirmed the preservation of islet mass, fluorangiography indicated a functional vascular barrier, and insulin secretion tests demonstrated increased insulin production during the MP sustained in the TP.

The preliminary results of spatial transcriptomic analyses have shown that the vascular compartment presents a pro-angiogenic and stable endothelium during the culture protocol and the preservation and activation of the endocrine compartment.

In the TP, hVIOs were used to assess inflammatory β cell damage via the IL-8-CXCR1/2 pathway. The human islets were positive for CXCR2, while BOECs did not express CXCR1/2, and the islet phenotype in hVIOs was preserved. IL-8 did not have a negative effect on islet function or human islet β cell death in a vascularized ECM environment. In fact, in the presence of IL-8, hVIOs exhibited a positive trend in insulin release. In long-term transplants in diabetic NSG mice, VEPs demonstrated an improved NPIs functional maturation with a significant engraftment associated to a prompt function after implantation. This led to the reversal of hyperglycemia within 2 days, sustained for 19 weeks after implantation compared to all the internal controls. The preliminary results of leukocyte trafficking have shown the ability of the pre-active PBMCs to attack the NPIs in standard culture conditions increasing the β cell death, detected by Incucyte Basic analyzer tool and miR-375. Preliminary experiment in VEP platform confirmed, after preactivated leucocyte perfusion, the increase of miR-375 that was associated, as expected, with a peak of β cell death.

CONCLUSIONS: Validating hVIO as a model for replicating the islet niche using human cells opens new possibilities for studying endocrine disorders. Additional experiments are necessary to understand the initial results of insulin secretion during the TP under inflammatory conditions to assess the role of IL-8 as a potential inducer for insulin release and to preserve the vascular and endocrine compartments. The *ex vivo* VEP enables NPIs' engraftment, maturation, and vascularization before

transplantation. To our knowledge, VEP is the first organ assembled with a relevant source of endocrine and endothelial cells suitable for future clinical translation. Further analyses are needed to understand the T-cell responses to pancreatic islets.

TABLE OF CONTENT

1. ACRONYMS AND ABBREVIATIONS 4

2. LIST OF FIGURES AND TABLES 7

3. INTRODUCTION 8

3.1. ENDOCRINE PANCREAS PHYSIOLOGY 8

3.1.1. Understanding the anatomical location and structure of the pancreas ..8

3.1.2. The endocrine pancreas: the role of the hormones 10

3.1.3. Physiological control of blood sugar 11

3.1.4. Insulin 12

3.1.5. Insulin physiological release: mechanism of action 14

3.2. ENDOCRINE PANCREAS DYSFUNCTIONS: DIABETES MELLITUS 18

3.2.1. Pancreatic endocrine disorders: type 1 diabetes mellitus (T1DM) etiopathogenesis and clinical characteristics 18

3.2.2. Current therapeutic approaches for diabetes treatment: advantages and disadvantages 20

3.3. AVAILABLE MODELS FOR UNDERSTANDING TYPE 1 DIABETES PATHOPHYSIOLOGY 22

3.3.1. Murine models for type 1 diabetes 23

3.3.2. Non-obese diabetic (NOD) mouse 23

3.3.3. BioBreeding (BB) rat 25

3.3.4. Komeda diabetes-prone (KDP) rat 25

3.3.5. Lew.1AR1-iddm rat 26

3.3.6. Chemical induction of Type 1 diabetes 26

3.3.7. Ex-vivo technology for studying islet's endocrine function. 28

3.4. TISSUE ENGINEERING SUPPORTING OF DYNAMIC CULTURE: AN EMERGING INNOVATIVE APPROACH 29

3.4.1. Tissue engineering strategies 31

3.4.2. Coexisting cells in the endocrine pancreatic niche 32

3.4.3. Synthetic biomaterial scaffold 35

3.4.4. Natural biomaterial scaffold 37

3.4.5. Decellularization methods of 3D ECM scaffold: Whole organ decellularization 39

3.4.6. TE applications to model endocrine dysfunction. 42

3.5. A UNIQUE FLEXIBLE MODEL THAT CAN BE USED FOR DIFFERENT PURPOSES 50

3.5.1. A novel system to restore the normoglycemia in vivo T1D model 50

3.5.2. A predictor platform for inflammatory or T cell-mediated β-cell damage 52

4. AIM OF THE WORK 54

5. RESULTS 55

5.1. EXTRACORPOREAL HUMAN VIOS (HVIOS) GENERATION AND PROTOCOL OF CULTURE 55

5.2. ENGINEERING THE VASCULAR COMPARTMENT: BOECS CHARACTERIZATION AND HVIOS AND VEP ASSESSMENT OF THE VASCULAR STRUCTURE AND FUNCTION 57

5.2.1. BOECs in vitro characterization 57

5.2.2. Evaluation of hVIOs vascular structure and function 59

5.3. ENGINEERING THE ENDOCRINE COMPARTMENT: EVALUATING ISLET VIABILITY AND FUNCTION 61

5.4. EVALUATION OF THE INTEGRATION OF HVIOS COMPARTMENTS 64

5.4.1. Understanding the cell's trajectory in hVIOs 65

5.5. TESTING CXCR1 AND CXCR2 EXPRESSION ON HVIO CELL COMPARTMENTS IN AN INFLAMMATORY CONTEXT: AN *IN VITRO* ASSESSMENT 73

5.5.1. Investigating the impact of the CXCR1/2 pathway on human islets 73

5.5.2. Investigating the impact of the CXCR1/2 pathway on BOECs 76

5.6. EXPLORING THE IMPACT OF IL-8 ON ENDOCRINE AND VASCULAR COMPARTMENTS IN HVIO: A CRITICAL ASSESSMENT 78

5.6.1. Evaluation of cell-on-scaffold distribution in the hVIOs setting 78

5.6.2. Assessment of β-cell preservation following IL-8 treatment 80

5.6.3. Evaluation of hVIOs secretory function after IL-8 treatment 81

5.7. FROM IN VITRO TO *IN VIVO*: EVALUATION OF THE VEP AS A POTENTIAL PLATFORM FOR FUTURE CLINICAL APPLICATION 82

5.7.1. Directed self-assembly of VEPs and functional assessment 83

5.7.2. VEP performance after transplantation into diabetic mice 86

5.8. VEP AS MODEL TO STUDY IN ENDOCRINE NICHE LEUCOCYTE TRAFFICKING: EVALUATION OF T CELL-MEDIATED B-CELL DAMAGE 90

6. DISCUSSION 95

7. MATERIALS AND METHODS 104

7.1. EXPERIMENTAL ANIMALS 104

7.2. DECELLULARIZATION AND PREPARATION OF LUNG LEFT LOBE SCAFFOLD 104

7.3. CELL SOURCES USED FOR HVIO GENERATION 106
7.4. CHARACTERIZATION OF BOECS' PHENOTYPIC AND FUNCTIONAL QUALITIES 107
7.4.1. Flow cytometry 108
7.4.2. Tube formation assay 108
7.4.3. Proliferation WST-1 assay 109
7.5. ISLETS EQUIVALENT COUNT 109
7.6. BIOREACTOR CUSTOMIZATION AND ASSEMBLY 111
7.7. *IN VITRO* SEEDING AND CULTURE OF HVIOS 112
7.8. CULTURE PROTOCOLS OF ISOLATED ISLETS BATCH-MATCH AS AN INTERNAL CONTROL 114
7.9. ISOLATION OF NEONATAL PANCREATIC ISLETS 115
7.10. FLUORESCENCE MICROANGIOGRAPHY 116
7.11. DEXTRAN PERMEABILITY ASSAY 116
7.12. MIRNAS QUANTIFICATION 117
7.13. HISTOLOGY AND IMMUNOFLUORESCENCE STAINING ON CELL AND TISSUE SAMPLES 118
7.14. DYNAMIC INSULIN SECRETION TEST (IST) OF HVIOS 120
7.15. DYNAMIC INSULIN SECRETION TEST (IST) OF BATCH MATCH HUMAN ISLETS AS CONTROLS 121
7.16. SPATIAL TRANSCRIPTOMICS ANALYSES 122
7.17. *IN VIVO* SYSTEM 127
7.17.1. Diabetes induction and metabolic monitoring 127
7.17.2. Device-less (DL), Kidney capsule (KC), and Liver (LV) NPIs transplantation 127
7.17.3. VEPs implantations in diabetic recipient mice 128
7.18. ACTIVATION AND EVALUATION OF PBMCS' ABILITY TO KILL NPIS 129
7.19. STATISTICAL ANALYSIS 130
8. REFERENCES 131

1. ACRONYMS AND ABBREVIATIONS

Pancreatic polypeptide (PP)
Glucose transporter 2 (GLUT2)
Endoplasmic reticulum (ER)
Human islets (HIs)
Type 1 Diabetes (T1D)
Type 2 Diabetes (T2D)
Human Leukocyte Antigens (HLA)
Insulin (INS)
Protein tyrosine phosphatase (PTPN22)
IL-2 receptor alpha subunit (IL2RA)
Protein tyrosine phosphatase kappa receptor kappa (PTPRK)
Thymocyte-expressed molecule involved in sorting (THEMIS)
Type 1 Diabetes Genetic Risk Score (T1D GRS)
Single nucleotide polymorphisms (SNPs)
T cell receptor (TCR)
Coxsackievirus and adenovirus receptor (CAR)
Blood-Mediated Inflammatory Reaction (IBMIR)
Islet equivalents (IEQ)
Non-obese diabetic (NOD) mouse
BioBreeding (BB) rat
Komeda diabetes-prone (KDP) rat
Specific pathogen-free (SPF)
Major histocompatibility complex (MHC)
Cytotoxic T-lymphocyte-associated protein 4 (CTLA-4)
Toll-like receptor (TLR)
Kilham rat virus (KRV)
Casitas B-lineage lymphoma b (Cblb)
Streptozotocin (STZ)
Glucose-stimulated insulin release (GSIR)
Tissue engineering (TE)
Extracellular matrix (ECM)
Endothelial cells (EC)
Basement membrane (BM)
Hepatocyte growth factor (HGF)
Vascular endothelial growth factor (VEGF)-A

Nerve growth factor (NGF)
Mesenchymal stem cells (MSCs)
Human umbilical vein endothelial cells (HUVECs)
Pluripotent stem cells (iPSC)
Blood-outgrowing endothelial cells (BOECs)
Polyethylene glycol (PEG)
Polyglycolic acid (PGA)
Polylactic-co-glycolic acid (PLGA)
Polydimethylsiloxane (PDMS)
Glycosaminoglycans (GAGs)
Growth factors (GFs)
Matrix-bound Vesicles (MBVs)
Sodium dodecyl sulfate (SDS)
Sodium deoxycholate (SD)
Ethylenediaminetetraacetic acid (EDTA)
Alginate/methacrylate-gelatin (GelMA)
Decellularized extracellular matrix (dECM)
Porcine native pancreatic ECM (pdECM)
Vascularized Islet Organ (VIO)
Neonatal porcine islets (NPIs)
Vascularized micro-organs (VMOs)
Human-vascularized islet organ (hVIO)
Pulmonary artery (PA)
Pulmonary vein (PV)
Trachea (T)
Angiogenic Medium (AM)
Stabilization medium (MSM)
Maturation phase (MP)
Testing phase (TP)
Ve-cadherin (VEC)
Von Willebrand factor(vWF)
BOEC culture medium (BCM)
Glucagon (GCG)
Somatostatin (SST)
Droplet digital PCR (ddPCR)
Insulin secretion tests (IST)
Cadherin related family member 5 (CDHR5)

Vascular endothelial growth factor C (VEGFC)
Vascular endothelial growth factor D (VEGFD)
Kinase insert domain receptor (KDR)
Vascular endothelial growth factor receptor 2 (VEGFR2)
Cathepsin S (CTSS)
Pumilio RNA-binding family member (PUM1)
Threonine tRNA ligase 1 (TARS1)
Lysyl oxidase-like 1 (LOXL1)
Polypyrimidine tract-binding protein 1 (PTBP1)
Gap Junction Protein Alpha 1 (GJA1)
Kinesin Light Chain 1 (KLC1)
C-type lectin-like receptor 1 (CLECL1)
RRAD And GEM Like GTPase 1 (REM1)
Prostaglandin-endoperoxide synthase (PTGIS)
MAF BZIP Transcription Factor A (MAFA)
Neuronal Differentiation 1 (NEUROD1)
Regulator of G Protein Signaling 2 (RGS2)
Transcription Factor A, Mitochondrial (TFAM)
Propidium Iodide (PI)
Endothelial Colony-forming Cells (ECFCs)
Vascularized Endocrine Pancreas (VEP)
Area Under the Curve (AUC)
Device-less (DL)
Kidney capsule (KC)
Liver (LV)
Dithizone (DTZ) Complete Final Wash Medium (cFWM)

2. LIST OF FIGURES AND TABLES

Figure 1: Central anatomical features of the human pancreas. 10
Figure 2: Biosynthesis and secretion of insulin. 13
Figure 3: Glucose-induced insulin secretion in human islets. 14
Figure 4: Insulin release from pancreatic b cells is controlled by a series of signals initiated by glucose entry into the cells. 15
Figure 5: Biphasic Insulin Secretion in Human Islets. 16
Figure 6: In vitro insulin secretion in response to glucose concentration. 17
Figure 7: Bioreactor design. 49
Figure 8: hVIOs and VEPs bioengineering timeline. 56
Figure 9: BOECs characterization. 58
Figure 10: Preservation of the structural integrity and functionality of the vascular network. 60
Figure 11: hVIOs' endocrine compartment at day 1, 7, and 14. 61
Figure 12: Analysis of b-cell death by miR-375. 62
Figure 13: Analysis of endocrine function from 1 to 14 days of hVIOs by IST. 63
Figure 14: hVIOs IF analysis. 65
Figure 15: Spatial transcriptomic analyses of vWF-Endothelial AOIs. 70
Figure 16:Spatial transcriptomic analyses of INS-islets AOIs. 72
Figure 17: Assessing the influence of the CXCR1/2 pathway on human islets:. 75
Figure 18: Assessing the influence of the CXCR1/2 pathway on BOECs. 77
Figure 19: Confocal microscopy of cellular distribution and integration into the vascular and endocrine compartments 79
Figure 20: Analysis of b-cell death by miR-375 during the TP. 80
Figure 21: IST during the TP. 81
Figure 22: VEP assembly and endocrine maturation assessment. 85
Figure 23: Ex vivo functional evaluation of VEPs. 85
Figure 24: Long-term in vivo performance of VEPs. 89
Figure 25: Long-term in vivo analysis of VEPs grafts. 90
Figure 26: Leukocyte trafficking in an in vitro model. 92
Figure 27: Leukocyte trafficking in VEP. 94
Figure 28: Representation of the lung anatomy. 105
Figure 29: Decellularization chamber and washing circuit. 106
Figure 30: Decellularized rat lung left lobe scaffold 106
Figure 31: Schematic representation of isolated pancreatic islets stained with DTZ. 110
Figure 32: Schematic representation of an ellipsoid 110
Figure 33:Schematic representation of the bioreactor composition 111
Figure 34: Representation of cell seeding. 113
Figure 35: Graphic summary of hVIOs TP protocol of culture. 114
Figure 36: Graphic summary of IL-8 treatment. 115
Figure 37: Schematic representation of microbeads infusion procedure. 116
Figure 38: Schematic representation of the perfusion machine. 122
Figure 39: GeoMx DSP workflow summary (GeoMx® DSP NGS Readout User Manual). 125
Figure 40: AMPure purification (GeoMx® DSP NGS Readout User Manual). 126

3. INTRODUCTION

3.1. ENDOCRINE PANCREAS PHYSIOLOGY

3.1.1. Understanding the anatomical location and structure of the pancreas

The pancreas is a retroperitoneal organ, and in healthy adults, it weighs around 100 g, is 14 to 25 cm long, has a volume of about 72.4 ± 25.8 cm^3, and has an elongated, lobular shape (Atkinson *et al*, 2020). The pancreas has five parts: head, uncinated process, neck, body, and tail (Fig.1A). The average weight or volume of the adult pancreas displays significant variability, with growth typically ceasing around age 30 (Saisho *et al*, 2007).

The pancreas is located in the upper abdomen near the spleen. The head lies directly against the descending and horizontal parts of the C-shaped duodenum. It has an uncinate process that extends towards the superior mesenteric artery, while the neck portion connects to the pancreatic body. The superior mesenteric artery and vein and the origin of the hepatic portal vein are located posterior to the neck. The pancreatic body is posterior to the aorta, superior mesenteric artery, left renal vessels, and left kidney. Finally, the tail is near the hilum of the spleen. Understanding these anatomical parameters is essential to understanding the function of the pancreas (Atkinson *et al*, 2020).

The pancreatic mass is divided into two parts:

The **exocrine pancreas** oversees the production and release of digestive enzymes into the duodenum. It consists of acinar and duct cells, along with surrounding connective tissue, blood vessels, and nerves in different ratios (Fig.1B). Acinar cells, arranged in clusters called acini, produce and secrete enzymes responsible for digestion and assimilation of nutrients (Atkinson *et al*, 2020). The pancreas has several ducts that connect to the duodenum. The Wirsung duct is the central pancreatic duct. Its dorsal lobe is the Santorini duct, which empties into the duodenum as the accessory pancreatic duct. The bile duct and the Wirsung duct merge to create the hepatopancreatic duct, also known as the ampulla of Vater. The flow through this ampulla is regulated by the sphincter of Oddi, which opens during digestion and closes afterward to prevent the backflow of duodenal contents into the pancreatic duct. The ductal epithelium produces bicarbonate-rich fluid that contains digestive enzymes. The output of pancreatic fluid is controlled by various hormones

and the autonomic nervous system. When food reaches the duodenum, it triggers the pancreas to release significant amounts of water, bicarbonate, and digestive enzymes. These enzymes are essential for breaking down food that moves from the stomach into the small intestine (Nishimori & Onishi, 2001).

Scattered patches of the **endocrine part** are located between the clusters of acinar cells, known as the islets of Langerhans (Fig.1C). These parts of the pancreas produce and release insulin, glucagon, somatostatin, and pancreatic polypeptide into the bloodstream. Approximately one to two million islets in the pancreas comprise about 1-2% of the organ's total mass (Veld & Smeets, 2015).

In the human body, approximately 40-60% of endocrine cells, called β cells, are responsible for producing insulin. The other cells, including α, δ, pancreatic polypeptide (PP), and ε cells, secrete glucagon, somatostatin, pancreatic polypeptide, and ghrelin, respectively (Kilimnik *et al*, 2012). The proportion of these cells within an islet can vary based on factors such as the size, age, and location of the organ (Bonner-Weir *et al*, 2015). Smaller islets mainly consist of β cells, compared to the larger ones which present an equal amount of β and α cells. In the ventral region, you can find islets richer in PP cells, while in the posterior head and uncinate regions there are islets with fewer β and α cells (Savari *et al*, 2013).

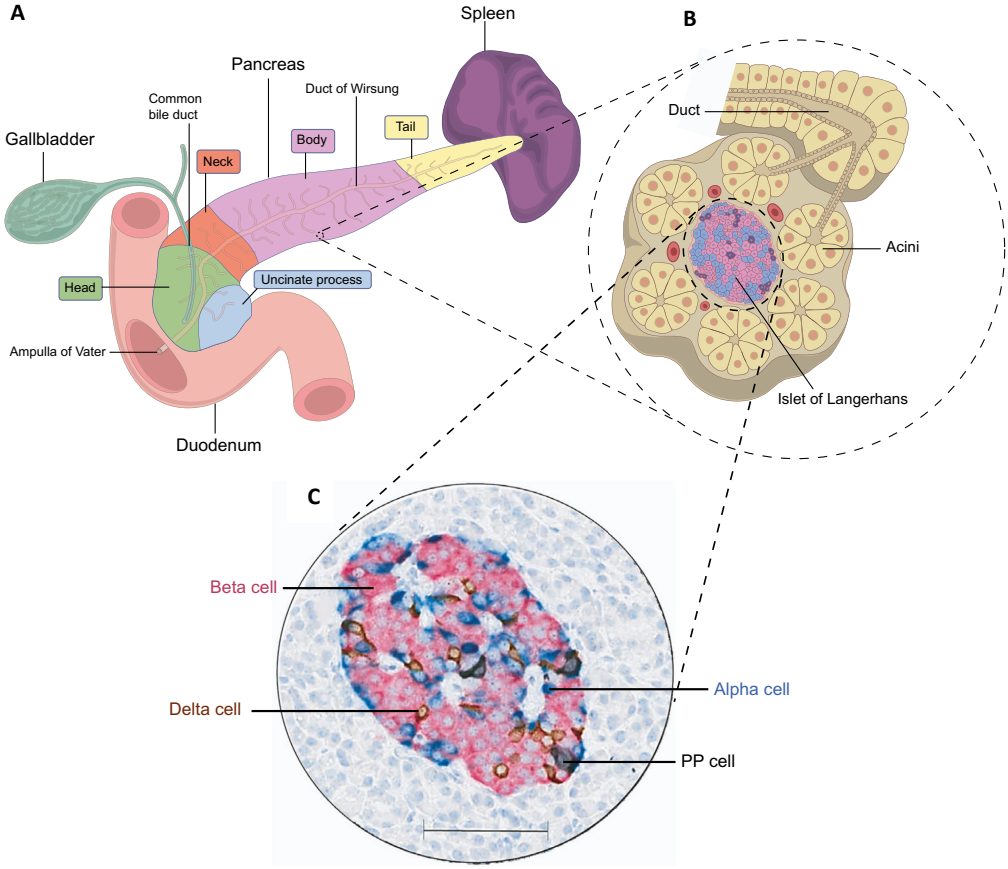


Figure 1: Central anatomical features of the human pancreas: A) Discover the intricacies of the pancreas and surrounding organs through a detailed diagram; **B)** Schematic representation of the intricate organization of the endocrine and exocrine pancreas at the cellular level; **C)** The human pancreatic islet shows the four endocrine cell types (Atkinson *et al*, 2020).

Each islet is supplied with blood from arterioles branching into capillaries. Capillaries merge outside the islet to form small veins. Additionally, the pancreas is innervated by parasympathetic and sympathetic fibers (Ahrén, 2012). The former fibers promote secretion of pancreatic juice and stimulate islets to produce insulin, glucagon, and other hormones essential for blood glucose control. The latter inhibits both exocrine and endocrine secretions (Rodriguez-Diaz *et al*, 2011). Thus, islets' function is finely regulated by a broad range of signals, as autonomic nerve fibers, circulating nutrients, hormones, and paracrine stimuli (Schwartz *et al*, 2013).

3.1.2. The human endocrine pancreas: the role of the hormones

Pancreatic islets are endocrine cells composed of α, β, δ, ε, and PP cells. These cells contain numerous hormone-filled secretory granules released upon receipt of the appropriate stimulus.

Insulin-producing β cells are the most common type of cells in the islets of Langerhans, accounting for 50-70% of the islet mass. Small islets contain more β cells than moderate or large islets (Bonner-Weir *et al*, 2015). In addition to insulin, β cells produce islet amyloid polypeptide (or amylin), which is packaged and released together with insulin. Amylin helps reduce post-prandial hyperglycemia by slowing the process of gastric emptying and promoting satiety (Kahn *et al*, 1990).

Glucagon-producing α cells comprise about 35% of islet mass in humans and primarily prevent hypoglycemia by stimulating glycogenolysis and hepatic gluconeogenesis (Brissova *et al*, 2005).

Somatostatin-producing δ cells are responsible for producing an inhibitory peptide hormone, are evenly distributed throughout the pancreas, and comprise less than 10% of islet mass. The hormone inhibits both endocrine and gastrointestinal hormones (Baetens *et al*, 1979).

PP-producing cells comprise less than 5% of islet mass and are most prominent in the head of the pancreas (like α cells). They have roles in the pancreas' exocrine and endocrine secretion functions (Barbieux *et al*, 2016).

Ghrelin-producing ε cells are the last discovered islet endocrine cell type. Although present in islets, ghrelin is predominately produced in the stomach; ghrelin suppresses insulin release and regulates energy homeostasis (Tong *et al*, 2010).

3.1.3. Physiological control of blood sugar

Normal fasting blood glucose levels range from 80 to 90 mg/dL. After a meal, glucose levels may increase to 120-140 mg/dL but return to normal within two hours. The liver synthesizes glucose through gluconeogenesis when starving (Chen *et al*, 2019). Plasmatic glucose levels are maintained in this range thanks to the coordinated action of all the hormones produced by the endocrine pancreas (see the previous paragraph).

Insulin is a hormone that helps reduce glucose levels in the blood after a meal by promoting glucose storage in peripheral tissues. On the other hand, glucagon is a hormone that encourages the breakdown of glycogen in the liver, which reduces the

amount of glucose in the blood. Glucagon is released to prevent hypoglycemia when blood sugar levels fall below the standard threshold (Brissova *et al*, 2004).
Somatostatin, ghrelin, and PP hormone indirectly regulate blood sugar levels by controlling food intake, digestion, insulin, and glucagon secretion. Somatostatin inhibits the secretion of insulin, glucagon, and PP, while ghrelin stimulates appetite and gastric acid secretion (Kieffer *et al*, 1996). PP hormone reduces intestinal motility and pancreatic juice secretion and inhibits gastrin release, lowering stomach acid production (Youos, 2011).
These hormones are released and coordinated to maintain normal blood sugar levels. When released in small amounts, glucagon stimulates insulin and somatostatin secretion. Somatostatin inhibits the secretion of insulin, glucagon, and PP. The latter, in turn, increases glucagon release, indirectly tuning β cell secretion (Youos, 2011). Disruptions in the regular release pattern of these hormones can result in abnormal blood sugar control. However, only disturbances in insulin secretion and its action can lead to life-threatening complications. Acute hyperglycemia can lead to ketoacidosis and nonketotic hyperglycemic hyperosmolar coma, while chronic hyperglycemia increases the risk of developing cardiovascular and peripheral vascular disease, retinopathy, nephropathy, and neuropathy (Nakrani *et al*, 2024).

3.1.4. Insulin

Insulin is a crucial hormone that plays a vital role in the body. Its synthesis, quality control, delivery, and action are intricately regulated in different organs throughout the body. These functions occur through specific cellular processes that start with hormone production in the pancreas' β cells. It is then partially cleared by hepatocytes, transported to the vascular endothelium, and exerts its effects on the brain, muscle fibers, and adipocytes—key action areas—before being broken down in the kidneys (Tokarz *et al*, 2018). This journey of insulin in the body provides an excellent example of integrated cellular physiology, and we will analyze biosynthesis first and then the mechanism of action (see next paragraph).
Humans have a single gene, INS, which produces insulin. This gene is situated on chromosome 11, and its transcription is controlled by several key transcription factors, such as PDX1, MafA, and NeuroD1, along with many coregulatory (Melloul *et al*, 2002) (Fig.2). These factors are necessary for the expression of the insulin gene in pancreatic β cells and also help regulate INS transcription in response to autocrine glucose and insulin signaling (Andrali *et al*, 2008). The enhancer elements,

transcription factors, and their coregulatory control the expression of insulin and other components of the β cell secretory pathway. They also play a crucial role in maintaining the β cell identity by regulating the expression of glucose transporter 2 (GLUT2) and insulin processing enzyme PC1/3. These factors are essential for the proper functioning of β cells (Gao *et al*, 2014).

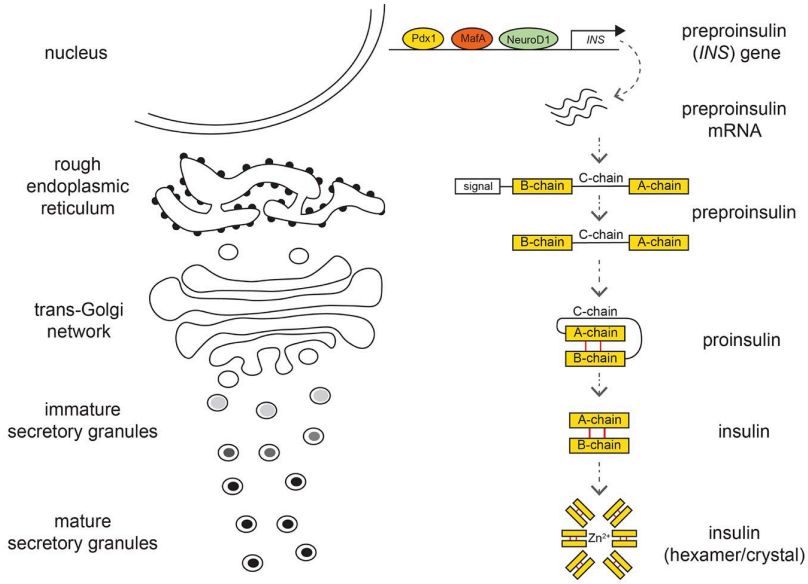


Figure 2: Biosynthesis and secretion of insulin: *Insulin maturation occurs along the granules' secretory pathway. Initially, pre-proinsulin mRNA is transcribed from the INS gene and translated into the pre-proinsulin peptide. As this peptide travels through the rough endoplasmic reticulum (ER) and the trans-Golgi network (TGN), it is converted into its mature form and stored as hexameric insulin/Zn2+ crystals within mature secretory granules* (Tokarz *et al*, 2018).

Insulin initially exists as pre-proinsulin, which the Endoplasmic Reticulum (ER) then transforms into proinsulin through the cleavage of its signal sequence by a signal peptidase. Proinsulin takes on its 3D structure in the endoplasmic reticulum (ER), forming three disulfide bonds that connect the A and B domains. Once it reaches the Golgi apparatus, the correctly folded proinsulin is sorted into immature secretory granules. Here, it undergoes processing by prohormone convertases PC1/3 and PC2, which cleave the C-peptide. Carboxypeptidase E then removes the essential amino acids from the C-terminal end of the resulting peptide chains, resulting in mature insulin, which consists of the A and B peptide chains linked by disulfide bonds (Hutton, 1994). Maturation is regulated by specific proteins, including the newly discovered vesicle-sorting proteins SORCS1 (Kebede *et al*, 2014) and HID-1 (Du *et al*, 2016).

Insulin biosynthesis is rapid and efficient, taking less than two hours. In mature secretory granules, only 1-2% of the protein is still in the proinsulin form. Insulin

binds to Zn^{2+} and forms crystal hexamers with the cation. The transport of these insulin hexamers into the granules is thought to be facilitated by ZnT8 or similar zinc transporters (Lemaire *et al*, 2009).

3.1.5. Insulin physiological release: mechanism of action

Approximately 75-95% of the estimated 10000 insulin granules are stored within the cytoplasm of β cells, away from the cell membrane (Rorsman & Renström, 2003) (Fig.3A).

Insulin release from β cells is a well-coordinated process involving multiple small G-proteins and their nucleotide exchange factors. To release secretory granules, they must first attach to the plasma membrane and undergo a "priming" process triggered by an intracellular calcium signal (Gandasi *et al*, 2017). The interaction of exocytic proteins with calcium channels helps create a complex at the insulin granule-exocytic site, ensuring that insulin can be released quickly when needed (Fig.3B). This process accounts for the biphasic nature of glucose-stimulated insulin secretion observed *in vitro*. The first phase, lasting up to 10 minutes in humans, is rapid and involves the release of granules that are already docked and primed. The second phase requires reorganization of the actin cytoskeleton, facilitating the recruitment of additional granules to the plasma membrane for insulin release (Wang & Thurmond, 2009).

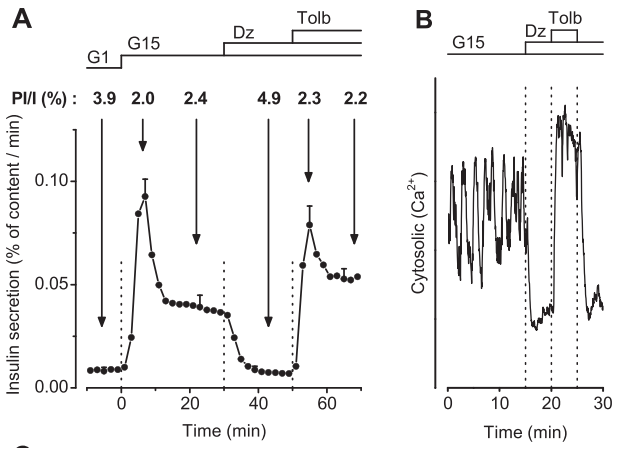


***Figure 3: Glucose-induced insulin secretion in human islets**:**A)** Insulin secretion increased with higher glucose levels. Opening β-cell KATP channels with diazoxide (100 μM) inhibited this increase while closing the channels with tolbutamide (100 μM) reversed the inhibition. Proinsulin levels were also measured, and the Proinsulin to Insulin (PI/I) ratio was shown; **B)** Measurements of islet [Ca $^{2+}$] indicate that the changes in secretion caused by diazoxide and tolbutamide result from alterations in the triggering Ca^{2+} signal* (Henquin, 2021).

Glucose-induced insulin secretion activates two pathways: triggering and amplifying (Henquin *et al*, 2009).

Regarding the triggering pathway, when the concentration of glucose in islets is low (<3 mM), the metabolism rate of β cells is slow. In this state, enough K_{ATP} channels are open in the plasma membrane to maintain the cells in a hyperpolarized state. Due to the minimal influx of Ca^{2+}, the concentration of cytosolic Ca^{2+} is low, leading to basal insulin secretion (Rorsman & Ashcroft, 2018). As the glucose concentration increases, islet cell metabolism accelerates (Doliba *et al*, 2012). This also leads to an increase in cytosolic ATP to ADP ratio in a concentration-dependent manner, (Doliba *et al*, 2012) closing K_{ATP} channels in the β cell membrane (Rorsman & Ashcroft, 2018). This results in depolarization, followed by several voltage-dependent calcium channels opening, allowing Ca^{2+} influx into the cell (Braun *et al*, 2008). The resulting increase in cytosolic Ca^{2+} concentration activates an effector system that promotes the exocytosis of insulin-containing granules. Micromolar concentrations of dihydropyridines can block L-type calcium channels, halting glucose-induced insulin secretion (Henquin, 2021)(Fig.4).

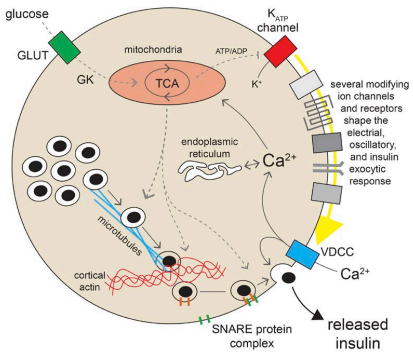


Figure 4: Insulin release from pancreatic β cells is controlled by a series of signals initiated by glucose entry into the cells: *Glucose is processed through several steps, including phosphorylation and entry into the TCA cycle. This process leads to the closure of ATP-dependent K+ (KATP) channels, which triggers a sequence of electrical events resulting in the entry of calcium ions (Ca2+) through voltage-dependent Ca2+ channels (VDCCs). The influx of calcium ions then prompts insulin release through exocytosis, mediated by SNARE complex proteins. Receptors, channels, intracellular calcium stores, metabolic signals, and cytoskeletal elements influence insulin secretion* (Tokarz *et al*, 2018)*.*

Generating a signal that triggers insulin secretion is essential. However, the effectiveness of Ca^{2+} is limited without an amplifying pathway that augments its effectiveness on exocytosis without raising the concentration of cytosolic Ca^{2+}. When islets are exposed to 15 mM glucose, insulin secretion is more significant in response to high glucose (Misler *et al*, 1992) (Fig.5). The amplifying action of glucose, which also depends on its metabolism, helps in increasing insulin secretion in response to a given triggering Ca^{2+} signal. It may account for up to 40-50% of the global response

(Henquin, 2021). However, we cannot modulate the amplifying pathway selectively in living subjects. Although early human studies of insulin secretion distinguished initiating and potentiating glucose actions, a direct demonstration that the amplifying pathway contributes to glucose-induced insulin secretion *in vivo* is still missing (Cerasi, 1975).

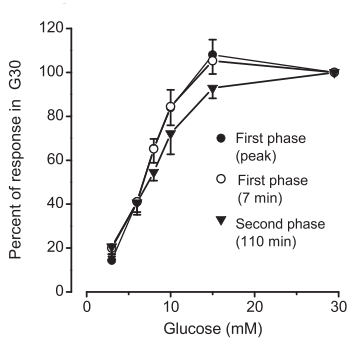


Figure 5: Biphasic Insulin Secretion in Human Islets (Henquin, 2021)***.***

Grodsky and his colleagues thoroughly investigated insulin secretion at the organ level (Wang & Thurmond, 2009). They perfused an isolated rat pancreas with a glucose-containing buffer to study insulin secretion dynamics. They examined responses to various glucose stimuli, including stepwise and staircase increments and short pulses (Grodsky *et al*, 1967),(Grodsky *et al*, 1969). These studies demonstrated that the β cell responds to a prolonged single step of glucose with a rapid and transient first phase of insulin secretion, followed by a slower, but increasing in time, second phase (Fig. 6). In response to a single-step glucose stimulus, the magnitude of the first phase increases with higher doses of glucose. The amount of insulin released during the first phase depends on glucose concentration and follows a sigmoidal function up to a point of 135 mg/dl. The first-phase insulin response is inhibited when the glucose stimulus is repeated in short intervals. However, if longer time intervals are used, the first-phase insulin response may be enhanced at the second stimulation. The first phase occurs almost instantaneously after the beginning of the stimulation, and at any glucose level, it lasts for approximately 3-4 minutes. The second phase may last several hours if the β cell is continuously exposed to glucose (Wang & Thurmond, 2009). Prolonged exposure to glucose can demonstrate a sustained but lower insulin release, known as a desensitization phase, lasting up to 24 hours (Caumo & Luzi, 2004).

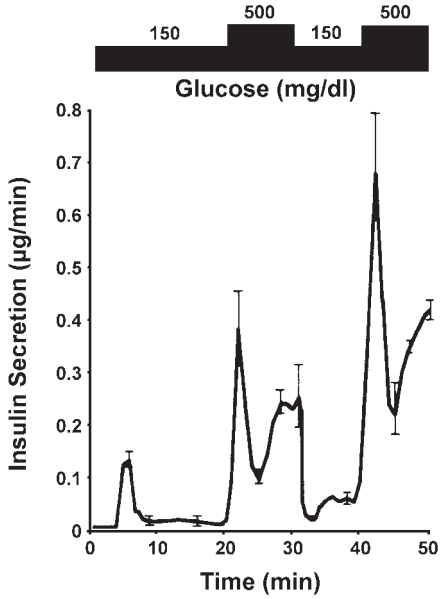


Figure 6: In vitro insulin secretion in response to glucose concentration.

Islets can be isolated from the pancreas of organ donors and dispatched to research laboratories for experimental studies (Henquin, 2021). Only exceptional results obtained with freshly isolated islets have been reported (Warnock *et al*, 1988). Studies on the insulin secretion process *in vitro* face a few challenges and limitations. Firstly, the characteristics of the tested islets, such as their purity and size, can vary, potentially influencing the results obtained, as has been recently reviewed. Secondly, due to their limited availability, human islets (HIs) are often incubated or perfused in small numbers that may only represent part of the islet population. Thirdly, all the solutions used *in vitro* differ significantly from plasma solutions. For instance, glucose is often tested at traditional but non-physiological concentrations and without other agents, such as fuels, hormones, and neurotransmitters, whose influence on insulin secretion by HIs would require a closer examination. No study has measured secretion in islets bathed in a medium that approaches plasma composition (Henquin, 2021).

It is important to note that certain limitations, often due to technical constraints, do not necessarily impact the results obtained in scientific experiments.

In summary, insulin secretion is a strictly controlled process highly dependent on the histological organization of the endocrine niche, which must be known to properly study the endocrine pancreas' (patho)physiology.

3.2. ENDOCRINE PANCREAS DYSFUNCTIONS: DIABETES MELLITUS

3.2.1. Pancreatic endocrine disorders: type 1 diabetes mellitus (T1DM) etiopathogenesis and clinical characteristics

Diabetes is a group of metabolic diseases caused by defects in insulin secretion, insulin action, or both. It leads to increased blood sugar levels. This disease has a complex origin that involves both environmental and genetic factors. Chronic hyperglycemia caused by diabetes can lead to long-term damage and failure of various organs, including the kidneys, eyes, heart, nerves, and blood vessels (Diagnosis and classification of diabetes mellitus., 2011).

Two forms of diabetes are most common: Type 1 Diabetes (T1D) and Type 2 Diabetes (T2D). Here, we will analyze T1D in detail.

T1D is a long-lasting autoimmune disease caused by the immune system mistakenly attacking and destroying insulin-producing cells in the pancreas. Both genetic factors and environmental triggers, particularly in the early stages of life, can contribute to the development of T1D. The progression of this disease (Atkinson & Eisenbarth, 2001) can be explained by identifying three main stages in its natural history.

In the first stage, individuals with a genetic predisposition may develop T-cell and humoral autoimmune responses against β cells due to environmental factors (Eisenbarth, 1986). The second stage is identified by two or more autoantibodies and changes in glucose metabolism, which are not diagnostic for diabetes but occur without any symptoms. This is known as "early metabolic alterations with an asymptomatic state." The third stage, "clinical diabetes," is characterized by the appearance of clinical symptoms (Insel *et al*, 2015).

Human Leukocyte Antigens (HLA) genes are responsible for up to 50% of the genetic risk of T1D, particularly HLA class II loci. This suggests that the selective presentation of specific auto antigenic peptides plays a role in developing the disease (Barrett *et al*, 2009),(van Lummel *et al*, 2016).

The first indication of autoimmunity during the development of T1D is the seroconversion of islet autoantibodies to insulin, glutamate decarboxylase, insulinoma antigen 2, or zinc transporter 8. The combined presence of these autoantibodies in the blood is the best predictor of both the loss of immune tolerance and the clinical manifestation of T1D. However, their exact role in destroying β cells remains unclear (Bottazzo *et al*, 1974),(Bloem & Roep, 2017).

It is important to note that less than 10% of individuals with HLA predisposition develop T1D (Craig *et al*, 2019). This means that our knowledge of HLA haplotypes

alone does not fully define the genetic risk of the disease (Krischer *et al*, 2017),(Bonifacio *et al*, 2014). Other genes, such as those that encode pre-proinsulin (INS), protein tyrosine phosphatase (PTPN22), or IL-2 receptor alpha subunit (IL2RA), have also been found to play a critical role in the development of T1D (Pociot *et al*, 2010). Genome-wide association studies have identified other genes that play a role in the pathogenesis of T1D, such as the chromosomal region 6q22.23 that encodes protein tyrosine phosphatase kappa receptor kappa (PTPRK) and the thymocyte-expressed molecule involved in sorting (THEMIS), which are engaged in thymic T cell development (Inshaw *et al*, 2018). In recent years, genetic scores have been proposed to evaluate the combined effects of different genes on the risk of T1D. The Type 1 Diabetes Genetic Risk Score (T1D GRS) is one such score that has been validated to predict the development of T1D in at-risk individuals. The T1D GRS incorporates HLA and non-HLA genes, single nucleotide polymorphisms (SNPs) associated with T1D, and discriminates T1D from T2D, monogenic diabetes, and controls (Oram *et al*, 2016),(Patel *et al*, 2016). Several studies have shown that the T1D GRS can predict the risk of pre-symptomatic T1D in children without affected first-degree relatives (Redondo *et al*, 2018),(Bonifacio *et al*, 2018).

As the disease progresses in T1D, immune cells infiltrate the pancreas and attack insulin-producing cells. This creates an inflammatory environment known as insulitis. Insulitis accelerates the development of T1D by increasing the exposure of islet antigens presented by HLA molecules class I to the immune system. However, the frequency of these autoreactive cells in peripheral blood is low and similar in T1D patients and healthy individuals (Culina *et al*, 2018). The increased frequency of CD8+ T cells in the pancreas of T1D patients implies differential peripheral activation and regulation in T1D patients (Coppieters *et al*, 2012),(Culina *et al*, 2018),(Kuric *et al*, 2017).

Autoreactive islet T cells have unusual characteristics compared to T cells that protect us from cancer and infections. They have low epitope binding affinity for HLA and low T cell receptor (TCR) avidity for HLA-epitope complexes, inclined or inverted. Since autoreactive T cells are part of a standard T cell repertoire, it is unlikely that the disease is entirely the result of dysfunctional immune cells. Instead, peripheral activation of the immune system is required locally in the target tissue (Culina *et al*, 2018),(Danke *et al*, 2004).

B cells in the pancreas play a role in their death (Bottazzo, 1986). Several triggers have been proposed to induce β cells to elicit an immune response, ranging from pancreatic size and β cell mass to viral infection and metabolic stress. The pancreas

of T1D patients is smaller than that of unrelated controls (Eizirik *et al*, 2009),(Campbell-Thompson *et al*, 2012),(Dotta *et al*, 2007).
Individuals at risk and patients with T1D have similar-sized pancreas (Campbell-Thompson *et al*, 2012), and there is currently no evidence to suggest that pancreas size decreases with disease progression. Lower β cell mass can result in lower functional capacity and increased pressure on β cells to manage glycemic control. Viral infections or leakage of inflammatory agents from the intestines into the pancreas could create a pro-inflammatory environment in addition to metabolic stress (Skog *et al*, 2013),(Dotta *et al*, 2007),(Krogvold *et al*, 2015). B cells express specific receptors and adhesion molecules, which makes them vulnerable to viral infections during insulin secretion. A coxsackievirus and adenovirus receptor (CAR) exclusive to β cells, present in insulin-containing granules, could make β cells vulnerable to viral infections. Although viral infection could be a risk factor in a small minority of patients with T1D, it is not the only contributing factor (Skog *et al*, 2013). Other viruses, such as rotavirus and cytomegalovirus, are also implicated in the development of T1D (Skog *et al*, 2013),(Krogvold *et al*, 2015).
It is important to note that the assumption that T1D is a single uniform disease is losing credibility as there is an increasing recognition of interpatient variability in every aspect of the disease, including epidemiology, potential environmental triggers, age of onset, sex differences, aggressiveness of autoimmunity, metabolic derangements, and insulin efficacy (Ilonen *et al*, 2019).

3.2.2. Current therapeutic approaches for diabetes treatment: advantages and disadvantages

Insulin replacement therapy is currently the primary treatment for T1D. In 1921, Banting and Best introduced animal pancreas extracts to lower glucose levels, beginning to use exogenous insulin therapy for T1D (Banting & Best, 1990). In 1922, commercialized crude insulin preparations from animal origins were introduced for clinical use. However, these preparations were associated with problems related to insulin absorption and inefficient action. These issues often led to inconsistent glucose-lowering effects or prolonged periods of hypoglycemia (Pathak *et al*, 2019).
Many insulin analogs have been developed to address the challenges posed by traditional insulin therapy. These analogs replicate the actions of natural insulin and have better pharmacokinetic profiles (Evans *et al*, 2011). However, despite these

advancements, insulin replacement therapy has limitations. Clinical evidence has shown that insulin preparations cannot fully replicate the biological actions of endogenous insulin (Cohen *et al*, 2016).

As the number of cases of T1D continues to rise, there is a growing need to find new and effective ways to restore normal blood sugar levels. The current treatment for T1D involves strict dietary management and lifelong use of insulin, delivered through multiple daily injections or insulin pumps. However, there is a need to explore novel therapies that could improve outcomes for people living with T1D (Yeh *et al*, 2012). Recently, there have been advancements in genetically modified insulin analogs such as Aspart, Lispro, and Delgludec insulins. These fast-acting and long-acting insulins provide more physiological hypometabolic control than traditional insulins (Franek *et al*, 2016). The current insulin-centric approach for treating T1D leaves patients vulnerable to severe hypoglycemic episodes, lifelong dependence on insulin, insulin resistance, mild obesity, and psychiatric conditions (Yeh *et al*, 2012),(Jacobson *et al*, 2013). Such observations highlight the importance of developing alternative strategies to restore glycemic control and complete insulin independence (Pathak *et al*, 2019).

An alternative approach to insulin injection involves replacing the endocrine mass by transplanting pancreas or pancreatic islets from a donor in T1D patients experiencing insulin-dependent hypoglycemia unawareness, severe hypoglycemia, and unstable glycemia (Bottino *et al*, 2018),(Chen & Gunton, 2021),(Cayabyab *et al*, 2021).

To date, pancreas transplantation is more commonly used than islet transplantation, despite the latter being a less invasive procedure with fewer post-surgery complications (Bellin & Dunn, 2020).

Islet transplantation has a limited success rate in achieving insulin independence after intrahepatic islet transplantation. However, it still has a significant impact on reducing hypoglycemic events and enhancing the quality of life of patients (Pignatelli *et al*, 2022). A decline in both graft function and insulin independence was observed within 5 years of islet transplantation (Cayabyab *et al*, 2021),(Pellegrini *et al*, 2016). Reestablishing endocrine pancreatic function can restore fine endogenous control over glucose homeostasis, which closed-loop artificial pancreas devices cannot precisely mimic in the long term (Peloso *et al*, 2017),(Trevitt *et al*, 2016).

After transplantation, the Instant Blood-Mediated Inflammatory Reaction (IBMIR) can cause a loss of 50% to 70% of the total infused islet mass within a few hours to days. Moreover, at the hepatic site, tissue reperfusion-related damage and thrombotic events can exacerbate the inflammatory state, leading to poor engraftment efficiency (Brusko *et al*, 2021),(Kourtzelis *et al*, 2015). After transplantation, islets are

dangerously exposed to hypoxic stress and lack of nutrients due to the delay in functional graft vascularization, causing cell death and apoptosis for at least two weeks (Gibly *et al*, 2011). Many islets are required to compensate for the intrinsic limitations of the procedure. Generally, at least 10000 islet equivalents (IEQ)/kg body weight are obtained from two or three donor pancreata, which increases the overall demand for organs (Shapiro *et al*, 2000),(Shapiro *et al*, 2006).

On the other hand, lifelong immunosuppressants are administered after the transplant to prevent immunological reactions against the graft. However, this can increase the risk of infection, cancer, and kidney failure(Samojlik & Stabler, 2021). To improve the success rate of allogeneic islet transplantation, researchers have proposed alternative sites for transplantation. However, the intrahepatic site has yet to be shown to have better outcomes (Chen & Gunton, 2021),(Cayabyab *et al*, 2021),(Pellegrini, 2019).

To improve the results and overcome current limitations, it is necessary to add several points (Pignatelli *et al*, 2022). Additionally, a model is required to study diabetes pathophysiology. The primary requirement is to increase the efficacy of currently available therapies by better understanding the disease's etiopathogenesis. The next chapter will examine current study models, analyze their advantages and disadvantages, and propose new strategies for understanding diabetes pathophysiology using available models.

3.3. AVAILABLE MODELS FOR UNDERSTANDING TYPE 1 DIABETES PATHOPHYSIOLOGY

Animal models have traditionally played a vital role in exploring and characterizing disease pathophysiology, identifying targets, and evaluating novel therapeutic agents *in vivo* (Al-Awar *et al*, 2016).

When studying diabetes, it is important to carefully select the appropriate animal models depending on the specific aspects of the disease being researched. These animal models allow for a better understanding of the pathogenesis of diabetes by combining genetic and functional characterization of the syndrome (Arndt *et al*, 2013). Achieving a deficiency in insulin production in T1D can occur through various mechanisms, including chemical ablation of β cells and breeding rodents that spontaneously develop autoimmune diabetes. Due to highly inbred animals used in

studying T1D, with limited pathways to T1D, the relevance to human T1D has been questioned (Phillips *et al*, 2011).

3.3.1. Murine models for type 1 diabetes

T1D is an autoimmune condition. To better understand its mechanisms, it is desirable to use an animal model that displays spontaneous autoimmunity. Insulitis is a key histopathologic feature of T1D. It is characterized by the infiltration of lymphocytes into the islets of Langerhans, which specifically target the β cells (Campbell-Thompson *et al*, 2013). This phenomenon is observed in human and animal models spontaneously developing T1D. Two main models of spontaneous T1D were the non-obese diabetic (NOD) mouse and the BioBreeding (BB) rat. Both were first identified and bred in the 1970s (Makino *et al*, 1980),(Nakhooda *et al*, 1977). In the 1990s and early 2000s, two rat models of spontaneous T1D were described: the Komeda diabetes-prone (KDP) rat (Kawano *et al*, 1991) and the LEW.1AR1 rat (Lenzen *et al*, 2001). The NOD mouse is widely used, primarily due to its compatibility with cross-breeding genetically modified strains and direct genetic manipulation. The cost of housing a mouse colony is also lower than that of a rat colony. In studies aimed at reversing or curing T1D, hyperglycemia can be induced by injecting streptozotocin or alloxan, which selectively kill pancreatic β cells. Alternatively, the Akita mouse model can be used, characterized by a deficiency in functional insulin caused by non-autoimmune mechanisms (Izumi *et al*, 2003).

When researching the pathogenesis of a disease, two main strategies are used. The first strategy involves utilizing an animal model that closely mimics the disease process in humans. The second strategy involves genetic manipulations that help assess the importance of specific genes in disease development. Often, both strategies are used together. To prevent the onset of the disease, the pathogenesis elements must reflect those of the human disease. Thus, similar models are often used (King & Bowe, 2016).

3.3.2. Non-obese diabetic (NOD) mouse

The NOD mouse develops insulitis around weaning in females, and in males, it occurs a few weeks later. Female NOD mice are more prone to overt diabetes than males. The onset of diabetes can vary between mice and colonies but usually happens between weeks 18 and 30 (Pozzilli *et al*, 1993). However, a specific pathogen-free (SPF) environment is necessary for the development of diabetes. If high standards of cleanliness are not maintained, the frequency of diabetes falls considerably.

Studying NOD mice has been crucial to understanding the genetics and pathogenesis of T1D (Jayasimhan *et al*, 2014). Some genes identified in NOD mice have been found to contribute to T1D susceptibility in humans (Driver *et al*, 2012). One of the most significant genetic predictors of T1D is the major histocompatibility complex (MHC), which confers susceptibility or resistance to T1D in both mice and humans (Driver *et al*, 2012). Genetic predictors are also associated with the immune system, including cytotoxic T-lymphocyte-associated protein 4 (CTLA-4) (Ueda *et al*, 2003). However, many susceptibility loci identified in NOD mice have not been found to be significant in human disease.

Studying NOD mice has helped understand much of the disease's immunopathology because obtaining human pancreas biopsies is challenging. Insulitis is present at the onset of both NOD and human disease and is associated with a decrease in β cell mass. In both cases, the infiltrate is predominantly T lymphocytes and contains autoreactive $CD8^+$ T lymphocytes, macrophages, and B lymphocytes (In't Veld, 2014).

MHC class I overexpression has been found in recent-onset NOD mice and human (In't Veld, 2014)cases. However, the way the disease develops is different in humans compared to NOD mice. In humans, insulitis is less severe, while in NOD mice, all the islets are significantly affected and show a strong infiltrate. In contrast, the infiltrate in human patients is much less pronounced (In't Veld, 2014).

It has been proposed that this model may exaggerate the effectiveness of an experimental drug in clinical settings. For instance, anti-CD3 therapy and oral insulin succeeded in NOD mice but not humans (Reed & Herold, 2015). Other factors to consider are the immunological differences between mice and humans and issues related to dosing (Reed & Herold, 2015). Additionally, while the incidence of diabetes in NOD mice rises in a clean environment (SPF) (Leiter, 1993), in humans, environmental influences like viruses can significantly impact disease development (Hober & Sauter, 2010). The underlying pathology of T1D likely varies among patients, as shown by distinct subgroups that respond differently to certain treatments (Herold *et al*, 2013). Therefore, the NOD mouse model may only reflect a subset of T1D patients (King & Bowe, 2016).

3.3.3. BioBreeding (BB) rat

The BB rats are known to develop diabetes spontaneously between 50 and 90 days, with an incidence of over 90% in both females and males when housed in a virus antibody-free environment (Mathews, 2005). As a control for the BBDP rats, a diabetes-resistant sub-strain called BBDR has been established. Although diabetes does not occur spontaneously in BBDR rats, it can be induced by T_{reg} depletion, toll-like receptor (TLR) ligation, or Kilham rat virus (KRV) infection (Bortell & Yang, 2012). Like humans and NOD mice, the MHC is involved in the risk of developing spontaneous disease in BB rats. However, a key difference from human disease is the presence of T-cell lymphopenia in these rats (Bortell & Yang, 2012). However, the morphology of insulitis in BB rats resembles that of humans more than that seen in NOD mice (In't Veld, 2014). Various interventions have been identified that can prevent or postpone the onset of the disease in BB rats, similar to NOD mice. These include significant measures that alter the immune system, such as thymectomy (Like *et al*, 1982), anti-lymphocyte therapy (Like *et al*, 1979), CD8 T-cell depletion (Groen *et al*, 2003), and cyclosporine treatment (Like *et al*, 1984). Other interventions involve administering insulin parenterally (Gotfredsen *et al*, 1985), making dietary changes (Scott *et al*, 1997), and performing intrathymic islet transplantation (Scott *et al*, 1997). However, many of these therapies have yielded disappointing results in clinical trials or are unsuitable for human use, similar to findings in NOD mice.

3.3.4. Komeda diabetes-prone (KDP) rat

The KDP rat model of diabetes shows overt diabetes symptoms around day 60, with approximately 80% of rats developing diabetes by day 120 (Komeda *et al*, 1998). These rats exhibit severe insulitis (Komeda *et al*, 1998) , unlike BB rats, but are not lymphopenic (Mordes *et al*, 2004). As in other models, the role of MHC class II in developing autoimmunity has been identified (Yokoi *et al*, 2012). The major non-MHC-linked susceptibility gene in these rats is Casitas B-lineage lymphoma b (Cblb) (Yokoi *et al*, 2007). Although the most common variants of this gene do not seem to

be associated with T1D in patients, some rarer missense mutations have been found in T1D patients (Yokoi *et al*, 2008). It is worth noting that this model has not been extensively used in prevention studies.

3.3.5. Lew.1AR1-iddm rat

The Lew. 1AR1-iddm rat model of T1D was developed by Lenzen et al. in Hannover (Lenzen *et al*, 2001). The onset of overt diabetes in Lew.1AR1-iddm rats occurs around day 60 and is equally common in both sexes (Jörns *et al*, 2005). Insulitis is observed in the pancreas, infiltrating $CD4^+$ and $CD8^+$ T lymphocytes, macrophages, NK cells, and B cells (Lenzen *et al*, 2001),(Mathews, 2005),(Jörns *et al*, 2004). Unlike other murine models of autoimmune T1D, the Lew.1AR1-iddm rat does not present with autoimmunity in other organs (Lenzen *et al*, 2001),(Jörns *et al*, 2004) and does not have lymphopenia like the BB rat. Genetic analysis of this strain also highlights the role of MHC class II in the pathogenesis of T1D (Lenzen *et al*, 2001),(Mathews, 2005). Diabetes in this model can be prevented by the immunomodulatory agent FTY720 (Jörns *et al*, 2010), which is like the results seen in the NOD mouse and BB rat (Popovic *et al*, 2004).

3.3.6. Chemical induction of Type 1 diabetes

Streptozotocin (STZ) and alloxan can harm β cells in the pancreas and cause high blood sugar levels within a few days of being administered. Both chemicals are transported into the β cell by the Glut-2 transporter (Szkudelski, 2001). STZ causes DNA alkylation, which activates PARP and reduces the amount of NAD^+. This leads to a decrease in ATP content and insulin secretion (Sandler & Swenne, 1983). Additionally, STZ creates free radicals that contribute to DNA damage. Eventually, the DNA damage, coupled with energy depletion, leads to the death of β cells. A single high dose of 100 mg to 200 mg/kg (depending on the mouse strain) of STZ is enough to destroy β cells rapidly (Srinivasan & Ramarao, 2007),(Hayashi *et al*, 2006). In rats, doses between 35 and 65 mg/kg are used (Srinivasan & Ramarao, 2007).

Alloxan is a chemical that can harm β cells in the pancreas. It produces highly reactive hydroxyl radicals that break down DNA (Szkudelski, 2001). β cells are particularly vulnerable to this damage as they are not well protected from reactive oxygen species (Nerup *et al*, 1994). However, it is important to note that alloxan can be toxic to the kidneys if even slightly overdosed, and it has a narrow range of doses that can cause diabetes (Szkudelski, 2001). Mice can tolerate doses of 50 to 200 mg/kg, while rats can tolerate doses of 40 to 200 mg/kg, depending on their strain and how the chemical is administered (Szkudelski, 2001).

Chemically induced T1D models are used in testing therapies that do not rely on β cells. Such models allow for diabetes to be induced quickly and predictably in various mouse strains, which makes it possible to perform isogenic (Rackham *et al*, 2013), allogeneic (King *et al*, 2003), or xenogeneic (Krishnan *et al*, 2015) transplants. In the case of islet transplant models, the transplantation site is often under the kidney capsule. This provides easy access and retrieval of the graft and allows for its removal in the living animal through nephrectomy of the graft-bearing kidney. However, this may exclude regeneration of the endogenous pancreas (Grossman *et al*, 2010), and an animal that has been cured should return to hyperglycemia after graft removal. Alternatively, islets can be implanted at the clinically relevant intraportal site in mice (Rackham *et al*, 2014). Although this procedure is much more technically difficult and does not allow for easy localization or removal of the graft.

It's important to note that using STZ as a treatment has some drawbacks. One of the main risks is the possibility of toxicity in case of overdose (Szkudelski, 2001). To avoid any risks, appropriate controls or study designs should be implemented. It is also important to exclude the possibility of endogenous β cell regeneration (Grossman *et al*, 2010).

Another thing to remember is that STZ can cause lymphopenia, which means there is a decrease in the number of lymphocytes in the blood. However, there is a relative increase in T_{reg} cells (Muller *et al*, 2011). This could potentially affect the interpretation of studies that involve immune tolerance to pancreas and islet transplants.

In summary, mouse models have advantages and disadvantages for studying T1D. Selecting the correct model to address a specific research question can be challenging and significantly impact the results obtained and their interpretation.

Although mouse models are useful for preclinical research, translating their results into clinical practice is challenging. Therefore, the success rate of therapies identified through mouse models is generally low.

3.3.7. Ex-vivo technology for studying islet's endocrine function.

Pancreatic endocrine disorders, such as T1D, are increasing globally, highlighting the urgent need for better models to develop targeted interventions.
It is difficult to study the human pancreas in real-time to assess treatments and metabolic and immunological features.
Recent research has focused solely on peripheral blood and explored mechanisms beyond pathogenesis.
The urgent need is the possibility to directly study the endocrine disorders during etiopathogenesis specifically in the tissue involved.
The most advanced *ex vivo* technology involves perfusing freshly isolated islets from healthy donors with varying concentrations of glucose while subjecting them to different treatments and stimulations, either alone or within a (micro)encapsulation system, to study their endocrine function (Buchwald *et al*, 2018).
Researchers are conducting dynamic perifusion experiments to study the effect of encapsulation on insulin secretion and to improve the ability to quantitatively describe glucose-stimulated insulin release (GSIR) of pancreatic islets. These experiments are performed using free (non-encapsulated) and immunoisolated HIs. An automated multichannel apparatus is used for parallel perifusion and sample collection with high temporal resolution (Buchwald *et al*, 2018).
Analytical, technical equipment enables quantitative characterization of insulin release kinetics under controllable experimental conditions of varying glucose concentrations and secretagogues of interest (Cabrera *et al*, 2008),(Buchwald *et al*, 2015),(Garcia-Contreras *et al*, 2017).
Perfusion studies are emerging as useful tools for analyzing islet quality and function in research and clinical applications (Kayton *et al*, 2015).
Another *ex vivo* approach for studying endocrine disorders involves utilizing publicly available virtual slides from the Network for Pancreatic Organ Donors with Diabetes (nPOD) project. For instance, one research utilized nPOD slides to assess the mass and distribution of β cells in non-diabetic subjects who were antibody-negative (Ab−) and antibody-positive (Ab+), as well as in patients with recent onset type 1 diabetes (T1D) (Diedisheim *et al*, 2016).

In this setup, the lack of a native organ vascular network and pancreatic islet niche limit endocrine physiological secretion mimicry (Nyman *et al*, 2008),(Olsson & Carlsson, 2006).

To overcome these limitations, tissue engineering started to collect innovative alternative approaches, which we will discuss in detail in the next paragraph.

3.4. TISSUE ENGINEERING SUPPORTING OF DYNAMIC CULTURE: AN EMERGING INNOVATIVE APPROACH

Tissue engineering (TE) is an interdisciplinary field that applies engineering principles and life sciences to create biological substitutes that restore, maintain, or improve tissue function (Langer & Vacanti, 2016). Three general strategies are utilized to create new tissue:

i) *Isolated cells or cell substitutes.* This method eliminates the risks and complications associated with surgery as it enables the replacement of only the necessary cells that carry out the required function. It also allows for the manipulation of cells before infusion. However, there are potential limitations, such as the inability of the infused cells to maintain their function in the recipient and the possibility of immunological rejection (Langer & Vacanti, 1993).

ii) *Tissue-inducing substances.* The success of this approach relies on the large-scale production and purification of appropriate signal molecules, such as growth factors, and the development of methods for their delivery to target cells (Langer & Vacanti, 1993)

iii) *Cells placed on or within matrices.* In closed systems, cells are enclosed by a membrane that permits the passage of nutrients and waste products but obstructs the entry of large entities like immune cells or antibodies that can damage the transplanted cells. These systems can be inserted inside the body or used externally. In open systems, cells are attached to matrices made of natural materials like collagen or synthetic polymers and are then implanted into the body. To avoid immunological rejection, immunosuppressive drugs or autologous cells can be used (Langer & Vacanti, 1993).

Cell biology holds the key to unlocking the potential of tissue engineering research. Understanding what controls cellular differentiation and growth and the impact of

ECM components on cell function is crucial for success (Yannas, 1990),(Grande Tovar *et al*, 2019). Immunology and molecular genetics can aid in developing cell transplant systems or designing cells (such as through gene therapy) not rejected by the immune system (SYKES *et al*, 1993).

It is crucial to take into account the source and preservation of cells used in transplantation. Cells can be sourced from cell lines or primary tissues from patients, human donors, animal sources, or fetal tissue. When selecting the source, ethical considerations, safety concerns, and effectiveness must be evaluated (Langer & Vacanti, 1993). While cryopreservation has been effective for specific cells, more extensive procedures are necessary to create cell banks for various tissues. Large-scale *in vitro* cell culture systems ensure cell proliferation before transplantation and resolve nutrient transport issues (Arutyunyan *et al*, 2022). Sterilization of the transplants is also critical.

Tissue engineering is a crucial study area, particularly regarding the materials used. Natural materials can contain information that enhances cell attachment or helps maintain differentiated function. However, natural materials are sometimes challenging to scale up, and variations may vary from batch to batch. Synthetic polymers provide exact control over factors like molecular weight, degradation time, and hydrophobicity. However, they might not engage with cells as effectively as desired. In contrast, natural polymers have beneficial cell interaction properties but lack precise control over molecular weight and other characteristics. Recently, researchers have merged the benefits of both types by grafting important amino acid sequences from natural polymers onto synthetic ones. This approach allows for the precise control of polymer properties while achieving desirable cell interactions (Guo *et al*, 2022). Polymer processing is essential for the effectiveness of many implants made from composite materials or highly porous structures, making reproducible manufacturing methods vital (Guo *et al*, 2022). Creating sustained-release systems that can deliver molecules over long periods will be important for administering different tissue-inducing growth factors and angiogenesis stimulants (Chua *et al*, 2017). Additionally, developing techniques for analyzing cell-material interfaces would be beneficial (Ratner *et al*, 1990). Mathematical models and *in vitro* systems can be used to predict cellular events *in vivo* (Williams *et al*, 2013).

Integrating all the biological elements relevant to the function of an organ within a single device has the potential to overcome the limitations of currently available *in vitro* models used in diabetes research (Huh *et al*, 2011). In the context of endocrine disorders, the endocrine niche consists of three building blocks: ECM, endocrine cells, and the vascular network (Citro *et al*, 2019a). The ability to create a platform that

combines three elements - physiological-like perfusion, inflammatory and immune processes - would be a significant advancement in engineering a functional endocrine compartment that can mimic the pathogenesis of diabetes (Huh *et al*, 2011). In addition, implementing such a system would create a dependable and precise platform for drug screening and physiological research.
The next chapter will outline the tissue engineering techniques used to create organs and tissues *ex vivo* and how they can enhance *in vitro* research methods.

3.4.1. Tissue engineering strategies

Rebuilding a complex tissue or organ involves recreating the interconnection between parenchyma, vasculature, and supportive structures in a 3D composition that facilitates biological function. There are two main strategies: i) scaffold-free TE and ii) scaffold-based TE.
The first technique, self-assembly, involves reconstructing tissues using only the patient's cells, without any external materials. This approach relies on the cells' ability to secrete and assemble their ECM (Saba *et al*, 2018).
The structure of a tissue or organ plays an important role in its function. Therefore, recreating the natural architecture is essential to obtain perfectly functioning tissues and organs. Indeed, scaffold-based TE exploits cellular or acellular 3D supports to preserve the natural architecture of the tissue/organ of interest (Clarke *et al*, 2018). The acellular 3D supports are implanted at the damaged site to provide structural support for functional regrowth and promote in situ regeneration by releasing pro-regenerative agents (Clarke *et al*, 2018). Cellular 3D support allows cells to grow, proliferate, move, rebuild the scaffolds, and produce new ECM.
The latter approach is the most popular, where the functional characteristics of these constructs depend on the cell source and the scaffold material. The cell source can be either fully differentiated or stem cells, while the scaffold material can be synthetic (made of polymers) or biological (derived from decellularized ECM) (Clarke *et al*, 2018).
In the field TE applied to the endocrine pancreas, recreating the endocrine niche *ex vivo* by TE might be advantageous, as it could overcome the lack of a better model to study endocrine disorders like diabetes and, if possible, apply those constructs in the field of β cell replacement.

Subsequently, we will examine the 3 primary building blocks necessary to engineer the pancreatic niche and which methods to use.

3.4.2. Coexisting cells in the endocrine pancreatic niche

Islets, clusters of endocrine cells, are encapsulated by an ECM and fibroblasts. The endocrine cells are not randomly distributed but rather are grouped. The islets are supplied with nutrients by a dense network of highly fenestrated capillaries, which allows each endocrine cell to be in close contact with the blood (Veld & Smeets, 2015). The specific organization of the ECM, cells, and microvasculature constitutes the endocrine niche. Owing to the evaluation of the endocrine niche, it was possible to identify the fundamental features useful for bioengineering endocrine pancreatic tissues (Pignatelli *et al*, 2022).

The interactions between endocrine and vascular cells are essential for the correct development and function of the endocrine network (Lammert & Thorn, 2020).

Vascular cells, such as endothelial cells (EC) and pericytes, typically comprise the cellular portion of the *tunica intima* of blood vessels. The structural component is the basement membrane (BM), which contains a specific ECM. In the endocrine pancreatic niche, endothelial cells form a fenestrated endothelium, ensuring high permeability and facilitating the exchange of nutrients, hormones, oxygen, and metabolic waste (Olsson *et al*, 2011),(Burganova *et al*, 2021). ECs can enhance β cell function by increasing insulin secretion and promoting β cell survival through the secretion of soluble factors such as hepatocyte growth factor (HGF), vascular endothelial growth factor (VEGF)-A (Stucker *et al*, 2021), and ECM proteins (Cao & Wang, 2014).

<u>Cells Source:</u>

The function of engineered tissue heavily depends on the type and source of cells used to repopulate a biomaterial scaffold. The cells can range from fully differentiated primary adult cells to undifferentiated progenitor and stem cells (Katari *et al*, 2014). Endocrine cell lines, spheroids, and induced pluripotent stem cells (iPSC) organoids could be integrated into 3D scaffolds (Loskill & Wu, 2019). Still, pseudo islets and/or spheroids do not present the cytoarchitectural complexity of native islets, failing to recreate the physiological signaling network (Zhang *et al*, 2022).

Thus, for our study, we chose to use human islet cells, the closest match to the human endocrine pancreas.

To recreate the interface between the endocrine and vascular systems, the *tunica intima*'s cellular components, such as ECs and pericytes, must form a complex network of capillaries that integrate with the 3D endocrine mass.

Pericytes are key in regulating endocrine niche homeostasis and function (Burganova *et al*, 2021). Landsman et al. have conducted a series of experiments that demonstrate the role of these cells in the growth and development of β cells during the neonatal stage and in maintaining their maturation and function in adulthood (Epshtein *et al*, 2017),(Sakhneny *et al*, 2018). They achieve this by regulating the production and deposition of islet ECM components and promoting the expression of β cell genes such as Ins1, Mafa, and Glut2 (Sakhneny *et al*, 2021). Moreover, pericytes are directly involved in β cell function by activating the release of insulin granules through nerve growth factor (NGF) pathways in the presence of high glucose levels (Houtz *et al*, 2016).

To promote functional vascularization and engraftment of endocrine cells in a natural and biomimetic manner, mesenchymal stem cells (MSCs), ECs, and fibroblasts have been employed *ex vivo* and *in vivo* to modify endocrine cell cluster composition (Brissova *et al*, 2004).

To achieve this, the ideal source of endothelial cells should meet the following criteria: i) it should have a high proliferative capacity while retaining its phenotypic and functional features; ii) it should display sustained vasculogenic potential by forming hollow tubes with physiological-like permeability properties; iii) it should be easily obtainable from both patients and healthy individuals, enabling comparative studies (Pellegata *et al*, 2018).

Human umbilical vein endothelial cells (HUVECs) are the most used endothelial cell sources. They were the first ECs to be isolated and cultured *in vitro*, and they are among the most commonly used ECs for demonstrating proof-of-concept in both *ex vivo* and *in vivo* scaffold-based islet treatments (Campo *et al*, 2023).

HUVECs are fully committed, primally adult human ECs. Therefore, they do not have a high proliferative capacity for many cellular passages, are obtained from pooled individual sources, and, therefore, are unsuitable for personalized medicine (Jain *et al*, 2016).

ECs derived from human iPSCs are becoming increasingly appealing as alternative sources for autologous vascular cells. While several studies have shown their feasibility and potential for future clinical applications (Rufaihah *et al*, 2011),(Samuel *et al*, 2013) ,several challenges must be addressed before iPSC-ECs can be used in

clinical practice. These include concerns about their potential tumorigenicity, the long-term effects of genetic and epigenetic changes, and issues related to their immunogenicity (Wu & Hochedlinger, 2011) .

BOECs, blood-outgrowing endothelial cells, have recently been introduced as an alternative and interesting source of EC in the TE context.

The discovery of BOECs offers a promising opportunity for clinical applications, as this type of ECs can be collected non-invasively, which may lower the immunogenicity of a potential bioengineered device (Martin-Ramirez *et al*, 2012).

BOECs are cells that can be isolated and expanded easily and at a much lower cost than iPSC-ECs. This makes them a preferable option for use in a GMP scenario. BOECs can also be engineered efficiently with viral vectors (Olgasi *et al*, 2021), further supporting their potential for clinical use. These cells are considered a valuable source for vascular engineering, as they possess similar growth kinetics, migration potential, and phenotypical markers expression as other sources of endothelial cells. Additionally, they retain similar expression profiles of endothelial-specific markers (Mathur *et al*, 2021). All the sources of endothelial cells offer valid alternatives for *in vitro* vessel engineering. BOECs are particularly appealing as they can be harvested non-invasively from patients, which presents a great possibility for developing personalized study platforms (Marei *et al*, 2022),(Sackett *et al*, 2018).

Scaffolds' material:

Finding a biomaterial with the right structure and composition for cell seeding is crucial.

TE is a field that uses 3D porous scaffolds to create an ideal environment for tissue and organ regeneration. These scaffolds act as a template for tissue formation and are typically seeded with cells. They may also be exposed to physical or chemical stimuli through a bioreactor, a device or system that applies various mechanical or chemical forces to cells (Martin *et al*, 2004). These scaffolds are used to seed cells for *ex vivo* bioengineering and culture. They can be used for *in vivo* transplantation or as a pathology model.

A scaffold's design and suitability for tissue engineering requires careful consideration of multiple factors:

i) Biocompatibility is a criterion for evaluating a substance's compatibility and toxicity for an organism. Cell adherence, normal function, and migration onto the surface are considered biocompatibility, followed by proliferation and the establishment of a new matrix (O'Brien, 2011).

ii) Stiffness refers to a material's ability to withstand deformation when subjected to an external force. In mechanobiology, substrate stiffness is typically determined by calculating the material modulus (Kennedy *et al*, 2017). Based on a literature review on tissue engineering, substrate stiffness has recently been crucial in determining cell fate (Yi *et al*, 2022).

iii) Scaffold architecture is extremely important in TE. Scaffolds should have a porous structure that allows cells to penetrate and receive nutrients. The scaffold should also allow waste products to diffuse out of the structure. The average pore size of the scaffold is another critical factor. Cells interact with scaffolds through chemical groups on the surface. Natural materials like collagen have the required chemical groups, while synthetic materials may need protein adsorption. The number of groups present depends on the specific surface area, determined by the average pore size (O'Brien, 2011).

iv) Mechanical properties are characteristic of scaffolds and should be comparable to the native tissue to support the regeneration process correctly (Kim *et al*, 2000). Stiffness, plasticity, mechanical integrity, flexibility, and resistance to compression strength, make the construct durable, all characteristics the scaffold retains over time (O'Brien, 2011).

All scaffold qualities depend on the biomaterials, classified into synthetic and biological materials, giving rise to synthetic and biological scaffolds.

3.4.3. Synthetic biomaterial scaffold

Synthetic biomaterials are compounds not present in nature and originated from chemical synthesis that provides greater control over composition, bio adhesive ligand presentation, mechanical properties, and degradation, offering enhanced reproducibility and scalability (Enemchukwu *et al*, 2016),(Spicer, 2020). Synthetic biomaterials in organoid culture precisely control the microenvironment's chemical properties (Guvendiren & Burdick, 2013). Many synthetic biomaterials can be functionalized with cell adhesive peptides derived from the ECM. These peptides have diverse functions and can be precisely conjugated to biomaterials (Collier & Segura,

2011). Synthetic mimics that imitate the ECM often do not match the functionality of the original protein. They may not be able to achieve high-affinity receptor binding or expose hidden binding sites when subject to mechanical activation or proteolytic degradation (Barker, 2011). Despite that, these tunable synthetic biomaterials can be engineered with versatile modularity to target specific cell-cell and cell-ECM interactions, eliciting signal transduction cascades that direct morphogenesis, differentiation, and cell function (Enemchukwu *et al*, 2016).

Some examples of synthetic biomaterials are polyethylene glycol (PEG), polyglycolic acid (PGA), polylactic-co-glycolic acid (PLGA), and polydimethylsiloxane (PDMS).

PEG hydrogels are commonly used in regenerative medicine applications(Spicer, 2020) due to their versatility. They have a wide range of polymer architectures and molecular weights, are easy to modify, resist biofouling and nonspecific protein adsorption, and can be crosslinked using various platforms. Additionally, they can be functionalized with numerous biological ligands (Spicer, 2020).

PEG hydrogels have been essential in bioengineering the pancreas for identifying the key adhesive ligands necessary for β cell adhesion (Hunckler & García, 2020). These ligands promote survival, function, and differentiation. Moreover, entrapping full ECM proteins with the PEG matrix significantly increases insulin secretion, decreases apoptosis, and increases islet survival (Weber & Anseth, 2008). Additionally, PEG–based conformal coating for encapsulating transplanted islets shows promise as a β-cell replacement therapy for T1D. This method avoids the need for chronic immunosuppression by reducing capsule thickness, graft volume, and the delay in insulin secretion (Stock *et al*, 2022).

Polyester Biomaterials, such as PGA and PLGA, are commonly used for cell encapsulation and for their biodegradation and ability to incorporate other growth factors and ECM proteins (Spicer, 2020).

All the polymers mentioned can be manipulated and designed to create 3D-porous structures or hydrogels via freeze-drying, phase separation, gas foaming, photolithography, stereolithography, and 3D printing (Jenkins & Little, 2019). 3D scaffolds have a uniform, interconnected porous structure, allowing cell penetration during seeding, efficient nutrient diffusion, and waste product removal (O'Brien, 2011).

Hydrogel scaffolds are highly hydrated structures created by cross-linking reactions of polymers with a hydrophilic nature. They resemble the tissue's ECM and have a water content ranging from 90% to 99%. This high-water content allows for safely incorporating biological entities such as proteins and cells. Furthermore, synthetic scaffolds are structures that are constantly changing. The polymer network in the

scaffold reacts to increases in temperature, which in turn affects the microenvironment of the scaffold. This means that the mechanical properties of the scaffold may also change. This helps mimic the dynamic nature of the ECM and regulate cellular changes. Overall, this process alters cellular behavior to better imitate the natural dynamism of the ECM (Jenkins & Little, 2019).
To sum up, synthetic scaffolds have both benefits and drawbacks in TE.

3.4.4. Natural biomaterial scaffold

Biological scaffolds can be composed of naturally occurring materials that are components of ECM, such as collagen (Glowacki & Mizuno, 2008), laminin (Iorio *et al*, 2015), and chitosan, among others (Rodríguez-Vázquez *et al*, 2015), or the entire ECM itself.
ECM-based bioscaffolds serve as a microenvironmental niche surgically placed to guide and support cell growth. These bioscaffolds are more than just mechanical support devices; they influence cells' mitogenesis, chemotaxis, and differentiation fate. This is not typically seen in bioscaffolds made up of individual components of the ECM. Studies have shown that ECM bioscaffolds have a positive impact on the remodeling process of the scaffold.
Unlike synthetic scaffolds made of individual matrix molecules, biological scaffolds retain the complex mixture of structural and functional ECM molecules and the native three-dimensional ultrastructure (Costa *et al*, 2017).
Creating an ECM bioscaffold that perfectly preserves both composition and structure is an unattainable goal. Mammalian tissues are composed of cells and a complex array of ions and soluble signaling molecules, including growth factors, cytokines, chemokines, and structural proteins, all organized in a tissue-specific three-dimensional ultrastructure. This ultrastructure is optimally designed to maintain homeostasis, facilitate mechanotransduction, and respond to injury (Costa *et al*, 2017).
The composition and structure of the ECM differ across tissues, yet many functional and structural molecules are common to multiple types:

i) Collagen accounts for about 85% of the dry weight of the ECM, with over 20 different types, each serving specific functions. Type I collagen is the main structural protein, providing significant strength and load-bearing capacity. Types IV and VII collagen, along with laminin, are key

components of the basement membrane in blood vessels. The epidermis offers anchoring sites and cell barrier functions, ensuring that ECs and keratinocytes are firmly secured (Akiyama, 1996). In the endocrine niche, collagen types I and IV are the most prevalent, supporting the structure and function of β cells (Jiang *et al*, 2019).

ii) Fibronectin, the second most abundant protein in the ECM, is a dimeric molecule made up of 250,000 MW subunits, which feature binding domains for various other ECM proteins, including collagen. Its RGD (arginine-glycine-aspartate) domains enable fibronectin to play a vital role as a cell-adhesion molecule (Plow *et al*, 2000).

iii) Laminin is a type of glycoprotein found in the basement membrane. It is made up of three cross-linked protein chains. Laminin helps cells interact with other components of the ECM, such as heparin sulfate and collagen (Plow *et al*, 2000),(Battaglia *et al*, 1992). For instance, it is crucial for adequately functioning the dystrophin-glycoprotein complex, which plays a key role in skeletal muscle contraction (Gumerson & Michele, 2011).

iv) Glycosaminoglycans (GAGs) are complex carbohydrates with a negative charge that can bind and retain water and other water-soluble molecules, such as growth factors (Alberts, 2015). GAGs are also known for their exceptional mechanical loading capacity, which enables them to distribute forces within the tissue. An example of this is hyaline cartilage. Hyaluronic acid, a type of GAG, is frequently used to deliver cells and bioactive molecules therapeutically. It has also been studied for its potential as a scaffold for the regeneration of cartilage and bone, stroke repair in the central nervous system, and forming vessel networks, among other applications (Collins & Birkinshaw, 2013).

v) Growth factors (GFs) are molecules that activate cellular pathways that affect cell survival, proliferation, and differentiation (Costa *et al*, 2017). However, their identity and relative abundance vary depending on the tissue. These molecules are trapped in the matrix and only exert their function when released during the physiological turnover of the ECM.

vi) Matrix-bound Vesicles (MBVs) are embedded in ECM full of micro-RNAs, intended to protect the latter (Huleihel *et al*, 2016).

vii) Matrix-cryptic peptides are fragments produced by parent proteins within the ECM that possess biological activity. They are released into the microenvironment during ECM degradation, and their biological activity

depends on the degradation rate (Badylak *et al*, 2011),(Londono & Badylak, 2015),(Reing *et al*, 2009).

These molecules' presence, three-dimensional ultrastructural organization, and integrity significantly impact the clinical outcome when using ECM bio-scaffolds for tissue repair and reconstruction (Costa *et al*, 2017).

3.4.5. Decellularization methods of 3D ECM scaffold: Whole organ decellularization

Decellularized tissues are scaffolds in regenerative medical research to help cells proliferate, differentiate, and organize into properly functioning tissues. The ECM provides physiochemical cues that regulate cell phenotype and function and is a foundation for the desired organ's natural structure. The native ECM is the best option for tissue engineering and regenerative medicine because it retains the original tissue anatomical structure. Therefore, the primary goal of decellularization is to preserve the native protein niches and physiochemical properties of the ECM (Moffat *et al*, 2022).

Decellularized ECM has proven to be a successful scaffold for generating various tissues and organs (Baptista *et al*, 2011). Upon decellularization, ECM retains large macromolecules (i.e., polysaccharides and collagens), while smaller ECM-associated components (i.e., growth factors, chemokines) are lost. Thus, ECM ability to act as a tissue-specific platform for recellularization might be hindered, impacting the final reconstituted tissue microenvironment (Emami *et al*, 2021).

To create an effective decellularization scaffold, it is important to ensure that the ECM produced should not contain: i) more than 50 ng of DNA / dry weight; ii) residual DNA fragments < 200 base pairs; iii) visible nuclei (Crapo *et al*, 2011). There are two main processes for decellularization: minced tissue and whole organ decellularization, used to generate ECM scaffolds for regenerative medicine. Possible applications of minced or sectioned decell-tissues include substrates for cell culture or injectable hydrogels to enhance cell proliferation, differentiation, and promote engraftment (Bi *et al*, 2020), or as a bio-ink in 3D bioprinting (Kort-Mascort *et al*, 2021).

Animal organs that have been decellularized retain their original 3D structure and vascular network, making them useful for repopulating with human cells for organ regeneration (Khan *et al*, 2014).

Decellularization can be achieved through chemical, physical, or a combination of both methods. This process aims to remove cells and genetic material while preserving the structural proteins. The effectiveness of these methods will be assessed by comparing the mechanical properties and ultrastructure of the tissue or organ both before and after treatment (Gilpin & Yang, 2017).

A range of chemicals, including acids, bases, and surfactants, have been employed in the decellularization process. Surfactants are the most frequently used agents for this purpose, as they disrupt the cell membrane by rearranging phospholipids (Nazari *et al*, 2012). Sodium dodecyl sulfate (SDS) is a widely used ionic surfactant that effectively removes cells and genetic material in various decellularization processes. For instance, SDS was the primary agent employed to decellularize the rat heart through perfusion (Ott *et al*, 2008). Perfusing entire organs with SDS is a technique that helps preserve the organ's ultrastructure. The constant flow of the solution through the blood vessels helps preserve their structure and prevents the deformation of the alveoli (Gilpin *et al*, 2014). This factor is essential for providing nutrients to the seeded cells (Orlando *et al*, 2011) and ultimately for restoring the organ's original function. However, it's important to highlight that SDS is cytotoxic. As a result, the tissue must be thoroughly rinsed to ensure the viability of the reseeded cells (Syed *et al*, 2014).

Nonionic surfactant Triton X-100 is often used to eliminate any remaining SDS during the perfusion decellularization of whole organs. This method has been widely prevalent and effective in various studies (Ott *et al*, 2008),(Gilpin *et al*, 2014),(Syed *et al*, 2014). Triton X-100 is a gentler decellularizing agent frequently used on its own. Its nonionic characteristics make it less harmful to the tissue's structural integrity than SDS. When used with ammonium hydroxide, it effectively removes all DNA while preserving more collagen I compared to treatments with SDS (Sullivan *et al*, 2012). The ultrastructure and mechanical properties of the decellularized tissue remain well preserved after this process (Mendoza-Novelo *et al*, 2011).

Sodium deoxycholate (SD), another ionic surfactant, disrupts the cell membrane and forms highly biocompatible scaffolds. Cells placed on SD-decellularized matrices show higher metabolic activity than those on matrices decellularized with SDS (Syed *et al*, 2014). Studies have shown that SD and agitation treatments can completely remove cells from different tissues (Gilpin *et al*, 2014),(Zhou *et al*, 2010). However, SD treatment can cause DNA to agglutinate on the tissue's surface (Meezan *et al*, 1975), even though it is not damaging. To address this problem, a 4% SD solution was combined with DNase I enzyme to break down the native DNA found in the tissue. This method was used for various structures like blood vessels (Meezan *et al*, 1975),

tracheas (Partington *et al*, 2013), diaphragm (Piccoli *et al*, 2016), aortic root (Friedrich *et al*, 2014), and small intestines (Syed *et al*, 2014). Nevertheless, it was noted that a considerable amount of DNA persists in the extracellular matrix after treatment, despite DNase I's role in breaking down DNA fragments (Syed *et al*, 2014),(Friedrich *et al*, 2014). Therefore, more extensive washing processes are required to eliminate DNA in the tissue to prevent immune rejection.

Enzymes like DNase I have been incorporated into decellularization protocols to enhance the effects of specific chemicals. For instance, DNase was combined with Triton X-100 and SD to decellularize some organs of humans (Wagner *et al*, 2014) and porcine (Rieder *et al*, 2004). This process effectively degraded leftover DNA fragments, minimizing potential immune responses in vivo. For instance, in lung treatment, a combination of perfusion and immersion was used, which helped preserve collagen types I and IV, along with fibronectin and laminin. However, the content of glycosaminoglycans (GAGs) was significantly reduced after treatment, while important smooth muscle proteins such as myosin and actin were retained. Although elastin levels decreased the overall lung's ultrastructure remained intact. A three-day washing cycle was carried out to achieve complete decellularization of the final organ product. The decellularized extracellular matrix was subjected to enzymatic digestion with DNase and RNase (Rieder *et al*, 2004), which eliminated cellular debris while preserving collagen and elastin.

Another multistep protocol was employed to decellularize specific organs, utilizing trypsin/ethylenediaminetetraacetic acid (EDTA), SDS, Triton X-100, peracetic acid/ethanol, and DNase (Zhang *et al*, 2016). The goal was to remove cells and DNA while retaining laminin, collagen type IV, and fibronectin. The ultrastructure and vasculature of the organs remained intact after treatment (Zhang *et al*, 2016). Although chemical methods can be enhanced by integrating enzymatic treatments, the success of the process relies on preserving the essential characteristics of the ECM that are crucial for regenerating the tissue's desired function (Gilpin & Yang, 2017).

Chemical and enzymatic treatments are the most commonly used methods, but they have limitations, including potential toxicity from the chemicals and damage to ECM proteins. To address these challenges, physical and mechanical methods are being developed. These approaches use temperature and pressure treatments to lyse cells and break down cell-matrix adhesive proteins. Examples of physical methods include freeze-thaw cycles, high hydrostatic pressure, and supercritical CO2 treatments (Gilpin & Yang, 2017). Regardless of the method, a washing step is always necessary to remove any remaining cellular debris and ensure the protocol's effectiveness.

Creating a three-dimensional, whole-organ ECM scaffold from a mammalian organ involves several steps that can significantly influence the structure and composition of the final product, as well as the host's response when it is used for organ reconstruction. During the decellularization process, the organ's cells are usually exposed to detergents, proteases, and chemicals via perfusion through the native vasculature, all while aiming to preserve the natural structure and composition of the matrix. It is essential to remove antigenic epitopes linked to cell membranes and intracellular components to reduce the risk of an adverse immune response in allogeneic or xenogeneic recipients of the ECM scaffold (Badylak *et al*, 2011).

Harald C. Ott led one of the initial teams that designed and successfully implemented a whole organ decellularization protocol. In 2008, Ott, et al. achieved the first entire heart scaffold with intact 3D geometry and vasculature from the hearts of cadavers (Ott *et al*, 2008). They began by comparing the effectiveness of several decellularization agents administered by antegrade coronary perfusion. They found that the optimal decellularization agent was 1% SDS detergent perfusion for 12 hours, which achieved sufficient decellularization without compromising the scaffold's vasculature and ultrastructure. They also included a washing step with TRITON X-100 to facilitate the removal of any residual SDS within the organ. This methodology was then successfully applied by Ott's team to lungs (Ott *et al*, 2010)and kidneys (Song *et al*, 2013), leading to the development of a standard process for pressure-controlled perfusion decellularization of entire organs. This process generated acellular 3D scaffolds with preserved ECM content, architecture, and vasculature. By modifying the protocol, researchers could achieve perfusion decellularization of small-animal experimental organs to use the scaffold as a study pathology model. The protocol must be tailored based on the target organ. It is worth noting that Peloso et al. were the first group to apply a decellularization protocol to a human pancreas in 2016, resulting in a human pancreata ECM scaffold (Peloso *et al*, 2016).

The bioengineering protocols used to obtain an endocrine pancreatic niche will be addressed in a specific chapter later.

3.4.6. TE applications to model endocrine dysfunction.

As previously mentioned, there is an urgent need to develop a better model for creating an endocrine pancreatic niche that can be used for targeted interventions (i.e. a screening tool for pharmacological compounds or as an immunological study

platform). It is crucial to be able to study endocrine disorders directly during the etiopathogenesis phase, specifically in the affected tissue.

Preclinical models have previously relied on basic *in vitro* assays and small animal *in vivo* models due to their simplicity, scalability, and efficiency. However, these models often fail to accurately mimic real-world scenarios. Additionally, the human cell lines used in *in vitro* models frequently exhibit abnormal genetic, epigenetic, and cellular phenotypes, further limiting their usefulness (Lorsch *et al*, 2014). New tools and advances at the intersection of biology and engineering provide a unique chance to produce and configure human cells and tissues. This can help increase the relevance of preclinical models to native human tissues and organs (Khalil *et al*, 2020).

It is possible to create an organ using tissue TE for transplantation purposes and to enable studies related to pathophysiology and pharmacology. As mentioned earlier, the essential components for building the endocrine pancreas are the islet niche ECM, vascular network, and endocrine cells (Citro & Ott, 2018).

The endocrine pancreas is divided into separate, vascularized areas where the islets are located within the ECM. These niches are essential for the survival of the islets, as they receive necessary oxygen and nutrients through their vascular distribution. Therefore, to successfully re-engineer the endocrine pancreas, it is crucial to consider these elements' preservation and proper functioning (Citro & Ott, 2018).

In the paragraph below, I will outline the most promising approaches for recreating the endocrine islets niche and their respective advantages and challenges.

Organ on chip

Microfluidic simulations of *in vivo* conditions have enabled the creation of organs-on-a-chip, which are micro-scale systems that mimic the human body. These systems serve both drug testing and disease modeling purposes, with the ethical goal of gradually replacing animal models. The development of organs-on-a-chip combines advanced expertise in cell co-cultures, stem cells, genome editing, sensors, 3D printing, and microfluidics. These chips replicate the functions of tissues and organs by integrating various tissues into 3D systems where biological and physical forces are applied to simulate in vivo conditions (Saorin *et al*, 2023). Organs-on-a-chip require specific conditions that can be met by microfluidics technology, which can improve the oxygen supply to the cells. Additionally, microfluidics can generate solute gradients that can be utilized for controlling the differentiation of stem cells into organoids (organoids-on-chip) or studying the absorption of a specific molecule by an organ simulated by an organ-on-a-chip (Saorin *et al*, 2023).

Organoids-on-chip can be derived from adult pancreatic tissues and utilized for drug development, regeneration, and disease modeling (Balak *et al*, 2019).

In a study, researchers designed a four-layered chip featuring microfluidic technology to create a biomimetic environment that facilitated the in situ differentiation of human pluripotent stem cells into islet organoids (Tao *et al*, 2019). The chip comprises two layers, one at the bottom and one at the top, made of PDMS material and enclosing a through-hole. The through-hole features polycarbonate membranes that allow for the perfusion of the organoids with a continuous flow, supplying nutrients and applying uniform fluid stress. This system enhances the generation and viability of perfused islet organoids, as well as their islet-specific functions. The organoids secrete insulin in response to glucose stimulation and generate a Ca^{2+} flux, resulting in the production of functional islet organoids from human iPSCs (Tao *et al*, 2019).

Taking into account the vascularization of different biological 3D tissues in an organ-on-chip model is crucial. Recent studies have shown a platform that can monitor the development of endothelial networks around mesenchymal and pancreatic islet spheroids, as well as blood vessel organoids derived from pluripotent stem cells. These structures can be cultured on-chip for up to 30 days. The research indicated that these networks successfully form functional connections with the endothelium-rich spheroids and vascular organoids, enabling intravascular perfusion to these structures. Additionally, the researchers reported enhanced functionality of pancreatic islet spheroids when using this platform. The research suggests that organoid growth, maturation, and function can be improved when cultured on-chip using their vascularization method (Quintard *et al*, 2024).

In the context of pancreatic organoids-on-a-chip, reported in the literature, it investigates organ development, diseases, and the effects of approved and experimental drugs (Balak *et al*, 2019). Researchers are developing organoids from different cell types to precisely model human physiology, often produced directly on chips and grown in coculture with other tissues or immune system cells (Quintard *et al*, 2024). Nevertheless, currently, no *ex vivo* platforms can model the entire immune-mediated. Still, the level of complexity required to reproduce such interactions is quite high and hardly reproducible on a chip. Indeed, one of the disadvantages of the organ-on-chip is that the cells are seeded in specific compartments and separated at different levels. It’s important to guarantee the interaction between all compartments, for example, the cell-to-cell interaction.

In this context, 3D bio-printing technologies can deposit different cell types spatially in a 3D space. This enables the encapsulation of various cellular components within different hydrogel preparations (Espona-Noguera *et al*, 2019).

3D Bioprinting

3D bio-printing technology has the potential to create tailored bioengineering devices for β cell replacement, offering several opportunities such as simultaneous 3D spatial deposition of different cell types, encapsulation of cellular components within different hydrogel formulations, and customization of the scaffold architecture based on the requested function (Gurlin *et al*, 2021),(Espona-Noguera *et al*, 2019),(Ghasemi *et al*, 2021).

Different types of bioprinters are available, including inkjet, extrusion-based, and light-based printers. Inkjet bioprinters use piezoelectric or thermal-driven mechanisms to deposit a small amount of polymeric solution (Hölzl *et al*, 2016). Still, they are not commonly used due to low cell density and weak mechanical properties. On the other hand, extrusion-based bioprinters use one or more nozzles to distribute the polymeric solution, or bioinks, through pneumatic systems (Hölzl *et al*, 2016),(Kirchmajer *et al*, 2015). These printers are widely used to distribute an appropriate cell density in three-dimensional space, providing optimal structural integrity. The bioinks used in extrusion-based printers can have a wider range of viscosities and be loaded with bioactive compounds, different cell types, cell aggregates, organoids, and tissue fragments (Bowers *et al*, 2019),(Hölzl *et al*, 2016),(Sarker *et al*, 2018). However, extrusion-based printers have a low printing speed and spatial resolution, and the pressure used during printing can affect cell viability (Espona-Noguera *et al*, 2019). Light-based printers, such as stereolithography, use lasers to induce polymerization and deposition with high-resolution photo-cross-linkable polymers. This type of printer has a limited range of bioinks and can expose cells to heat during polymerization (Gurlin *et al*, 2021),(Kang *et al*, 2014). Overall, extrusion-based 3D printers are widely used due to their flexibility, good biocompatibility, and minimal risk of damage to cellular components. Current research in 3D-bioprinting for β cell replacement focuses on recreating endocrine pancreatic tissue's insulin-producing and vasculature components. While the aim is not to recreate the entire pancreas, researchers are exploring using bio-mimicking scaffolds made of ECM-based materials. One study showed improved islet viability *in vitro* using 3D-bioprinted alginate/gelatin bioink to encapsulate HIs (Marchioli *et al*, 2015). However, the hydrogel's high viscosity and reduced porosity

hindered glucose and insulin diffusion, which affected insulin secretion analysis (Marchioli *et al*, 2015). Another study used a porous ring scaffold of PCL to favor vessel formation. The scaffold was modified with VEGF-binding heparin with a high degree of functionalization, while the hollows of the ring were filled with human islet-encapsulating alginate solution. The specific porous structure of the scaffold provided a high surface-to-volume ratio, and the slow release of VEGF augmented the vascularization capability of the system *in vivo* (Marchioli *et al*, 2016). However, the efficacy of the technology in sustaining endocrine function *in vivo* was not demonstrated in this study.

Previous studies were limited in their ability to investigate and reconstruct the endocrine compartment and vasculature without considering the functional and structural integration in physiological conditions. To address this issue, another report used coaxial extruders to fabricate 3D-bioprinted alginate/methacrylate-gelatin (GelMA) strands with a core-shell structure. These strands encapsulated EC and murine islets in the shell and core, respectively, resulting in a uniform distribution of both cellular components in the bioengineered compartments (Akkouch *et al*, 2015),(Liu *et al*, 2019).

Studies have shown that while a certain system supported the viability of islets, its small pore size made it difficult to analyze insulin secretion (Liu *et al*, 2019). Therefore, recent research has focused on developing bioinks for 3D bioprinting using decellularized extracellular matrix (dECM) due to its ability to sustain endocrine pancreatic components. Porcine native pancreatic ECM (pdECM) was used as a source of bioink and was embedded with insulin-producing cells and HUVEC for 3D bioprinting. The study successfully induced optimal insulin secretion efficiency while supporting the viability and function of β cells and the pro-vascularizing ability of HUVEC *in vivo*. This validated the efficacy of pdECM as a source of bioink and demonstrated the possibility of replicating tissue-specific conditions in 3D constructs (Kim *et al*, 2019). Another study developed alginate/pdECM and alginate/fibrin bioinks and encapsulated porcine islets, HUVEC, and MSCs. The study found that alginate/pdECM hydrogel composition sustained the viability and insulin secretion activity of porcine islets. In contrast, alginate/fibrin hydrogel supported the viability of HUVECs, inducing them to acquire sprouting morphology. Scaffolds with three different configurations were successfully fabricated, indicating that the complexity of the 3D-printed scaffold could be easily increased (Idaszek *et al*, 2021).

It's important to note that despite the advantages of controlling cell placement accurately, the way cells organize themselves naturally changes over time. Therefore, understanding the underlying physiological processes is necessary to

create effective bio-mimicking structures that promote graft survival, integration, and function. Studies using decellularized organs have shown that pre-vascularizing scaffolds can improve insulin-producing cell viability and facilitate rapid *in vivo* revascularization and engraftment. To replace β cells, 3D-bioprinted constructs should follow this strategy by creating channel or tubular architectures (Pignatelli *et al*, 2022). Various bio-fabrication protocols have proposed different approaches to achieve this, such as using coaxial nozzles to create hollow tubular strands, introducing sacrificial polymers like Pluronic or gelatin in extrusion-based bioprinting, which can be removed by changing the temperature, pH, or through enzymatic degradation, leaving hollow structures; and producing light-based printed structures that can be embedded in the 3D printed scaffolds, making them perfusable (Gurlin *et al*, 2021),(Bowers *et al*, 2019),(Miri *et al*, 2019),(Datta *et al*, 2017),(Grigoryan *et al*, 2019). It is possible to recreate a functional vasculature *in vitro* by re-endothelializing different structures using a medium flow connected to a perfusable system. This allows for a dynamic culture promoting cell infiltration and revascularization *in vivo* (Gurlin *et al*, 2021). However, creating such complex systems for β cell replacement is challenging due to technological and biological limitations. The 3D-bioprinting field needs to overcome these limitations to fabricate systems that can recreate the physiological mechanisms of insulin-producing cells, which are highly sensitive.

Developing a bioengineered artificial endocrine pancreas is an interesting solution in the field of β cell replacement. However, using a bioengineered decellularized whole organ to recreate the endocrine pancreatic niche is a concrete and clinically strategic solution for treating T1D.

Whole organ re-cellularization for engineering an endocrine pancreatic niche: bioreactor design and seeding strategies.

The ECM scaffold serves as the foundational structure for the biofabrication of an entire organ. Recellularization is the process of repopulating acellular ECM scaffolds with organ-specific cell types or stem cells, intending to restore the organ's microanatomy and recreate its specific functions (Hillebrandt *et al*, 2019) . Therefore, successful recellularization entails using physiologically relevant culture methods, an optimal seeding procedure, and the appropriate cell type and source to regenerate the intended organ. These factors pose significant challenges that must be overcome to achieve successful recellularization.

Decellularized organs such as lungs (Abualhassan *et al*, 2016),(Citro *et al*, 2019a), kidneys (Willenberg *et al*, 2015), spleens (Vishwakarma *et al*, 2018), livers (Fathi *et al*, 2021),(Zhou *et al*, 2016), and pancreas (Huang *et al*, 2019),(Peloso *et al*, 2016),(Guruswamy Damodaran & Vermette, 2018) have been re-cellularized using the existing architecture of the native organs to recreate their complex endocrine microenvironment (Tapias & Ott, 2014),(Badylak *et al*, 2011). The decellularization process does not alter the physical and chemical properties of the native organ, and the scaffolds preserve the native ECM composition (Peloso *et al*, 2016). However, depending on the decellularization protocol, it may cause glycosaminoglycan loss (Goh *et al*, 2013). Seeding insulin-secreting cells within these scaffolds, regardless of the organ source, has improved insulin expression and efficacy in response to high-glucose stimuli *in vitro* (Peloso *et al*, 2016).

Using a native scaffold has allowed researchers to reconstruct the vasculature side of the endocrine pancreas by exploiting pre-existing vessel structures within the decellularized organs. However, only few studies have reported successful reconstruction of the endothelial barrier *in vitro* and obtaining an *ex vivo* vascularized organ (like lung (Citro *et al*, 2019a) and pancreas (Peloso *et al*, 2016)) by seeding HUVEC within the native decellularized organ vasculature structure (Citro *et al*, 2019a),(Peloso *et al*, 2016).

Interestingly, bioengineered devices have been found to support the reconstitution of vasculature and improve the efficiency and viability of insulin-producing cells compared to those grown in standard conditions. This suggests the potential for successful *ex vivo* engraftment of endocrine cellular components (Citro *et al*, 2019a),(Peloso *et al*, 2016). However, it can be challenging to regenerate organs *in vitro* that accurately mimic the physiological conditions present *in vivo*, such as a constant supply of nutrients, biophysical stimuli, oxygen, correct temperature, flow rate, and shear stress (Badylak *et al*, 2011). Bioreactors can support cell survival and function for an extended period, which is useful in promoting the engineered construct's engraftment and *in vitro* maturation (Bijonowski *et al*, 2013). The apparatus is designed as an in-line circuit (Fig.7), composed of an organ chamber where the engineered construct is located, a reservoir for culture medium storage, a perfusion peristaltic pump that can mimic the physiological peristalsis of the heart, a gas debubbler to eliminate bubbles that can disrupt flow rate and cells seeded in the construct, a gas exchanger able to oxygenate the media, and at least one inlet and one outlet (Bijonowski *et al*, 2013),(Scarritt *et al*, 2015). Sensors can also be present to monitor culture features and adjust them in real-time. Each bioreactor apparatus

can be customized with specific components and tailored to the target organ, allowing for a wide range of possible applications (Murphy & Atala, 2013).

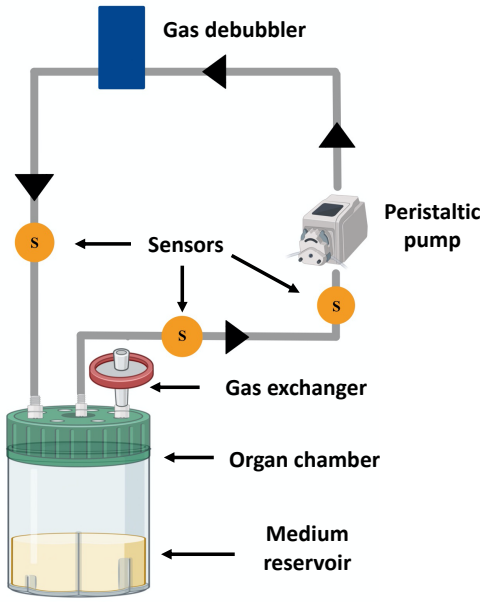


Figure 7: Bioreactor design.

Our group utilized a decellularized left lobe of a rat lung to create a vascularized islet organ (VIO). HUVECs were introduced through the pulmonary artery and vein, successfully recreating the native lung's vasculature. Rodent islets and more HUVECs were co-seeded through the trachea, allowing them to reach the native decellularized alveolar structure where they were retained. This location provides metabolic support to the rodent islets because of the dense capillary network surrounding the already vascularized alveoli (Citro *et al*, 2019a). The importance of restoring vascularization *in vitro* was observed when the VIO platform was implanted in an immunocompromised diabetic murine model. Almost 80% of recipient mice showed its function just 5 days after subcutaneous implantation. This demonstrated the need for a rapid vascular connection *in vivo*, which shortens the hypoxic phase and limits the loss of insulin-producing cells (Citro *et al*, 2019a). The results displayed the significant impact of the ECM shaped native-like architecture in optimizing pre-vascularization and engraftment ex vivo, leading to the acceleration of anastomosis and endocrine function *in vivo* (Pignatelli *et al*, 2022). Following the same idea, a new version of the platform was proposed with the integration of immature neonatal porcine islets (NPIs) and BOECs, which are healthy subject-derived endothelial cells. The platform facilitates *in vitro* NPIs maturation and *in vivo* primary function after transplantation for over 18 weeks (Citro *et al*, 2019a).

The tailored composition and microarchitecture of the decellularized organ created a coupled effect that functionally and structurally intertwined the endocrine pancreatic and vascularizing components (Pignatelli *et al*, 2022). The promising results obtained from whole decellularized organs with their specific features have highlighted their potential to efficiently transplant endocrine cells by recreating the native endocrine pancreatic niche. Moreover, the flexibility of these systems could allow for their integration with alternative sources to HIs and local immune-protection strategies to create an immune-privileged endocrine site. These important advances suggest that bioengineered endocrine pancreas based on whole organ decellularized scaffolds have the potential for clinical translation.

Our concept for engineering the pancreatic niche involves utilizing the established VIO platform. We aim to create a vascular compartment using BOECs and an endocrine compartment using HIs modified with an engineered ECM. By doing so, the VIO platform can be transformed into a platform that enables the exploration of physiological and immunological mechanisms beyond poorly understood endocrine dysfunctions.

3.5. A UNIQUE FLEXIBLE MODEL THAT CAN BE USED FOR DIFFERENT PURPOSES

3.5.1. A novel system to restore the normoglycemia in vivo T1D model

Exogenous insulin administration is the gold standard treatment for controlling blood glucose levels. This treatment mimics the action of human insulin produced by β cells, maintaining a basal level of the hormone and creating peaks during mealtimes. The standard of care involves administering regular insulin before each meal and basal insulin at bedtime (Mathieu *et al*, 2017).

Nevertheless, the disadvantages of exogenous insulin are:

1. Insulin is administered peripherally, while natural release targets the liver first, affecting blood glucose levels and β cell secretion.
2. There are no feedback mechanisms to suppress insulin release, increasing the risk of hypoglycemia (Mathieu *et al*, 2017).

Insulin therapy, while life-saving, does not fully restore the body's natural regulation of blood glucose. It is unable to prevent severe hypoglycemia or long-term complications. As a result, the life expectancy of patients relying on insulin therapy is still shorter than that of the general population (Pellegrini *et al*, 2016).

For this reason, a potential treatment for severe T1D patients involves replacing the damaged β cell mass through transplantation. These transplanted cells can sense blood glucose levels and secrete appropriate amounts of insulin in response to glucose levels.

There are 2 different strategies for transplantation: pancreas transplantation and pancreatic islet transplantation.

The pancreas transplantation procedure improves glycemic control for patients with T1D without the risks associated with insulin injections (Robertson, 1999). However, this procedure has limitations, such as the shortage of organ donors, the requirement for ongoing immunosuppression to prevent rejection, and its surgical invasiveness. As a result, pancreatic islet transplantation stands out as an appealing alternative from a surgical perspective.

Pancreatic islet transplantation involves injecting endocrine cells into the recipient's portal vein using a catheter, which requires only a minimally invasive surgical procedure.

The first attempt at isolating and transplanting islets was performed in 1972 by Ballinger and Lacy in chemically induced diabetic rats (Ballinger & Lacy, 1972). This was followed by Kemp et al. establishing the liver as the most suitable site for islet transplantation (Kemp *et al*, 1973). A significant development for clinical islet transplantation was introducing the "automated method" of dissociation and isolation of pancreatic islets, developed by Ricordi et al (Ricordi *et al*, 1988). This method is based on a dissociation/filtration chamber, which allows pancreatic fragments and islets freed from the gland to be promptly removed from the system to avoid over-digestion while preserving cluster integrity (Piemonti & Pileggi, 2013).

Following this, efforts were made regarding human islet isolation and the development of new immunosuppressant strategies. These efforts resulted in a breakthrough protocol published in 2000, the Edmonton protocol. Shapiro et al. achieved 100% insulin independence after 1 year of transplant in seven patients with T1D treated with a steroid-free immunosuppression protocol and receiving islets from multiple donors (Shapiro *et al*, 2000).

However, pancreatic islet transplantation has different limitations:

shortage of pancreas for clinical use, ii) need for immunosuppressive strategies, iii) host instant blood-mediated reaction (IBMIR), iv) multiple donor pancreases needed for each patient, v) islet isolation challenges and vi) islets vulnerable to stress and decreased oxygenation (Atkinson & Eisenbarth, 2001),(Citro & Ott, 2018),(Frisch & Screaton, 2001).

Overall, these events lead to a loss of 50-75% of the islets (Citro *et al*, 2019a) and result in low engraftment, often requiring additional transplantation to maintain the results, which makes the treatment very resource-intensive (Peloso *et al*, 2018).
In this situation, whole organ engineering becomes increasingly essential for β cell replacement. Specifically, whole pancreas engineering could provide a feasible solution to support immediate vascularization and islet cell engraftment, eliminating the avascular phase and improving endocrine function after transplantation.
As mentioned before, in 2019, Citro et al. proposed a new approach in our lab. They suggested repurposing a whole lung scaffold to address the significant loss of islets after transplantation, caused by poor engraftment and vascular supply. An ideal scaffold for creating a bio-artificial pancreas should include an islet compartment that promotes islet engraftment and a vascular compartment that provides blood supply through its vessel network to the islets. Additionally, the vascular compartment should be able to integrate with the islet's capillary network.
This platform represents a flexible system in which different types of cells, such as neonatal pig islets, can be seeded to overcome the shortage of organ donors for transplantation.

3.5.2. A platform for inflammatory or T cell-mediated β cell damage

Our system can better study endocrine disorders during etiopathogenesis, specifically in the involved tissue's microenvironment.
Our endocrine-like pancreatic organ may serve as a platform for studying T cell-mediated or inflammatory damage of β cells that may occur after transplantation on in T1D onset.
When T1D first appears, the immune system's inflammatory response targets the pancreatic islets, a significant aspect of the disease's pathology (Coppieters *et al*, 2012). As a result, managing this inflammatory response is a crucial strategy that could potentially impact the progression of the disease. However, this approach is still relatively unexplored (Nepom *et al*, 2013).
Chemokines are a group of small cytokines that can attract other cells towards them. They have a wide range of effects on different physiological and pathological processes. These effects include immune surveillance, inflammation, viral infection, and cancer. One possible explanation for how leukocytes enter mouse, and human pancreatic islets is that β cells release chemokines that attract leukocytes to the area (Citro *et al*, 2015b).

For example, B-cells release CCL2 to attract monocytes and macrophages to pancreatic islets (Kriegel *et al*, 2012) , while insulin-producing cells secrete CXCL10 to encourage T-cell infiltration (Roep *et al*, 2010).

My lab's previous work demonstrated that pancreatic islets in culture release abundant CXCR1/2 ligands (CXCL1 and CXCL8). Pancreatic islets produce and release chemokine ligands CXCL8, CXCL1, and CXCL2 in response to pro-inflammatory cytokines. These ligands bind to CXCR1/2 receptors, which are elevated in the blood of both rodents and humans with autoimmune diabetes. Furthermore, some studies suggest that neutrophils, the primary target of CXCR1/2 inhibitors, play a crucial role in the development of T1D (Citro *et al*, 2012).

We will evaluate the effects of the CXCL8-CXCR1/2 pathway on islets and endothelial cell functions by infusing CXCL8 into the system to induce inflammation.

A recent study proposed a new method to assess the interactions of immune cells and the resulting destruction of pancreatic β cells, which is a key factor in developing type 1 diabetes. The approach involves using vascularized micro-organs (VMOs) that contain isolated HIs, endothelial colony-forming endothelial cells, and commercial stromal cells within a three-dimensional hydrogel matrix supplied with living, perfusable blood vessels. However, the study found that the islets only responded to glucose for one week in the platform, and the model cannot be used to evaluate the effect of T cell-mediated islet damage in an autologous model. Therefore, further studies using this model to investigate T1D must rely on human leukocyte antigen matching or alternative tissue sources to derive an autologous model (Bender *et al*, 2024).

Our platform has enabled the creation of an *ex vivo* model that simulates leukocyte trafficking through the scaffold's vascular architecture, using PBMCs isolated from the same subject as the BOECs. This model is capable of studying T cell responses to xenogeneic neonatal porcine islets.

4. AIM OF THE WORK

As of now, the available platforms for studying pancreatic endocrine (dys)function *in vitro* and validating their potential *in vivo* are based on isolated pancreatic islets removed from their natural environment. This method has limitations because the lack of a supportive ECM and proper vascular plexus negatively impacts both islet viability and endocrine functionality. There is an urgent need to develop a flexible platform with a dual potential (*in vitro* and *in vivo*) that integrates the endocrine cell mass, vasculature, and ECM as a single entity. We hypothesized that the microarchitecture of the whole decellularized rat lung would provide a strategic architecture to bioengineer the endocrine niche *ex vivo*. Specifically, we aimed to seed pancreatic islets in the alveolar space and re-vascularize the original vascular plexus. In this study, we built upon the established VIO platform and bioengineered an extracorporeal vascularized islet organ using human pancreatic islets and BOECs (namely hVIO) for *in vitro* platform evaluation and vascularized endocrine pancreas (namely VEP) using NPIs and BOEC for *in vivo* application. Different endocrine sources are utilized due to the reduced availability of human islets and to assess the plasticity of the engineered platform. For the *in vitro* study: we evaluated the predictive potential of this platform in pathophysiological studies. Our first milestone was verifying that the rat lung's ECM preserved the viability and functionality of human islet and BOEC in long-term culture, restoring endocrine and vascular function. Secondly, considering the potential involvement of the IL-8-CXCR1/2 inflammatory pathway in T1D pathophysiology, we used the hVIO to dissect the effect of this pathway on the endocrine function.

For the *in vivo* study: we used VEP to evaluate its potential in the preclinical model of islet transplantation as a potential platform for future clinical application.

Additionally, as a link to the *in vitro* and *in vivo* project, we decided to preliminarily evaluate whether the VEP platform, in *ex vivo* fashion, may represent a good model to assess the xenogenic reaction by perifusion-activated leucocytes against the endocrine niche before moving the technology to an *in vivo* humanized mouse model.

5. RESULTS

5.1. EXTRACORPOREAL HUMAN VIOS (hVIOs and VEPs) GENERATION AND PROTOCOL OF CULTURE

To bioengineer hVIO, we first repopulated acellular lung matrices by seeding BOECs from the pulmonary artery (PA) and pulmonary vein (PV). The following day, we repopulated the airspace with a combination of BOECs and HIs through the trachea (T) (Fig. 8A). The culture protocol for hVIOs consists of two consecutive phases: the maturation phase (MP—day 0 to day 7) and the testing phase (TP—day 7 to day 14), which include the first 7 and last 7 days of culture, respectively (see Figure 8A). The re-cellularized scaffold was dynamically cultured in our custom bioreactor for up to 14 days, with 12 days in the Angiogenic Medium (AM) (Citro *et al*, 2019a) and 2 days in the modified stabilization medium (MSM) (Citro *et al*, 2019a).

Based on our previous work, we hypothesized that the endocrine and vascular compartments would integrate and functionally mature after 7 days. The remaining 7 days would be used to test the platform's stability and conduct inflammatory studies.

The same culture protocol was used to bioengineer VEP, but 4000 clusters of NPIs were used as an endocrine source. The culture protocol ended after 7 days, obtaining the mature VEP. We cultured the resulting constructs for 4 days in AM and 2 days in MSM (Fig. 8B).

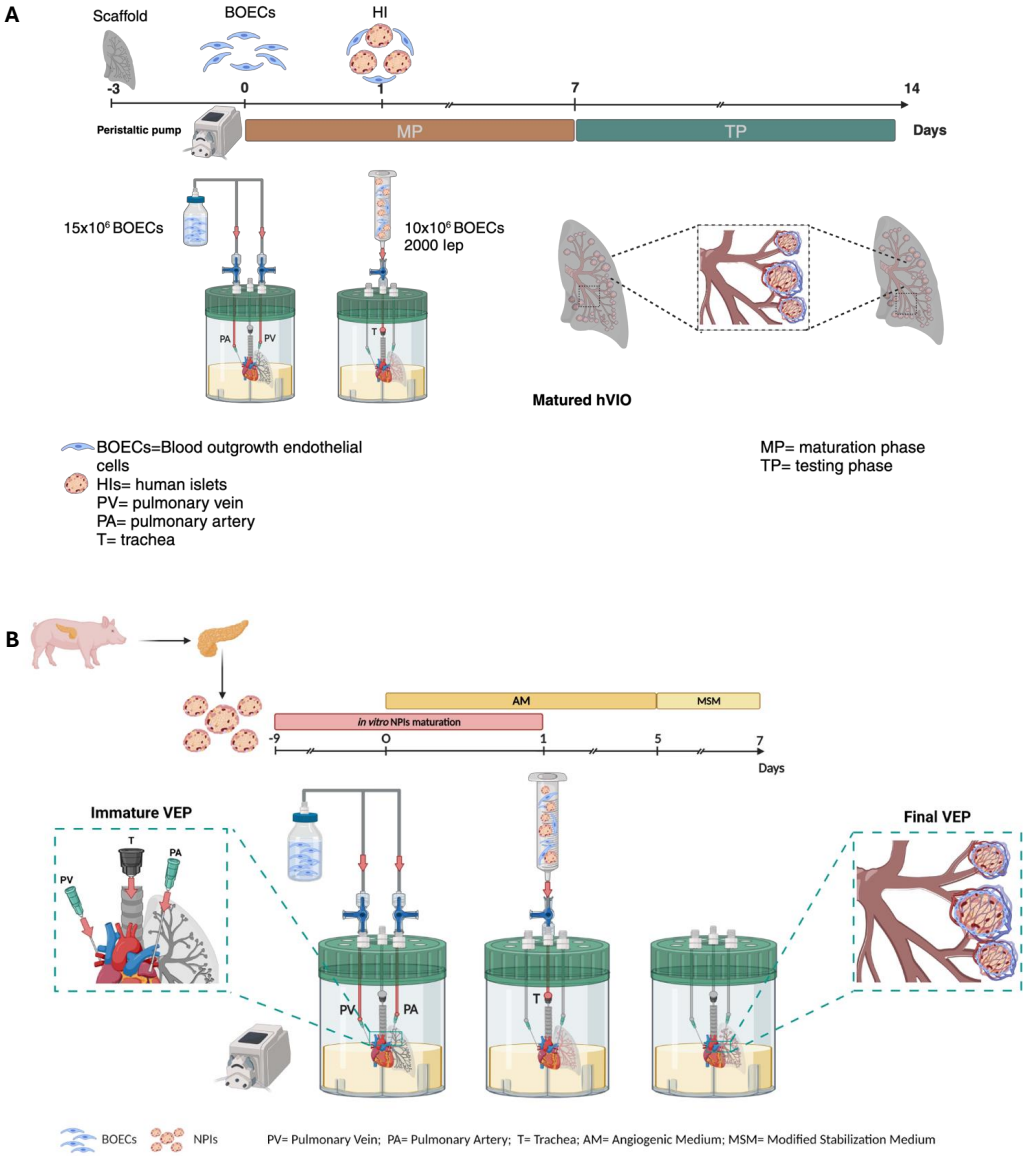


Figure 8: hVIOs and VEPs bioengineering timeline: A) *On Day 0, BOECs are seeded into the PA and PV, and the reendothelialized scaffold is cultured in the AM. On Day 1, a mixture of HIs and BOECs is seeded into the tissue, and the resulting recellularized organ is cultured in a perfusion system for 12 days;* ***B)*** *Schematic drawing of customized bioreactor and steps in VEP assembly.*

5.2. ENGINEERING THE VASCULAR COMPARTMENT: BOECs CHARACTERIZATION AND hVIOs AND VEP ASSESSMENT OF THE VASCULAR STRUCTURE AND FUNCTION

5.2.1. BOECs in vitro characterization

Current works have shown that it is possible to completely re-engineer the hierarchical vascular architecture of a decellularized organ by infusing and grafting endothelial cells into the organ (Ren *et al*, 2015). This self-assembly process regenerates the vascular architecture and restores the organ's endothelial function (Ren *et al*, 2015). Specifically in vascular engineering, BOECs can be utilized for this purpose. Thus, we investigated the endothelial phenotype, vasculogenic potential, and proliferative capacity of the colony isolated in our lab from a healthy subject. BOEC colonies appeared after approximately 14-28 days. They were characterized through flow cytometry at low passage (passage 3) and after expansion (passage 8), confirming the persistence of an endothelial phenotype ($CD31^+$/CD144 (VEC) $^+$/ KDR^+/$CD34^-$/$CD45^-$) (Fig.9A). Furthermore, immunofluorescence analysis confirms the endothelial phenotype, showing BOECs positivity for CD31, VEC, vWF, and VEGFR2 (Fig.9B).

One major bottleneck in engineering devices is the use of balanced culture media to preserve the function and phenotype of all cell types.

To use BOECs to generate hVIOs, which require the combination with pancreatic islets, we compared the *in vitro* "performance" of the isolated BOEC both in standard conditions (using the BOEC medium) and in the presence of the culture protocols for our scaffold. To confirm BOEC endothelial function, we performed a WST-1 proliferation assay in the presence of both standard medium and the combination of hVIO media. The results indicated a significant increase in cell growth after 24 and 48 hours of using the hVIO media combination compared to the standard BOEC medium (Fig. 9C, ***WST1 test. hVIO; p=0.0002 for both time points).

We also performed a tube formation assay. The results show a significant increase in the capacity of BOEC to form an endothelial network in the presence of the hVIO medium compared to the standard condition (Fig.9D, E). Moreover, the overall results demonstrate a significant improvement in the BOEC performance in the presence of the hVIO medium combination, suggesting their compatibility with a designed culture media protocol to preserve endocrine function.

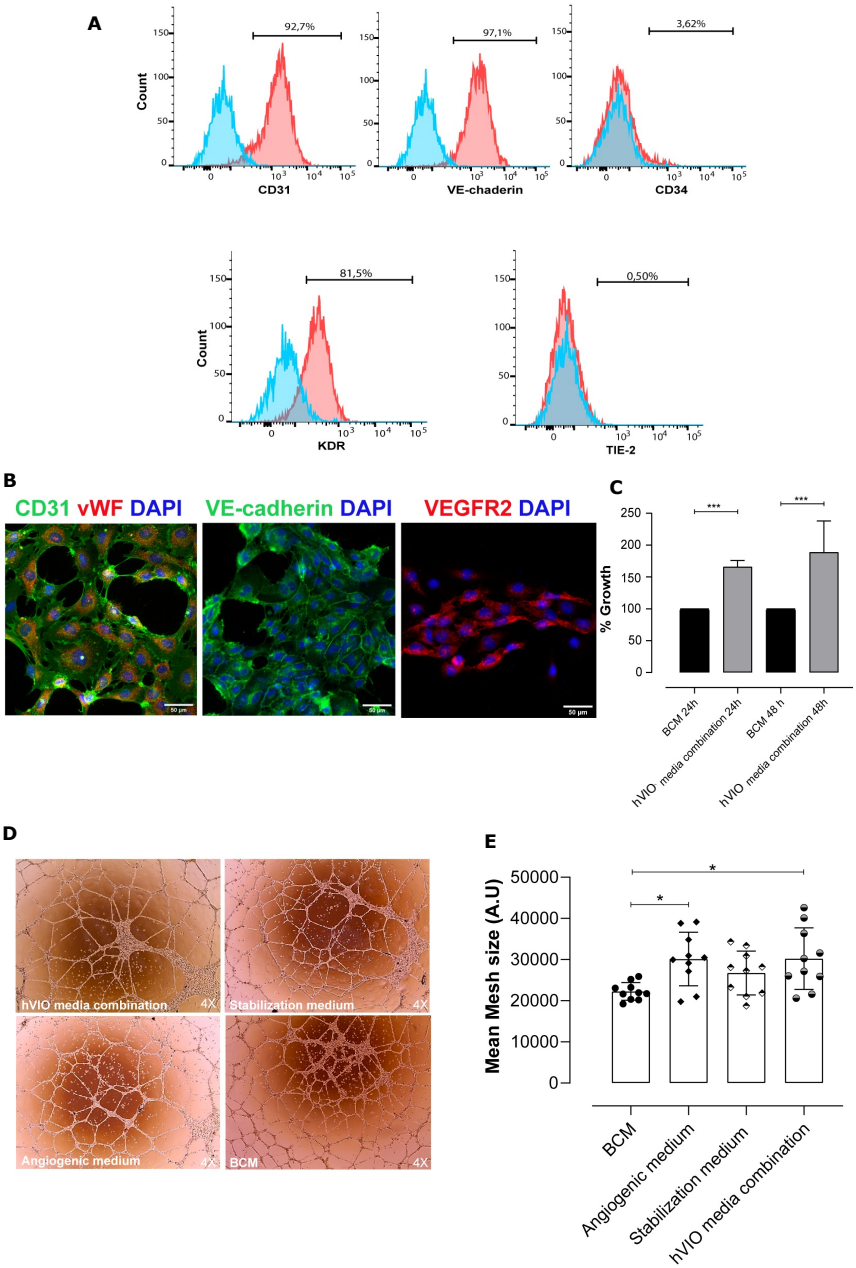


Figure 9: BOECs characterization: A) *Representative histograms of endothelial marker expression: cells are positive for endothelial markers CD31, VEC (Ve-cadherin), and KDR (VEGF receptor), and negative for CD34 and CD45;* ***B)*** *Immunofluorescence image of BOEC endothelial phenotyping CD31 (green), Von Willebrand factor (vWF - red), and DAPI (blue). Scale bar in µm;* ***C)*** *WST-1 assay for BOEC proliferation in the presence of standard BOEC culture medium (BCM) (n=8) or hVIO media combination (n=8) for 24 or 48 hours (p<0.0001);* ***D)*** *Morphology of BOECs tube formation assay in the presence of hVIO media combination, AM,MSM and BCM magnification 4x;* ***E)*** *Analysis of the formed vascular mesh for vascular density analysis in the presence of BCM, AM, MSM, and hVIO media combination, (n = 10 biological replicates), values presented as mean ± SD (BCM vs. Angiogenic medium *p = 0.0166; BCM vs. hVIO media combination *p = 0.0235), one way ANOVA with Dunn's correction.*

5.2.2. Evaluation of hVIOs vascular structure and function

Evaluating the vascular barrier function in a vascularized scaffold is crucial for sustaining scaffold perfusion and nutrient distribution. To validate the hVIO and VEP engineered vascular network, we performed a fluorangiography assay and a dextran perfusion assay 7 and 14 days after the engineering process.

The fluorangiography assay (Fig. 10A) demonstrated that blue beads, perfused in a low-melting agarose solution through PA (for more details, see section 7.10), were retained within the endothelial, vWF^+ continuous vascular network without any spillage into the air space. Our results show that the blue beads are correctly trapped within the endothelial tissue engineered using BOECs (vWF^+—red) 14 days after seeding (Fig. 10A).

This step is crucial because it indicates that the flow of the medium in and out of the lung is controlled by a dynamic perfusion that can replicate the physiological distribution of nutrients.

In addition, we evaluated the functional perfusion of the hVIO/VEP vascular compartment by conducting FITC-dextran of various molecular weights (20-150 KDa) perfusion tests (Fig. 10B and C, respectively). The control group is represented by the left lobe of the rat lung, which is decellularized and not repopulated with BOECs. Our results show that hVIOs can release dextran early, with better kinetics than the control group, confirming the presence of a continuous and functional vascular structure (* $p<0.05$ min 5 of the test at both 20 and 150 KDa). We conclude that the newly formed human BOEC endothelium is preserved and effectively distributes the perfusate in a dynamic 3D organization.

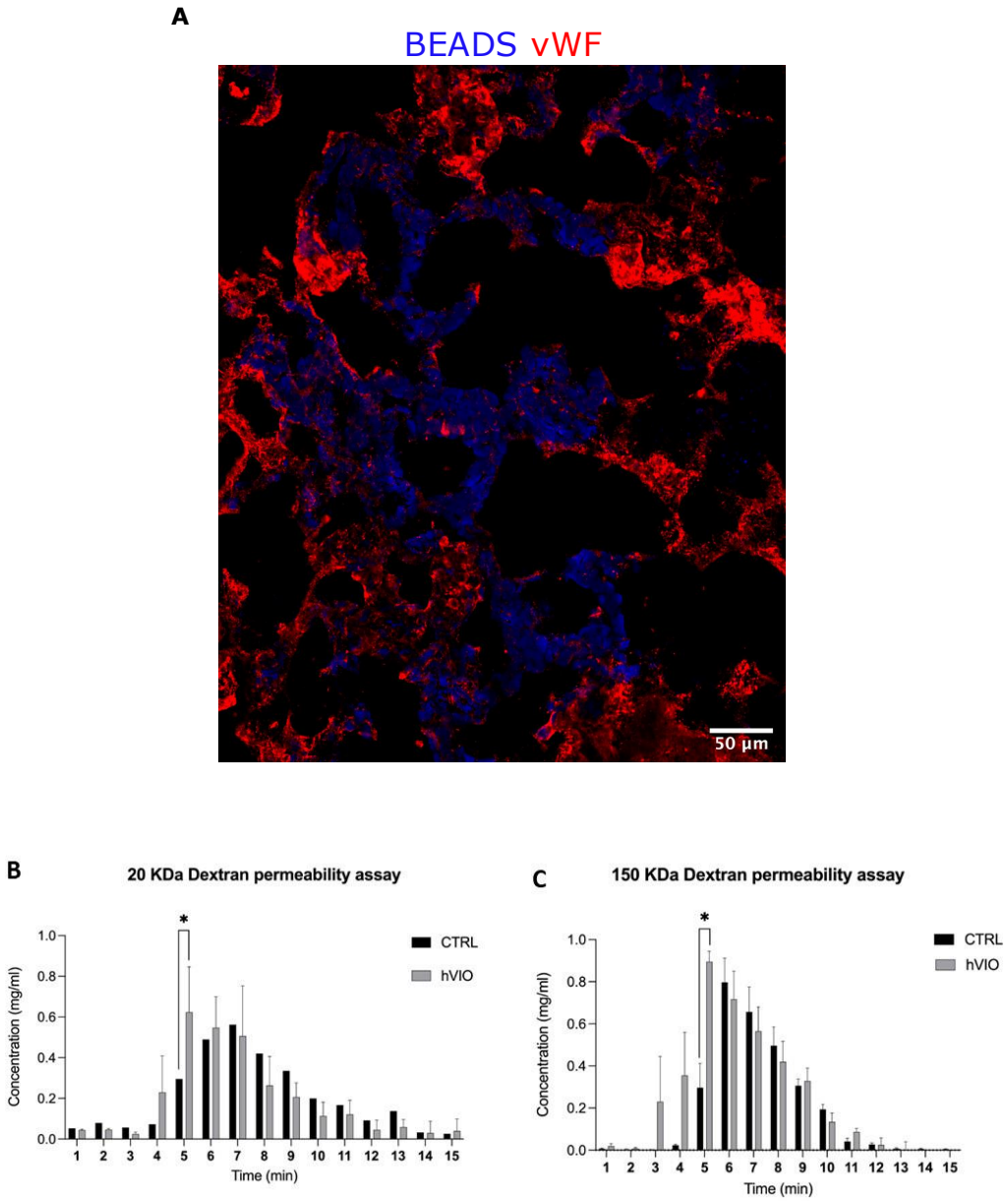


Figure 10: Preservation of the structural integrity and functionality of the vascular network: A) *Fluorescence microsphere perfusion. 0.2-µm microspheres (Beads, blue) present and trapped in newly formed hVIO vasculature (human vWF, red). Scale bars in µm;* ***B-C)*** *Analysis of the endothelial function of hVIOs after 14 days of culture using labeled dextran (20 kDa and 150 kDa) at different molecular weights.*

5.3. ENGINEERING THE ENDOCRINE COMPARTMENT: EVALUATING ISLET VIABILITY AND FUNCTION

To evaluate the engineering process of the endocrine compartment, the major milestones are: i) validating the stability of the endocrine phenotype throughout the entire culture protocol, ii) assessing the ability of hVIO to preserve β cell mass, and iii) evaluating hVIO's ability to respond to insulin in the presence of glucose stimuli. Firstly, we assessed the preservation of islet structure and endocrine phenotype throughout the entire culture period by performing an IF analysis on hVIOs after 1, 7, or 14 days of dynamic culture. Islets in all the samples, at different time points, showed preserved conventional architecture and were positive for the canonical endocrine markers insulin (INS), glucagon (GCG), and somatostatin (SST) (Fig. 11). This data confirms that the scaffold can maintain human islets' structural composition, organization, and viability over a 14-day culture period.

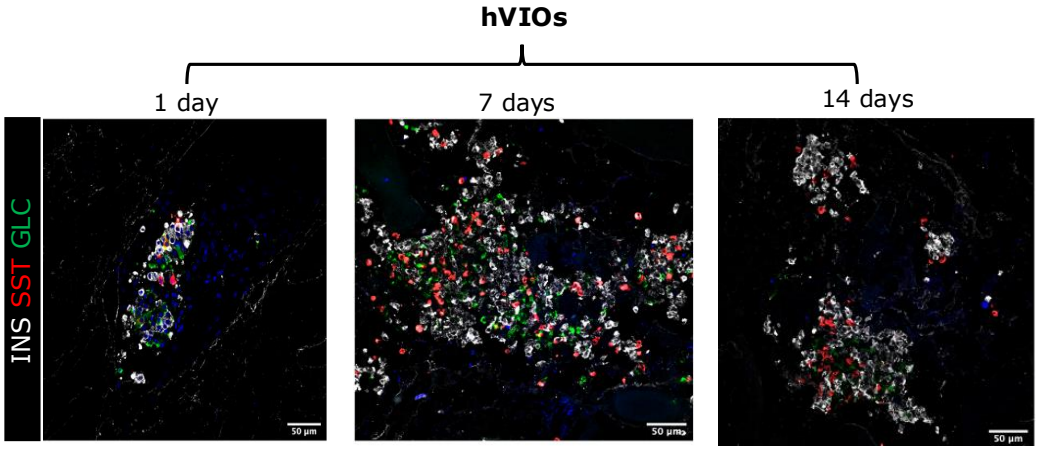


Figure 11: hVIOs' endocrine compartment at day 1, 7, and 14: *IF analysis, insulin (green), somatostatin (red), and glucagon (green). Scale bars in µm.*

To evaluate the preservation of β cell mass in hVIO technology, we adopted miR-375, a recognized marker of β cell damage (Kanak *et al*, 2015),(Erener *et al*, 2013), measured at 1, 3, 7 (MP), 10, and 14 (TP) days after seeding. To normalize the overall β cell death, we compared batch-matched miR-375 levels measured by HIs in standard culture conditions vs batch-matched HIs seeded in an hVIO fashion. To dissect the role of BOECs in miR-375 evaluation, we first traced the contribution of miR-375 from BOECs in an hVIO engineered exclusively with BOECs. As demonstrated, BOECs do not contribute to the kinetic release of miR-375, confirming the assay's specificity for tracing β cell death (Fig.12A). The results show the absolute number of copies of miR-375 in hVIOs, with a peak on day 3 during the MP and a

complete absence of miR-375 copies during the TP (Fig. 12A). Additionally, based on the estimated number of miR-375 copies per cell and the miR-375 copies measured in the hVIO supernatants at each time point, we estimated the percentage of β cell death during the hVIO culture protocol. The results indicate a peak of about 15% β cell death during the MP (Fig. 12B). Finally, the comparison of β cell death in the hVIO culture with standard culture conditions shows a statistically significant reduction (HIs 7 days and hVIOs 7 days (***p = 0.001), HIs 14 days and hVIOs 14 days (** p=0.0159)) in β cell death in the HIs seeded in hVIO compared to the batch-matched HIs in standard culture conditions (Fig. 12C). This data confirms that our protocol develops hVIO that matures in 7 days (MP) and stably preserves the endocrine mass until day 14 (TP).

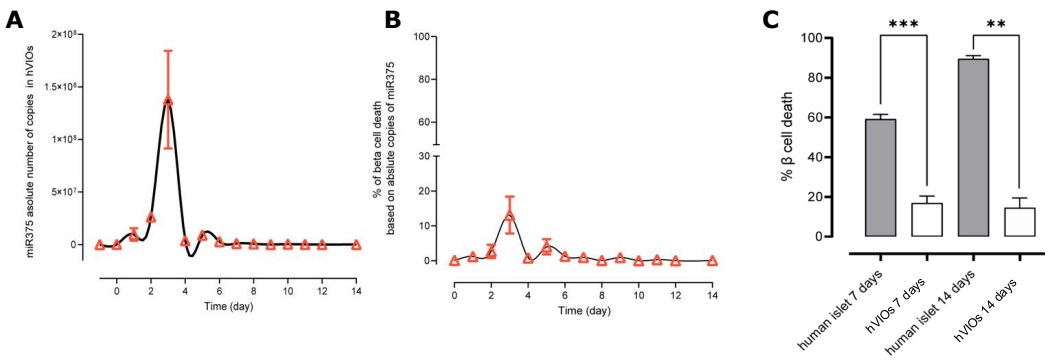


Figure 12: Analysis of β-cell death by miR-375: A) *Analysis of the release kinetics of miR-375 absolute copy numbers in hVIOs during the entire culture protocol(n=8);* ***B)*** *Conversion of miR-375 release kinetics from absolute copies into the percentage of β cell death (n=8);* ***C)*** *Comparison of β-cell death 7 and 14 days of culture of HIs in standard conditions compared to hVIOs; * p< 0.05, statistical analysis carried out using Mann Whitney U test.*

Lastly, we assessed the endocrine function of the hVIOs by testing their ability to produce insulin when exposed to controlled levels of glucose (ranging from 2 to 20 mM). We conducted dynamic insulin secretion tests (IST) for this evaluation. The curves were analyzed as an increase in insulin compared to the basal value, expressed as a fold change over the basal. This allowed for a comparison of the "performance" of freshly isolated HIs with that of hVIOs after 1 day of culture. The results indicate that the insulin secretion of hVIOs 1 day after seeding is not different from that of isolated islets simultaneously. This confirms that the decellularized lung matrix with an endothelial draft does not improve the secretory function of HIs (Fig. 13A).

In contrast, the data show that hVIOs released significantly higher insulin levels on day 7 compared to day 1, indicating a substantial increase in secretory activity

(min=3 *p=0.039, min=4 **p=0.023, min=5 *p=0.035), (Fig. 13B). Furthermore, hVIOs released significantly higher insulin levels on day 14 than on day 1, as shown by the point-by-point analysis (min=1 *p= 0.0221, min=2 *p=0.021, min=4 *p=0.0221, min=6 *p=0.035, min=9 *p=0.014, min=10 *p=0.035, min=12 **p=0.0082, min=13 *p=0.0221, min=14 *p=0.012, min=20 *p=0.0167), statistical analysis carried out using the Mann-Whitney U test) (Fig. 13C).
Additionally, batch-matched hVIOs compared at 7 or 14 days of culture exhibited preserved biphasic insulin secretion kinetics, with the acquisition of physiological biphasic kinetics (the second peak of secretion matured between 10 and 20 minutes after the stimulus) (Fig. 13D).

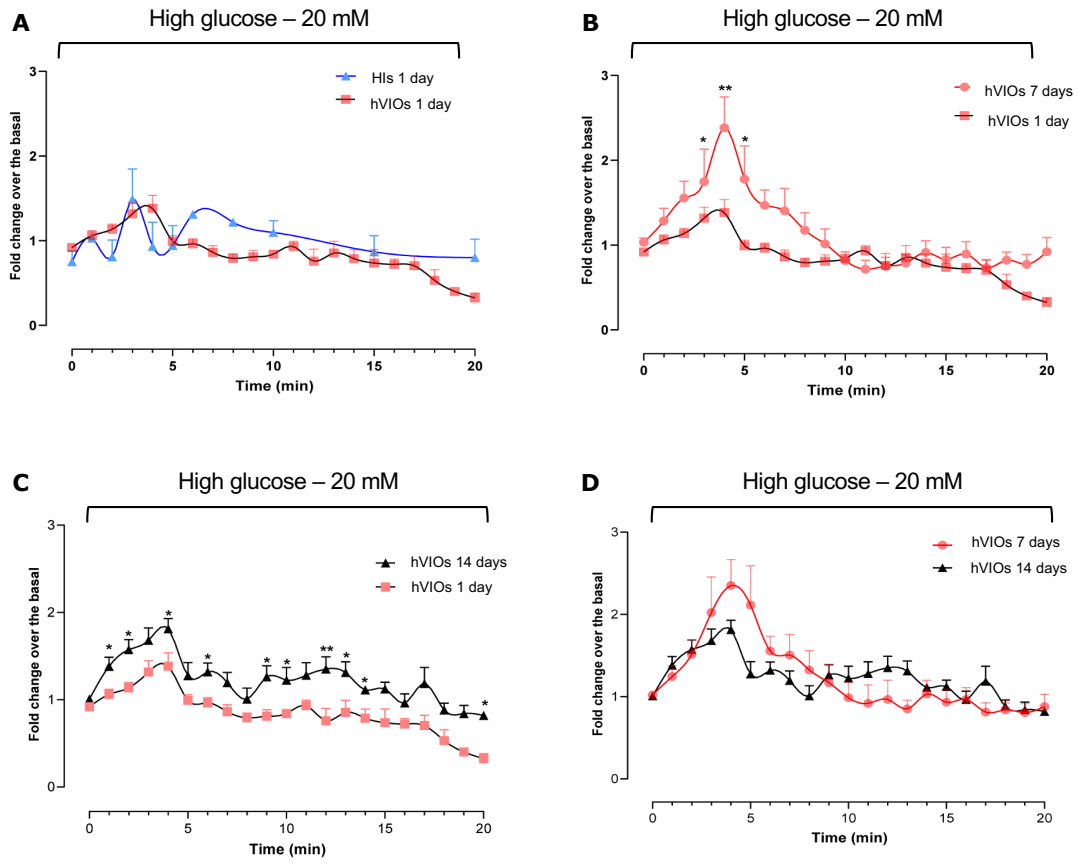


Figure 13: Analysis of endocrine function from 1 to 14 days of hVIOs by IST: A) *comparative endocrine function of HIs compared to hVIOs at day 1 (n=8);* ***B)*** *comparative endocrine function of hVIOs at day 1 vs hVIOs at day 7 (n=8);* ***C)*** *comparative endocrine function of hVIOs at day 1 vs hVIOs at day 14 (n=8);* ***D)*** *comparative endocrine function of hVIOs at day 7 vs hVIOs at day 14 (n=8); * p< 0.05, statistical analysis carried out using Mann Whitney U test.*

5.4. EVALUATION OF THE INTEGRATION OF hVIOs COMPARTMENTS

After confirming the engineered vascular and endocrine compartments of the hVIOs, we assessed their ability to integrate during the MP and to maintain this integration during the TP. Samples collected 1, 7, and 14 days after seeding were fixed and used for morphological evaluation through IF analyses. We evaluated the integration of the vascular and endocrine compartments and the cellular distribution of the samples at these time points. We conducted IF staining of vWF/CD31 and INS on hVIOs. Confocal microscopy images revealed a preserved endocrine compartment (INS^+) at all three time points, with a progressively structured vasculature (vWF^+ and $CD31^+$) from day 1 to day 14. This suggests that the vascular engineering requires 7 days to reshape the vascular architecture, achieving close contiguity with the endocrine compartment within the alveolar space (Fig. 14A). Additionally, we observed that from day 7 to day 14 (TP), the spatial compartment distribution in hVIOs is qualitatively stable. In hVIOs cultured for 14 days, we noted a uniform distribution of islets (INS^+) and BOECs ($CD31^+$) across a transverse section of the scaffold (Fig. 14B). This further confirms the structural integrity of both compartments throughout the entire culture period.

We can affirm that the hVIO platform has been thoroughly engineered and functionally validated for model generation and is now ready for the testing phase.

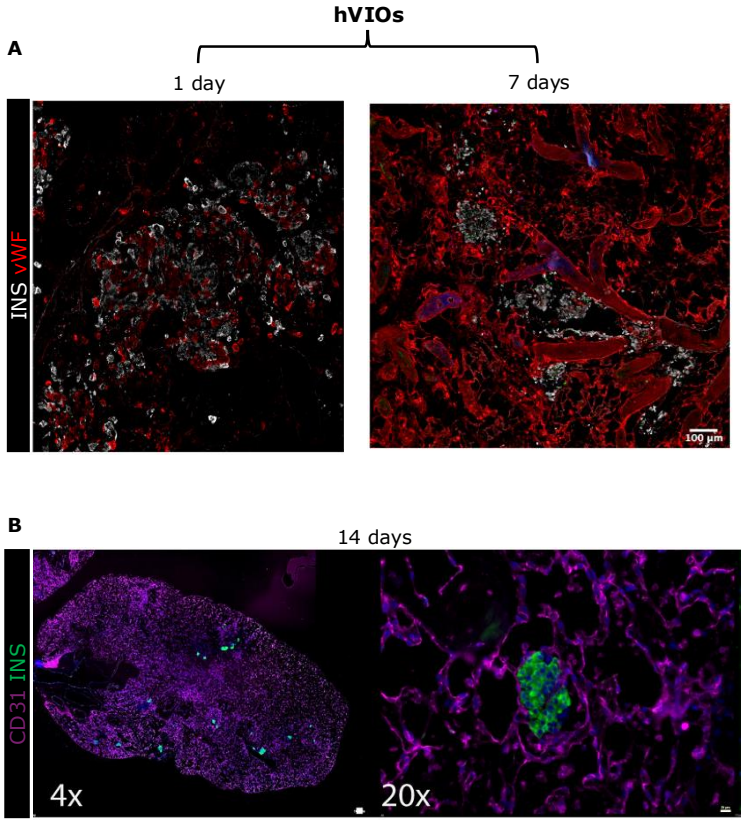


Figure 14: hVIOs IF analysis: A) *Day 1 and 7: Evaluation of the endothelial texture vWF+ (red) and the endocrine component INS+ (white);* ***B)*** *Day 14: Evaluation of the endothelial texture CD31+ (purple) and the endocrine component INS+ (green).*

5.4.1. Understanding the cell's trajectory in hVIOs

We conducted spatial transcriptomics analyses to track the hVIOs cell composition trajectory at three-time points: day 1, day 7, and day 14. For each time point, we analyzed a single hVIO slide. Multiple regions of interest (ROIs) were outlined and labeled for vWF- and INS for the vascular and endocrine hVIO compartments, respectively. On day 1, we traced 14 vWF-Endothelial areas of interest (AOIs) and 10 INS-islets AOIs. On day 7, we traced 15 vWF-Endothelial AOIs and 30 INS-islets AOIs. On day 14, we traced 12 vWF-Endothelial AOIs and 29 INS-islets AOIs (Fig.15 A, B and 16A). The experimental plan is detailed in paragraph 7.16.

Regarding the endothelial cells, we found that the canonical endothelial genes are expressed during the culture period (Fig. 15C): CDHR5 (Ve-Cadherin) is more expressed on day 1 than on days 7 and 14, with a fold change of 1.7 and 2,

respectively. During the TP (between day 7 and day 14), it is 1 time more expressed on day 7 than on day 14.

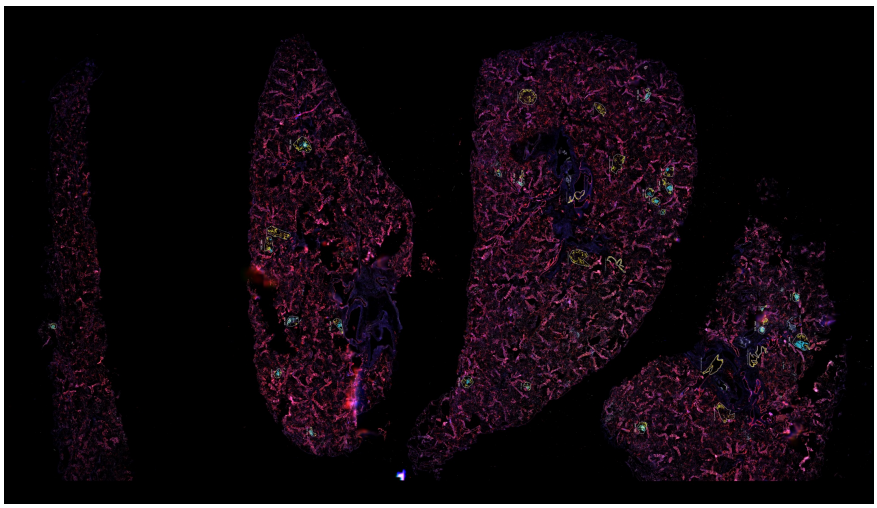
VEGFC (Vascular Endothelial Growth Factor C) is more expressed on day 1 than on day 7 and day 14, with a fold change of 1.3 and 1.8, respectively. During the TP, it is 1.4 times more expressed on day 7 than on day 14. VEGFD (Vascular Endothelial Growth Factor D) is more expressed on day 1 than on day 7 and day 14, with a fold change of 1.8 and 1.6, respectively. During the TP, it is 0.9 times more expressed on day 7 than on day 14. KDR (Kinase insert Domain Receptor, also known as VEGFR2, vascular endothelial growth factor receptor 2) is more expressed on day 1 than on day 7 and day 14, with a fold change of 0.9 and 1, respectively. During the TP, it is 1.1 times more expressed on day 7 than on day 14. Finally, VEGFA (Vascular Endothelial Growth Factor A) is more expressed on day 1 than on day 7 and day 14, with a fold change of 0.7 for both time points. During the TP, it is 0.9 times more expressed on day 7 than on day 14.

We also detected some interesting genes that contribute to the pro-angiogenic activity of the endothelial cells (Fig. 15 C,D), like CTSS (Cathepsin S), which plays an active role in blood vessel permeability and angiogenesis (Xu *et al*, 2023). It is more expressed on day 1 than on day 7 and day 14, with a fold change of 3.9 and 2.4, respectively. During the TP, it is 0.6 times more expressed on day 7 than on day 14. PUM1 (Pumilio RNA-binding family member) plays a role in the proliferation, migration, invasion, and tube formation capacities of endothelial cells (Dai *et al*, 2022). It is more expressed on day 1 than on day 7 and day 14, with a fold change of 2.9 and 3.4, respectively. During the TP, it is 1.6 times more expressed on day 7 than on day 14. TARS1 (Threonine tRNA ligase 1), whose secretion is induced by VEGF, regulates endothelial cell migration and angiogenesis (Barai & Chen, 2024). It is more expressed on day 1 than on day 7 and day 14, with a fold change of 4.3 and 3.7, respectively. During the TP, it is 0.8 times more expressed on day 7 than on day 14. LOXL1(Lysyl oxidase-like 1) plays an important role in hypoxia-triggered angiogenesis, but the specific mechanism involved is still unknown (Xie *et al*, 2017). It is more expressed on day 1 than on day 7 and day 14, with a fold change of 6.2 and 5.3, respectively. During the TP, it is 0.8 times more expressed on day 7 than on day 14. Finally, PTBP1 (Polypyrimidine tract-binding protein 1), which characteristically colocalizes with endothelial cells, and its deficiency affects the migration of endothelial cells, thereby disrupting proliferation (Liu *et al*, 2023). It is

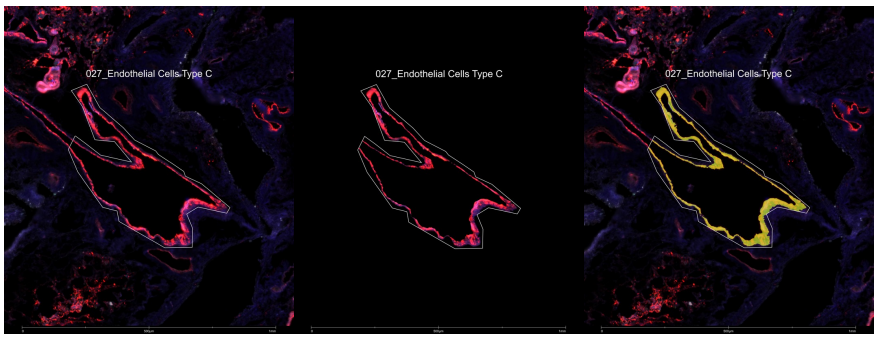
more expressed on day 1 than on day 7 and day 14, with a fold change of 4 for both time points. During the TP, it is expressed 1 time more on day 7 than on day 14.
We also detect other interesting genes (Fig. 15 C, D): GJA1 (Gap Junction Protein Alpha 1) is a significant gap junction protein implicated in endothelial stability (Behrens *et al*, 2010). It is more expressed on day 1 than on day 7 and day 14, with a fold change of 4 for both time points. During the TP, it is 1 time more expressed on day 7 than on day 14. KLC1 (Kinesin Light Chain 1) is a microtubule-associated force-producing protein that may play a role in organelle transport with pro-inflammatory activity (Cyrus & Muller, 2016). It is more expressed on day 1 than on day 7 and day 14, with a fold change of 3.3 and 2.7, respectively. During the TP, it is 0.8 times more expressed on day 7 than on day 14. CLECL1 (C-type lectin-like receptor 1) has recently been described as playing crucial roles in immunity and homeostasis since these proteins can recognize pathogens and self-Ags, has an immune modulation activity (Thebault *et al*, 2009). It is more expressed on day 1 than on day 7 and day 14, with a fold change of 4.9 and 2.7, respectively. During the TP, it is 0.6 times more expressed on day 7 than on day 14. REM1 (RRAD And GEM Like GTPase 1) is a human gene that encodes a GTPase protein expressed in endothelial cells. It is more expressed on day 1 than on day 7 and day 14, with a fold change of 0.2 and 0.8, respectively. During the TP, it is 4.3 times more expressed on day 7 than on day 14. In the end, PTGIS (Prostaglandin-endoperoxide synthase), which under physiological conditions, constitutive PTGIS interacts with thromboxane-A synthase to regulate prostacyclin–thromboxane A2 metabolism, essential for homeostasis and functional endothelium (Liu *et al*, 2023). It is a gene that defines a pulmonary endothelial phenotype and is more expressed on day 1 than on day 7 and

day 14, with a fold change of 5.6 and 4, respectively. During the TP, it is 0.7 times more expressed on day 7 than on day 14.
These results indicate that the hVIOs endothelium is active in terms of proliferation and stable during the culture period.

A



B



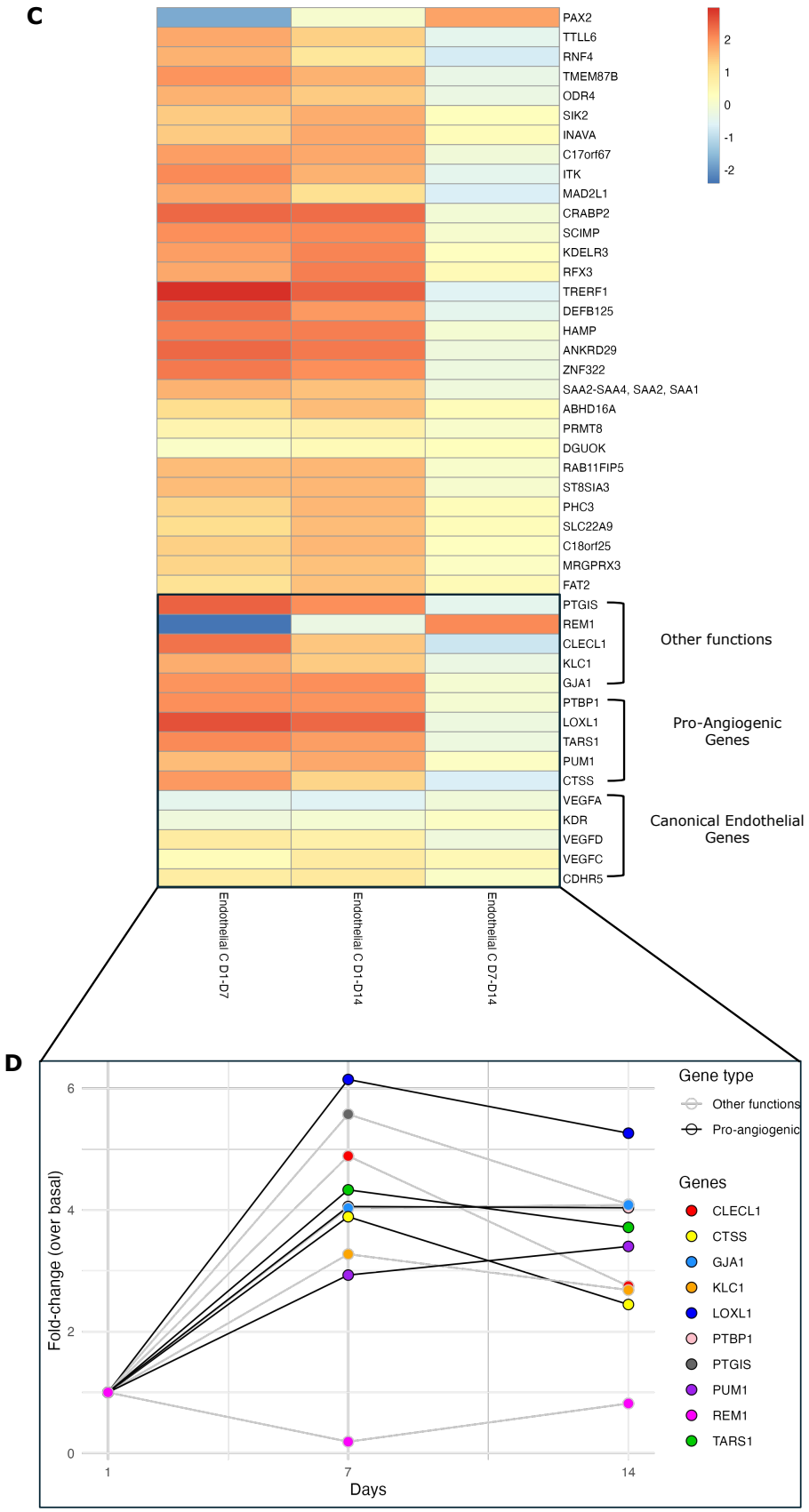

C
PAX2
TTLL6
RNF4
TMEM87B
ODR4
SIK2
INAVA
C17orf67
ITK
MAD2L1
CRABP2
SCIMP
KDELR3
RFX3
TRERF1
DEFB125
HAMP
ANKRD29
ZNF322
SAA2-SAA4, SAA2, SAA1
ABHD16A
PRMT8
DGUOK
RAB11FIP5
ST8SIA3
PHC3
SLC22A9
C18orf25
MRGPRX3
FAT2
PTGIS
REM1
CLECL1
KLC1
GJA1
PTBP1
LOXL1
TARS1
PUM1
CTSS
VEGFA
KDR
VEGFD
VEGFC
CDHR5
Other functions
Pro-Angiogenic Genes
Canonical Endothelial Genes
2
1
0
-1
-2
Endothelial C D1-D7
Endothelial C D1-D14
Endothelial C D7-D14
D
Fold-change (over basal)
Days
Gene type
Other functions
Pro-angiogenic
Genes
CLECL1
CTSS
GJA1
KLC1
LOXL1
PTBP1
PTGIS
PUM1
REM1
TARS1

Figure 15: Spatial transcriptomic analyses of vWF-Endothelial AOIs: A) *Representative immunofluorescence image of the hVIO slice analyzed;* ***B)*** *Representative immunofluorescence image explaining the segmentation strategy of vWF-endothelial AOIs;* ***C)*** *Heatmap of endothelial genes generated using the "pheatmap" function from the pheatmap package in R (version 2024.09.0+375). The input data consisted of a numeric matrix containing the fold-change expression data of the selected genes (log-transformed), calculated in each sample comparison;* ***D)*** *Line plot of the most represented genes for endothelial cells.*

Regarding the human endocrine cells, we found that the canonical islet genes are expressed during the culture period (Fig.16B): GCG is more expressed on day 1 than on day 7 and day 14, with a fold change of 1.2 and 1, respectively. During the TP, it is 0.85 times more expressed on day 7 than on day 14; SST is more expressed on day 1 than on day 7 and day 14, with a fold change of 0.8 and 0.7, respectively. During the TP, it is 0.8 times more expressed on day 7 than on day 14; INS is more expressed on day 1 than on day 7 and day 14, with a fold change of 1.6 and 0.6, respectively. During the TP, it is 0.4 times more expressed on day 7 than on day 14; MAFA (MAF BZIP Transcription Factor A) is more highly expressed on day 1 than on day 7 and day 14, with a fold change of 1.5 and 1.3, respectively. During the TP, it is 0.9 times more expressed on day 7 than on day 14; and at the end, NEUROD1 (Neuronal Differentiation 1) is more expressed on day 1 than on day 7 and day 14, with a fold change of 0.9 and 1, respectively. During the TP, it is 1.1 times more expressed on day 7 than on day 14.

We also detected two interesting genes that contribute to the islet's survival (RGS2) and the metabolic activity of the islets (TFAM) (Fig. 16B): RGS2 (Regulator of G Protein Signaling 2) is a key regulator of pancreatic β cell survival and is essential for retention of normal function and mass of β cells and RGS2−/− islets are more vulnerable to β cell apoptosis *in vitro* and *in vivo* (Dong *et al*, 2017). It is more expressed on day 1 than on days 7 and 14, with a fold change of 4.7 and 4.1, respectively. During the TP, it is 0.9 times more expressed on day 7 than on day 14; TFAM (Transcription Factor A, Mitochondrial) is a gene connected to PDX1, which regulates both pancreatic embryonic development and mature β cell function. Disruption of PDX1 activity in β cells leads to decreased TFAM expression and subsequent mitochondrial dysfunction, which can be reversed by reintroducing TFAM expression (Mulder, 2017). It is more expressed on day 1 than on days 7 and 14,

with a fold change of 4 and 4.2, respectively. During the TP, it is 1 time more expressed on day 7 than on day 14.

These results indicate that the islets in the hVIOs are preserved during the entire culture time, confirming the data obtained from the quantification of miR-375 and presenting active mitochondrial activity.

Interestingly, we also detected the presence of IL-8 receptors, CXCR1/2, on the islets (Fig.16B):

CXCR1 is more highly expressed on day 1 than on days 7 and 14, with a fold change of 0.8 and 0.9, respectively. During the TP, it is 1.2 times more highly expressed on day 7 than on day 14; CXCR2 is more highly expressed on day 1 than on days 7 and 14, with a fold change of 1.2 for both time points. During the TP, it is 1 time more highly expressed on day 7 than on day 14.

In the following paragraphs, we evaluated the presence of CXCR1/2 receptors in the cellular components of hVIO, in the presence or absence of an inflammatory insult given by IL-8.

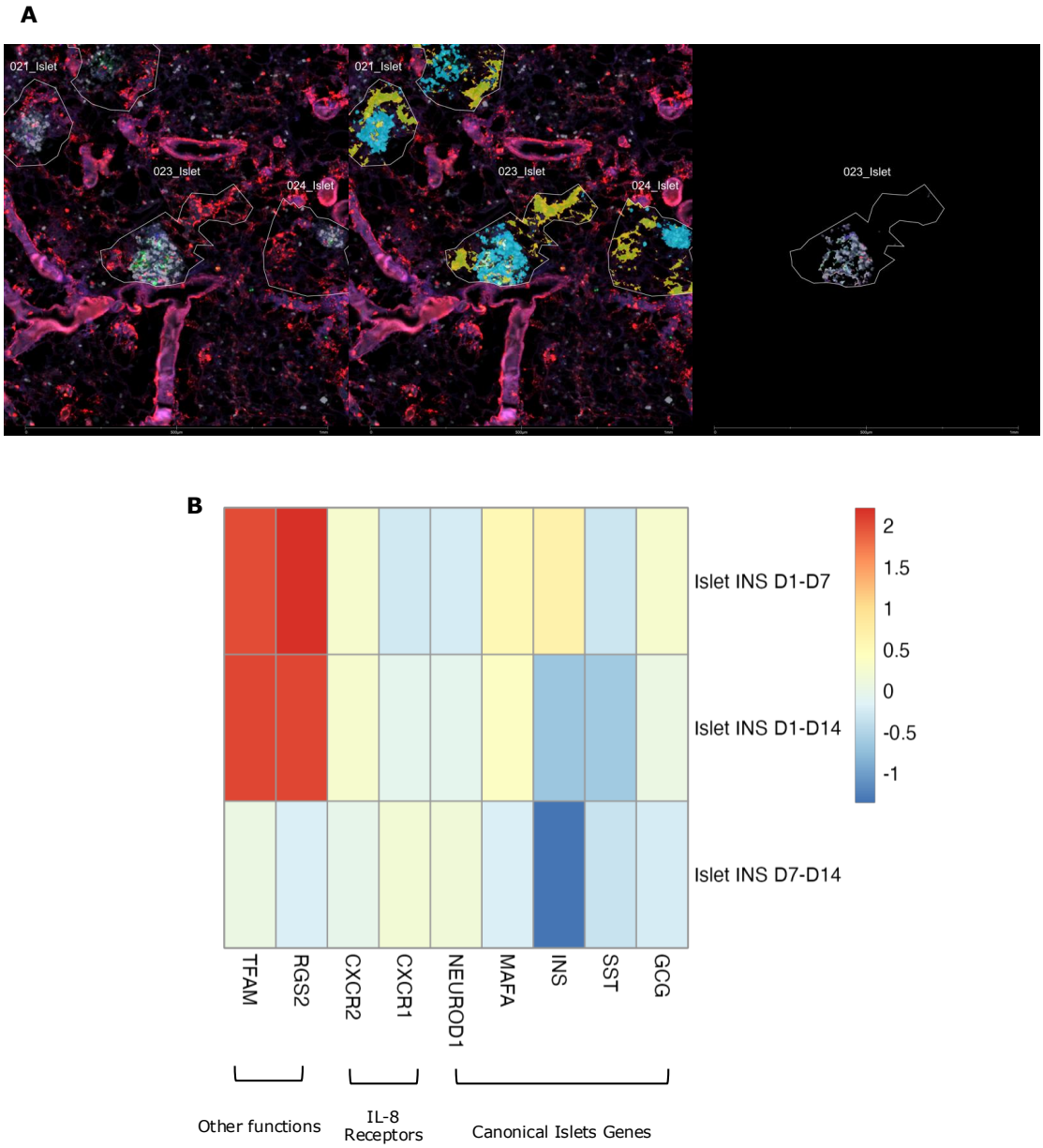


Figure 16: Spatial transcriptomic analyses of INS-islets AOIs: ***A)*** *Representative immunofluorescence image explaining the segmentation strategy of INS-islets AOIs;* ***B)*** *Heatmap of islets gene generated using the "pheatmap" function from the pheatmap package in R (version 2024.09.0+375). The input data consisted of a numeric matrix containing the fold-change expression data of the selected genes (log-transformed), calculated in each sample comparison.*

5.5. TESTING CXCR1 AND CXCR2 EXPRESSION ON hVIO CELL COMPARTMENTS IN AN INFLAMMATORY CONTEXT: AN *IN VITRO* ASSESSMENT

In previous sections, we demonstrated that hVIO could be engineered within 7 days, and its structure and function can be preserved from day 7 to day 14. This opens the possibility of using hVIO as a study platform during the TP. We focused on evaluating hVIO technology as a tool for studying inflammatory β cell damage. To achieve this goal, we selected an inflammatory stimulus that could impact both the vascular and endocrine compartments. The IL-8-CXCR1/2 pathway has recently been suggested as a significant contributor to the development of diabetes (Citro *et al*, 2015a). Additionally, it is known to alter the endothelium's permeability, viability, and proliferative capacity (Li *et al*, 2003). Previous laboratory studies have shown that HIs release high levels of IL-8, which mediate interactions between the immune and endothelial systems during the onset of T1D and after transplantation(Citro *et al*, 2012).

Thus, our focus has been on the role of IL-8 within the context of hVIO compared to standard internal controls. We decided to i) confirm the presence of CXCR1/2 on both hVIO cellular components (BOECs and HIs – sections 5.5.1 and 5.5.2) and later ii) evaluate the impact of IL-8 administration on the hVIO system (section 5.6).

5.5.1. Investigating the impact of the CXCR1/2 pathway on human islets

Firstly, we examined the presence of the CXCR1/2 receptors using IF. We conducted IF analysis immediately after pancreas isolation (T0) and subsequently exposed the samples to IL-8 (100 ng/ml) for 7 days to evaluate the role of IL-8 in relation to CXCR1/2 detection. We analyzed a total of 87 HIs from 4 different preparations (with 70 and 75 % purity). We did not find CXCR1 in any of the samples, but we did observe CXCR2 positivity in all analyzed islet preparations. In particular, preparation 1 showed 87% positivity, preparation 2 showed 85% positivity, preparation 3 showed 65% positivity, and preparation 4 showed 100% positivity (Fig.17A). Interestingly, we found that CXCR2 was present alone or alongside insulin ($CXCR2^+/INS^+$), glucagon ($CXCR2^+/GCG^+$), and somatostatin ($CXCR2^+/SST^+$), indicating a diverse distribution of CXCR2 within the human pancreatic islets. We measured the presence of CXCR2 in each batch by calculating the percentage (%) of $CXCR2^+$ islets. Furthermore, we

quantified the percentage of $CXCR2^+$ islets that also had α, β, or δ cells positive for the receptor, defining $CXCR2^+/INS^+$ (β) (preparations 1 and 2 showed 20% positivity, preparation 3 showed 15% positivity, and preparation 4 showed 37% positivity), $CXCR2^+/GCG^+$ (α) (preparations 1 showed 55% positivity, preparation 2 showed 25% positivity, preparation 3 showed 10% positivity, and preparation 4 showed 0% positivity), $CXCR2^+/SST^+$ (δ)(preparations 1 showed 40% positivity, preparation 2 showed 70% positivity, preparation 3 showed 45% positivity, and preparation 4 showed 35% positivity) islets (see Figure 17B). Overall, these findings supported the expression of CXCR2, but not CXCR1, in pancreatic islets in a heterogeneous manner.

These data suggest that human pancreatic islets may be influenced by the IL-8 pathway, enabling an investigation into the role of this chemokine in regulating their endocrine function.

Then, we evaluated how IL-8 treatment could impact islet function. We performed a dynamic insulin secretion test on 100 HIs equivalents in the presence of IL-8 (100ng/mL – n=4) or vehicle (n=4) at different time points (1,3,12, and 24 hours). We observed no statistical differences between IL-8 treatment groups at all time points compared to the control one (Fig.17C). Our results show that acute administration of IL-8 (from 1 to 24 hrs) does not have a negative effect on isolated islet function.

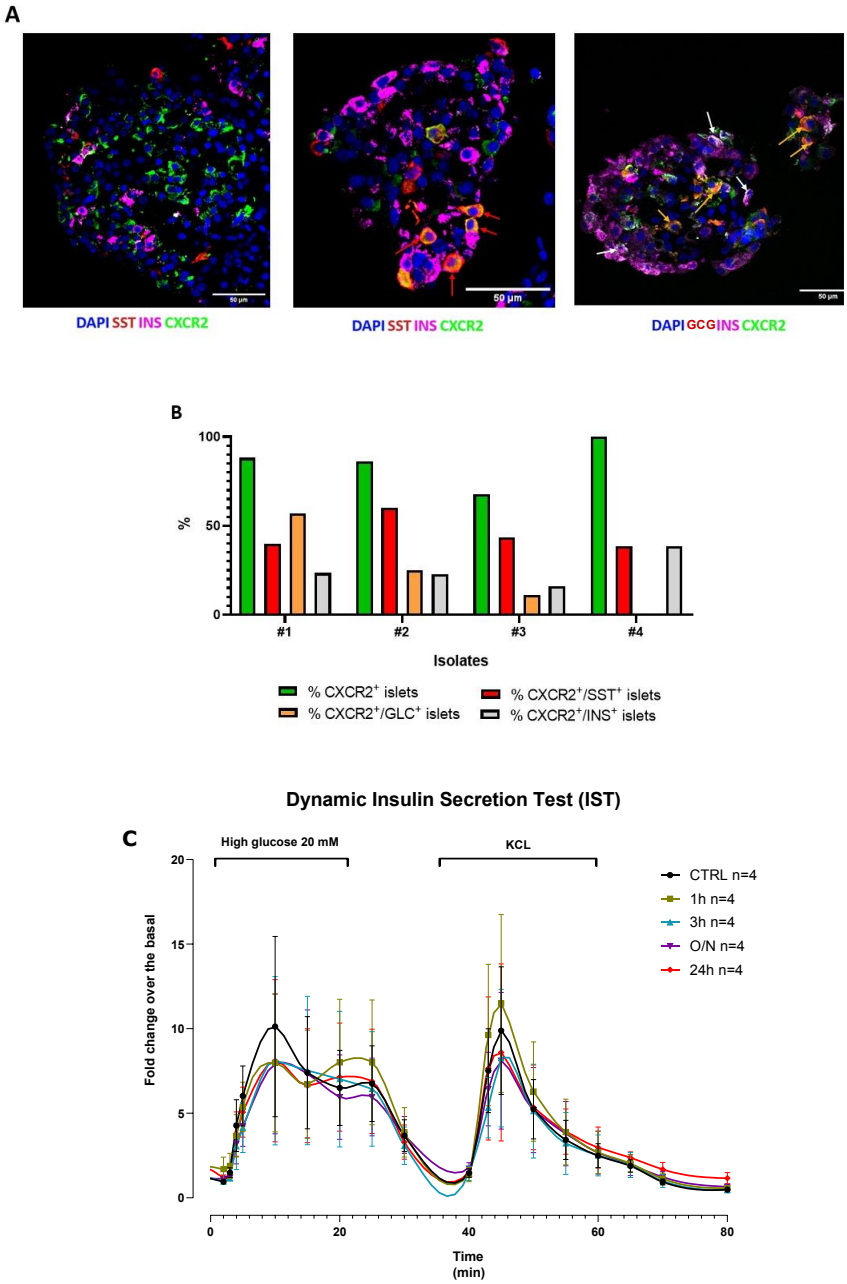


Figure 17: Assessing the influence of the CXCR1/2 pathway on human islets: A) *IF analysis of isolated HIs stained with DAPI (blue), Insulin (INS) (purple), CXCR2 (green), SST (red) or GCG (red). Red, orange, and white arrows indicate SST$^+$, CXCR2$^+$ cells; GCG$^+$, CXCR2$^+$ cells, INS$^+$, CXCR2$^+$ cells. Scale bars in µm;* ***B)*** *quantification of CXCR2$^+$ islets (green), CXCR2$^+$/SST$^+$ islets (red), CXCR2$^+$/GCG$^+$ islets (orange), CXCR2$^+$/INS$^+$ islets (grey) in 4 different preparations of pancreatic islets. A total of 78 islets were analyzed, 21+/-8 for each isolate;* ***C)*** *IST on 100 HI equivalents (n=4) in the presence of IL-8 (100ng/mL) or vehicle at different time points (1,3,12, and 24 hours).*

5.5.2. Investigating the impact of the CXCR1/2 pathway on BOECs

The literature on IL-8 and endothelial cells is well-defined, with a general consensus that IL-8 is a proangiogenic chemokine. However, little is known about its effects on BOECs alone or in the presence of decellularized ECM. Since BOECs are a key component of hVIOs, we evaluated their role in this context, focusing initially on the role of IL-8 on BOECs under standard conditions.

The expression of CXCR1/2 by Endothelial Colony-forming Cells (ECFCs; i.e., BOECs) is controversial, with some studies failing to detect these receptors on cord blood-ECFCs(Blandinières *et al*, 2021), while others indicate that IL-8 stimulation may induce their expression (Medina *et al*, 2013),(Yoon *et al*, 2005).

In this regard, we decided to investigate the role of the CXCR1/2 pathway on BOEC function and proliferation. Here, we isolate BOEC from 3 subjects (3 healthy males) and evaluate the presence of CXCR1/2 receptor in basal and IL-8 chronic stimulated condition (6 days).

Flow cytometry analysis showed that BOECs do not express CXCR1/2 receptors in all 3 subjects analyzed, both in the absence of treatment and after exposure to IL-8 for 6 days (Fig.18A, B).

We tested BOEC proliferation capacity with EssenBio IncuCyte S3 Live-Cell Analysis System in the presence of IL-8 (100 ng/mL) during 6 days of culture. IL-8 was added to the culture medium every other day. We observed similar proliferation to the internal control, suggesting that IL-8 does not negatively affect BOEC activity or compromise their proliferative capacity (Fig.18C).

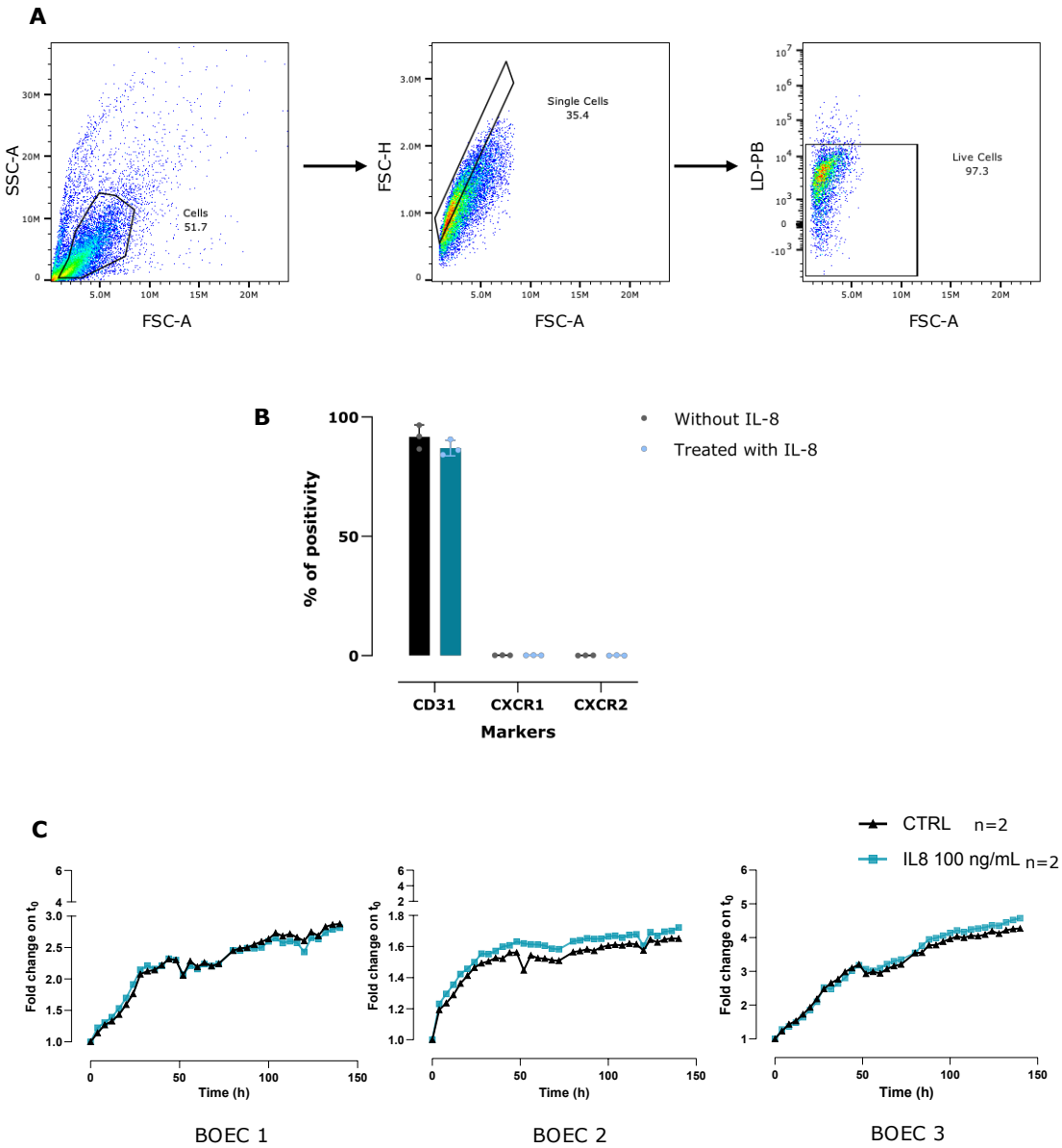


Figure 18: Assessing the influence of the CXCR1/2 pathway on BOECs: A) *Flow cytometric analysis of BOEC utilized a gating strategy. Cells were selected based on dimension (FSC-A vs SSC-A), followed by the isolation of single cells (FSC-A vs FSC-H), and live cell identification using a live/dead marker;* ***B)*** *Percentage of positivity for markers CD31-APC-A700, CXCR-PE, and CXCR2-PerCP. The dots represent the analysis of 3 subjects treated with IL-8 (100 ng/mL) or without the treatment;* ***C)*** *Proliferation assay using the EssenBio IncuCyte S3 Live-Cell Analysis System for 3 subjects with or without treatment with IL-8 (100 ng/mL).*

5.6. EXPLORING THE IMPACT OF IL-8 ON ENDOCRINE AND VASCULAR COMPARTMENTS IN hVIO: A CRITICAL ASSESSMENT

After initially testing the effects of IL-8 on HIs and BOECs in standard culture conditions, we moved to the hVIO setting. We aimed to observe the hVIO response to IL-8 treatment during the TP. To achieve this, we used a customized bioreactor to perfuse IL-8 or a control solution through the hVIO PA. This exposure allowed us to assess the impact on vascular and endocrine compartments using modified culture media. The fresh medium was supplemented with IL-8 or the control solution before each media change, which occurred every other day. In this setup, the perfusion of hVIO imitates a chronic inflammatory state, and the bioreactor enabled us to collect daily biological samples to evaluate the treatment's effects.

5.6.1. Evaluation of cell-on-scaffold distribution in the hVIOs setting

Firstly, we assessed the impact of IL-8 on the structural integrity of both compartments by performing a confocal evaluation of hVIO at the end of the TP.
The hVIOs were histologically analyzed after 7 and 14 days of culture. We evaluated cellular distribution and integration into the vascular and endocrine compartments. Confocal microscopy showed a uniform distribution of BOEC in the vascular tree (vWf^+), and after 7 days, the islets showed positive results for INS, GCG, and SST (Fig.19A). Interestingly, islets seeded in the lung showed positive results for both CXCR1 and CXCR2, which differed from the results observed in batch-matched control islets, suggesting that the vascularized ECM may have contributed to this difference (Fig.19A).
During the TP period, both the hVIOs treated and hVIOs control were examined. We observed a preserved vascular bed (vWf^+) and no alteration of the islet phenotype in hVIO after IL-8 treatment. Indeed, we observed islets positive for INS, GCG, and SST (Fig.19B, C). Additionally, we consistently detected human islet CXCR1/2 within hVIO in the presence of IL-8 treatment and the control group (Fig.19B, C). For each condition, we analyzed a single slide; 18 islets were positive for CXCR1 out of 18 islets detected in a lung slice, and 27 islets were positive for CXCR2 out of 31 islets detected in a lung slice. Further analysis is required to understand if the presence of vascularized ECM affects CXCR1/2 expression, considering that islets isolated without vascularized ECM did not express both receptors.

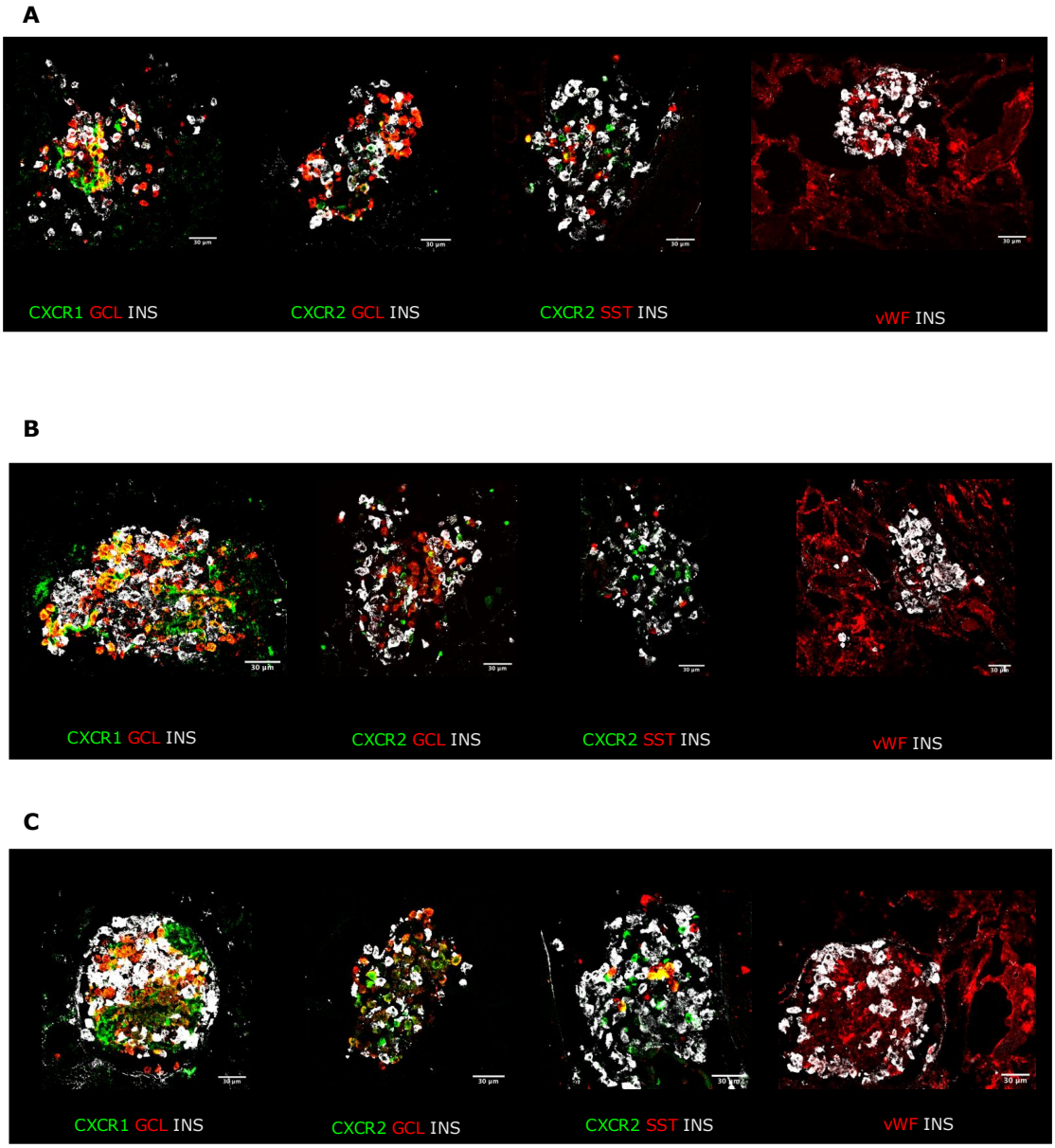


Figure 19: Confocal microscopy of cellular distribution and integration into the vascular and endocrine compartments: A) *During the MP, analyses of hVIO show CXCR1$^+$, CXCR2$^+$, GCG$^+$, INS$^+$, and SST$^+$ in HIs and BOECs, resulting in vWF$^+$;* ***B)*** *During the TP in the present of IL-8, analyses of hVIO show CXCR1$^+$, CXCR2$^+$, GCG$^+$, INS$^+$, and SST$^+$ in HIs and BOECs, resulting in vWF$^+$;* ***C)*** *During the TP without the IL-8 treatment, analyses of hVIO show CXCR1$^+$, CXCR2$^+$, GCG$^+$, INS$^+$, and SST$^+$ in HIs and BOECs, resulting in vWF$^+$.*

5.6.2. Assessment of β cell preservation following IL-8 treatment

To evaluate the preservation of HIs during the TP, we quantified miR-375 by ddPCR to track β cell death in the presence or absence of IL8 treatment. We detected an absolute number of copies of miR-375 and compared the hVIOs control group with the hVIOs treated with IL-8. The microenvironment plays a crucial role in maintaining islet viability and our results show, during the MP, similar kinetics as expected, given that treatment has not yet started. During the TP, we don't observe any β cell death in either control hVIOs or in hVIOs treated with IL-8 (Fig.20A), suggesting that eventually, IL-8, in the absence of the immune system or during the engraftment process, is not affecting β cell death.

We translate the number of copies into the percentage of β-cell death, and the peak corresponds to about 25% β cell death in hVIOs with IL-8 (day=0 0±0; day=1 1±0,632; day=3 17,368±8,378, day=5 4,334±3,378; day=7 0,206±0,206; day=9 0,018±0,018; day=11 0,026±0,026; day=13 0±0, day=14 0,002±0,002) and about 25% in hVIOS controls treated (day=0 0.002±0.002; day=1 1,202±0,734; day=3 27,482±13,707; day=5 5,998±4,348; day=7 0,61±0,402; day=9 0,004±0,004; day=11 0,002±0,002; day=13 0±0; day=14 0,002±0,002) during the MP (Fig.20B). This result is important because IL-8 is typically thought to promote β cell death in the islet field. Here, IL-8 treatment on HI does not affect β cell survival.

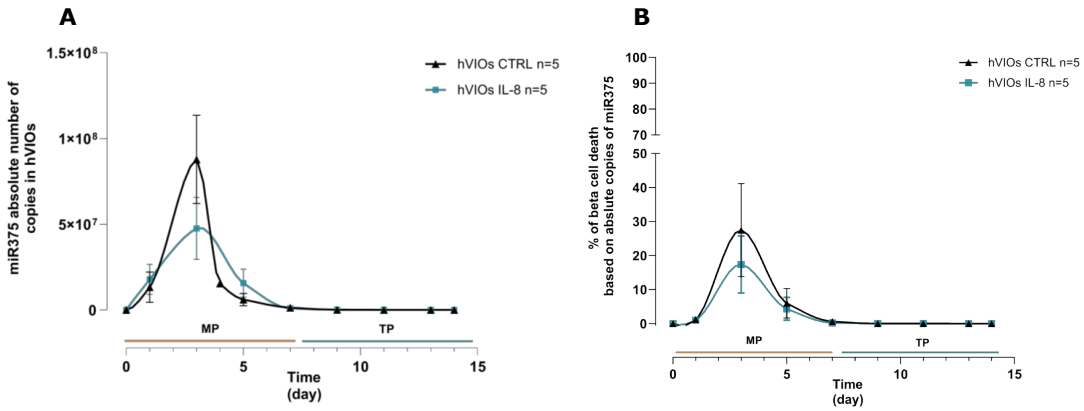


Figure 20: Analysis of β-cell death by miR-375 during the TP: A) Analysis of the release kinetics of miR-375 absolute copy numbers in hVIOs during MP and TP, comparing the hVIOs treated with IL-8 and the control hVIOs(n=5); **B)** Conversion of miR-375 release kinetics from absolute copies into the percentage of β-cell death (n=5).

5.6.3. Evaluation of hVIOs secretory function after IL-8 treatment

Next, we assessed whether IL-8 altered the hVIO's endocrine function.

hVIOs and the islets from the same preparation were tested by dynamic IST in controlled glucose stimuli (2-20 mM) during the TP (n=7_see the table below for the % of purity of HIs, Fig. 21A). Insulin was measured by ELISA assay, and the results were used to describe the hVIO's insulin secretion kinetics. The results indicated an increased trend in insulin secretion during the first phase-peak in hVIOs treated compared to the controls (Fig.21B) (min=9 p=0.0221; 0.863±0.05), suggesting a potential influence of IL-8 on hVIO's insulin secretion capacity. Additional studies will be required to understand the role of IL-8 in islet insulin secretion as a potential inductor in inflamed conditions.

A

hVIOs	% of Purity of HIs
#1	70%
#2	70%
#3	75%
#4	60%
#5	70%
#6	55%
#7	55%

B

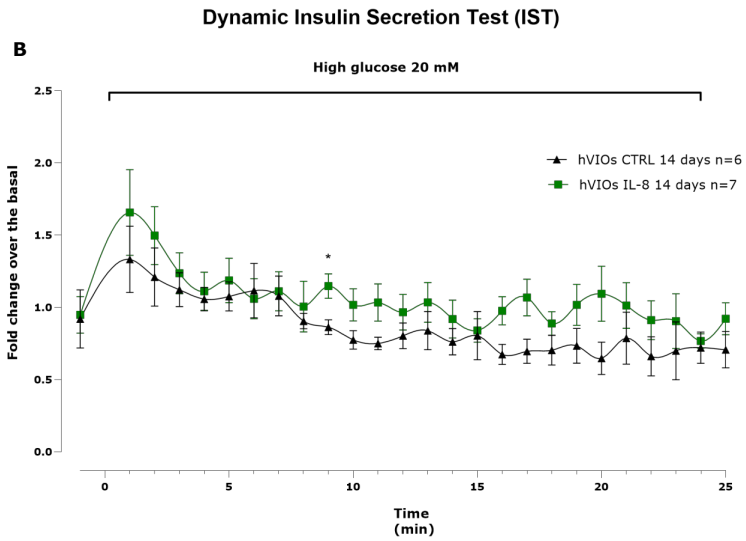


Figure 21: IST during the TP: A) *Table with the purity percentages of HIs preparations;* ***B)*** *Evaluation of hVIOs' endocrine function by dynamic IST upon 7 of chronic treatment with IL-8 (100 ng/ml) or vehicle.*

5.7. FROM IN VITRO TO *IN VIVO*: EVALUATION OF THE VEP AS A POTENTIAL PLATFORM FOR FUTURE CLINICAL APPLICATION

Based on previous laboratory work (Citro *et al*, 2019a), we have decided to test hVIO *in vivo* to evaluate the system's ability to restore normoglycemia in a mouse model. For this study, based on the shortage of organ donation and human islet availability, we decided to use a different source of pancreatic islet for the *in vivo* study. Since we are setting up a new complex technology, we moved to the neonatal pancreatic islets (NPIs). We selected those islets since they have similar i) architecture, ii) composition of human islets, and, once the endocrine activity is matured, iii) the same insulin-secreting performance. From a clinical standpoint, pigs are becoming a clinical reality for organ transplantation thanks to the removal of PERVs and the gene engineering manipulation that may improve their compatibility to the human recipient. As of now, different organs like heart (Fischer & Schnieke, 2022) and kidney(Zhao, 2024) have been clinically transplanted, and recent clinical trials with encapsulated NPI islets demonstrated that pig pancreatic islets may serve to increase the transplant option in the field of T1D. From a bioengineering perspective, we also want to validate our platform in the presence of different endocrine cells with the idea of generating a reliable *in vivo* platform for potential clinical use in the field of β cell replacement. It is important to note that the current supply of organ donors will never be enough to meet the clinical demand. The search for alternative sources of islets for transplantation is ongoing, focusing on stem cell-derived products (Melton, 2021) and pig islets (Kemter & Wolf, 2018). Pigs are the preferred donor species for xeno-islets for several reasons: 1) porcine insulin is effective in humans, 2) pigs have a high reproductive rate and a short generation time, 3) they can be kept under specific pathogen-free conditions, and most importantly, 4) genetic engineering and gene editing tools have been adapted for pigs to address rejection mechanisms, enhance islet function, and reduce the risk of zoonosis (Kemter *et al*, 2018).
Additionally, the isolation of NPIs is simple and can be scaled up for therapeutic use (Kemter & Wolf, 2018),(Kemter *et al*, 2018). The insulin content of NPIs is only 10–20% compared to adult pig islets, and they need to undergo functional maturation to exhibit normal endocrine activity (Hassouna *et al*, 2018),(Li *et al*, 2018). Immature NPIs have been tested in both lab settings and living organisms with the support of natural or artificial ECM components to encourage endocrine maturation. Still, they have not shown immediate, mature function (Mourad & Gianello, 2019),(Katsuki *et al*, 2016). Research suggests that the microenvironment is crucial in cell behavior, differentiation, and function (Hogrebe *et al*, 2020),(Zbinden *et al*, 2021). Therefore,

decellularized organ ECM could positively impact the survival and maturation of endocrine cells/clusters (Hogrebe *et al*, 2020).
First, we assessed the *ex vivo* maturation of NPIs using our scaffold, which we named VEP. Subsequently, we evaluated the *in vivo* performance of VEPs.

5.7.1. Directed self-assembly of VEPs and functional assessment

After 10 days of NPIs *in vitro* maturation, isolated clusters were seeded with BOECs in decellularized lung rat left lobes to bioengineer the VEPs.
We used the same culture protocol to generate hVIO (see paragraph 5.1, Fig. 8B). At the end of this maturation process, we observed a precise spatial organization in the bioengineered organ. It consisted of distinct tissue compartments with a continuous network of human endothelial cells and mature insulin-positive NPIs integrated into the newly formed BOEC vascular bed (Fig. 22A, B).
We further researched the endocrine maturation of NPIs in VEP by analyzing the insulin, glucagon, and somatostatin IF and quantified the fluorescence intensity (Fig. 22B–F). We compared batch-matched NPIs in standard culture to those in VEP on days 1 and 7 (Fig. 22B–F). Our findings showed that on day 7, VEPs exhibited significantly increased insulin staining at the protein level while maintaining glucagon and somatostatin positivity compared to day 1 VEPs (Fig. 22C–E).
Additionally, higher insulin and glucagon fluorescence levels were observed in NPIs seeded in VEP compared to batch-matched NPIs in standard cultures at days 1 and 7 (Fig. 22C-E). In our analysis of INS positivity, we examined several groups across different time points: NPIs on day 1 (n = 56 islets) and day 7 (n = 114 islets), as well as VEP on day 1 (n = 36 islets) and day 7 (n = 71 islets). The comparisons yielded significant differences, particularly between VEP day 7 and NPIs day 1 (p = 2.23e-13) and between VEP day 7 and NPIs day 7 (p = 2.23e-13). Notably, VEP day 1 showed significant differences compared to NPIs day 1 (p = 4.74e-06) and NPIs day 7 (p = 1.98e-05). Additionally, VEP day 1 was significantly different from VEP day 7 (p = 2.23e-07) (Fig. 22C). Turning to GCG positivity, we again analyzed multiple groups: NPIs on day 1 (n = 29 islets) and day 7 (n = 111 islets), alongside VEP on day 1 (n = 77 islets) and day 7 (n = 70 islets). We also found significant differences, particularly between VEP day 7 and NPIs day 7 (p = 4.5e-07) and between VEP day 7 and NPIs day 1 (p = 6.65e-05). Additionally, comparisons between VEP day 1 and NPIs day 7 (p = 9.59e-06), as well as VEP day 1 and NPIs day 1 (p = 4.72e-04), also showed significant results (Fig. 22D). Finally, for SST

positivity, we looked at NPIs on day 1 (n = 56 islets) and day 7 (n = 110 islets), and VEP NPIs on day 1 (n = 41 islets) and day 7 (n = 69 islets) (Fig. 22E). Overall, these findings indicate robust differences in positivity across time points and conditions, highlighting the dynamic nature of the islet response during the experimental timeline.

This confirms that the presence of the vascularized ECM induces maturation.

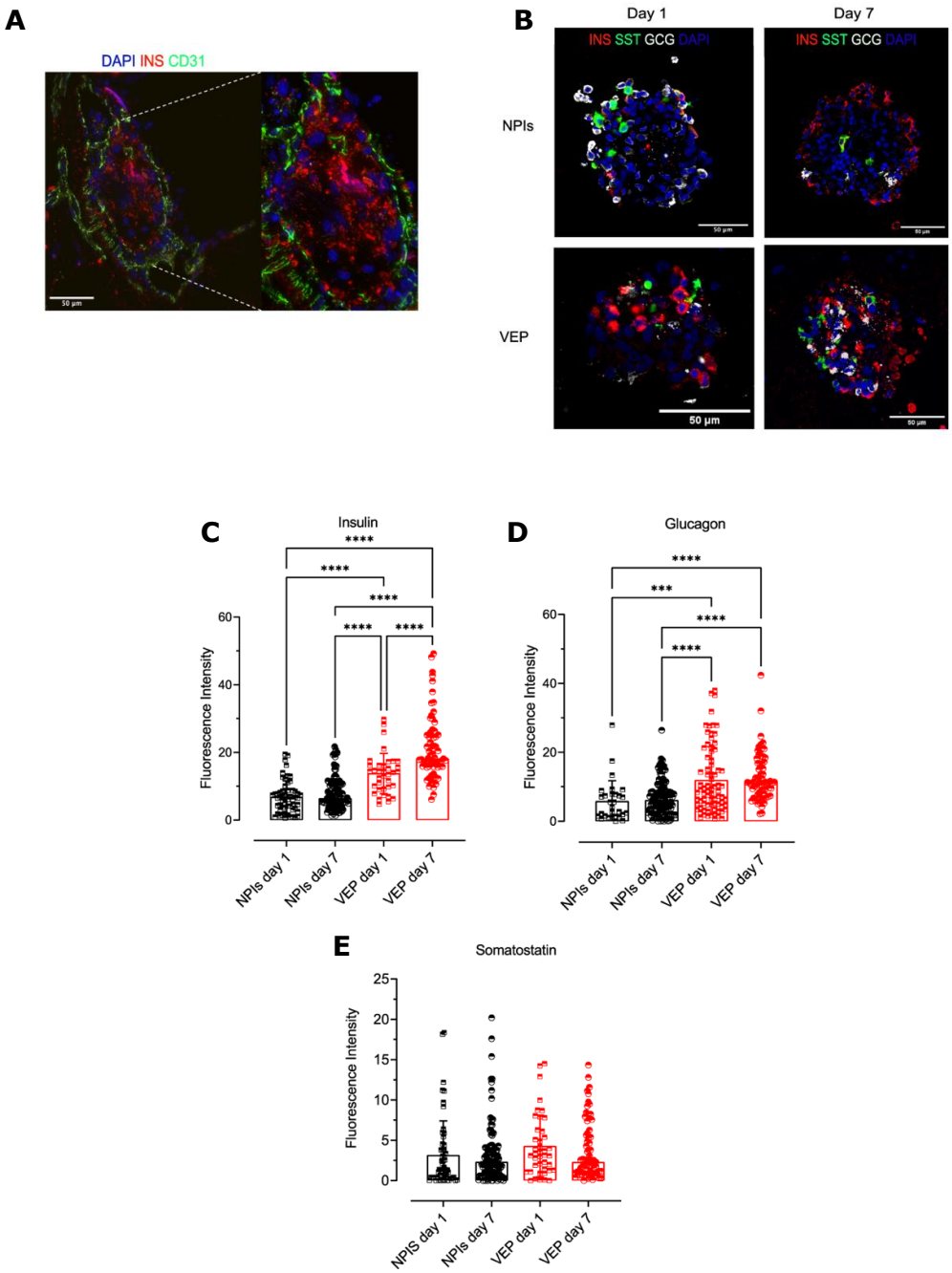


Figure 22: VEP assembly and endocrine maturation assessment: ***A)*** *Representative immunofluorescence of 7 days mature VEP after culture in a bioreactor system. (INS-red, CD31-green, DAPI-blue) Scale bars in µm;* ***B)*** *Immunofluorescence comparison of 1 (left) and 7 days (right) batch matched NPIs alone or in VEP. (INS -red, STT- green, GCG-white, DAPI-blue) Scale bars in µm;* ***C-E)*** *INS, GCG, and SST immunofluorescence intensity quantification on VEP (day 1 and day 7) and batch-matched NPI (day 1 and day 7) one-way ANOVA for multiple comparisons corrected by Tukey, values presented as mean ± SD.*

We also examined the endocrine function of VEPs. We evaluated NPIs using a dynamic IST in VEPs and compared them to NPIs cultured in standard conditions on day 7 (see Fig. 23A–C). When exposed to high glucose concentration (20 mM), VEPs (n = 8) demonstrated a regular insulin release, while NPIs (n=10) in standard culture conditions did not show a coordinated insulin response. Additionally, VEPs released significantly higher levels of insulin, as shown by the point-by-point analysis (VEP vs. NPIs min 2 p=0.026; min 3 p<0.0001; min 4 p=0.0002; min 5 p = 0.0155; min 7 p = 0.0085). The peak of insulin release during the initial phase was significantly higher in matured VEPs compared to NPIs in standard culture conditions (min 3: VEP fold change 2.02 ± 0.43 vs. NPIs fold change 0.89 ± 0.03; p < 0.0001). A significant difference was also observed in the second phase of insulin secretion (min 7: VEP 1.27 ± 0.3 vs. NPIs 0.74 ± 0.32 fold-change; p = 0.0085, see Fig. 21A). The Area Under the Curve (AUC) of insulin release during the insulin response was significantly higher in both phases for VEPs (n=8) (AUC VEP first phase: 3.43 ± 0.9; second phase: 2.37 ± 0.5) compared to NPIs (n=10) in standard culture conditions (AUC first phase NPI 1.6 ± 0.2, p < 0.0001; second phase: 1.43 ± 0.5, p = 0.0031, see Fig. 23B).

Additionally, comparisons of batch-matched VEPs (n = 5) at 7 and 14 days of culture demonstrated preserved biphasic insulin secretion kinetics, along with a trend of improving overall insulin production over time (Fig.23C).

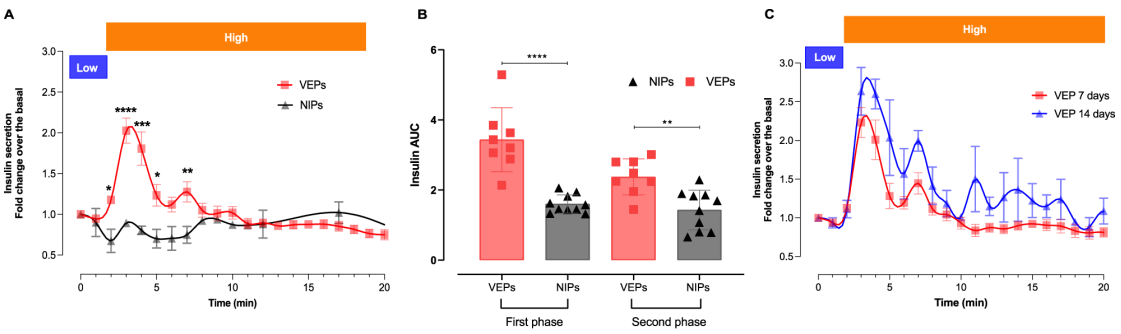


Figure 23: Ex vivo functional evaluation of VEPs: A) *IST of VEPs (red line, n = 8 scaffolds) vs. NPIs (black line, n = 10, NPIs preparations) after 7 days of culture in the presence of 2 mM and 20 mM glucose. Values are expressed as fold change over the basal;* ***B)*** *AUC analysis of IST. Analysis of VEPs (n = 8 scaffolds) and NPIs (n = 10 NPIs preparations) performance within the first and second insulin secretion phase after glucose stimulus. Mann-Whitney U test, Values presented as mean ± SEM;* ***C)*** *IST of VEPs (n = 5 scaffolds) after 7 or 14 days of culture. Values are presented as mean ± SEM.*

5.7.2. VEP performance after transplantation into diabetic mice

The mature VEPs were tested *in vivo* using a preclinical model of severe diabetes in immune-compromised NSG mice (see Fig. 24). The performance of the VEPs was compared to batch-matched NPIs that were transplanted in different ways: in a device-less, pre-vascularized subcutaneous pouch (DL-NPI_ (n = 8), under the kidney capsule (KC-NPIs_ n=10), or in the liver through the portal vein (LV-NPIs_ n=4) (Fig. 24A). As previously reported(Citro *et al*, 2019a), the VEP was divided longitudinally into two different portions to facilitate organ integration within the unmodified subcutaneous implantation area and anastomosed the VEP's to the recipient vasculature in subcutaneous site (Fig. 24A). The function of the graft was monitored by measuring glucose levels over 9 weeks for DL-NPIs and LV-NPIs, and over 18 weeks for KC-NPIs and VEPs experimental groups. The non-fasting blood sugar levels in mice with VEP implants were significantly lower compared to the other groups (VEP vs. DL-NPIs p = 4.98e-39; VEP vs. KC-NPIs p = 3.85e-29 and VEP vs. LV-NPIs p = 2.01e-25; using a general linear model with repeated measures corrected by Bonferroni, as shown in Fig. 24B). It is worth noting that 37% of mice with VEPs did not need insulin pellets because their endocrine cells matured quickly, and the graft functioned immediately after implantation. Conversely, all animals in the other experimental groups exhibited suboptimal glucose control, requiring insulin pellets (p = 0.025, chi-square test). In the follow-up, all 20 out of 20 (100%) VEP-implanted mice achieved normal blood sugar levels. In comparison, only 1 out of 8 (12.5%) DL-NPI-implanted mice, 4 out of 9 (44.4%) KC-NPI-implanted mice, and 1 out of 4 (25%) LV-NPI-implanted mice achieved normoglycemia. The median time to achieve normal blood sugar levels was 3 ± 0.6 days for VEPs, 65 ± 5.55 days for KC-NPIs, and ≥ 60 days for DL-NPIs and LV-NPIs (p < 0.0001, log-rank analysis) (Fig. 24C). An oral glucose tolerance test was performed in all groups 9 weeks after transplantation (Fig. 24D). After glucose loading, VEP mice (n=5) showed significantly lower blood glucose concentrations compared to DL-NPI mice (n=3) (AUC VEPs vs DL-NPIs p = 0.0463), confirming the superior function of the engrafted scaffold (Fig. 24D, E). At 9, 14, or 18 weeks of follow-up, the VEPs were explanted to confirm the graft’s contribution to the mice’s glucose control.

As expected, immediately after the removal of VEP, the mice returned to a diabetic state and exhibited hyperglycemia for at least an additional week (see Fig. 24B)

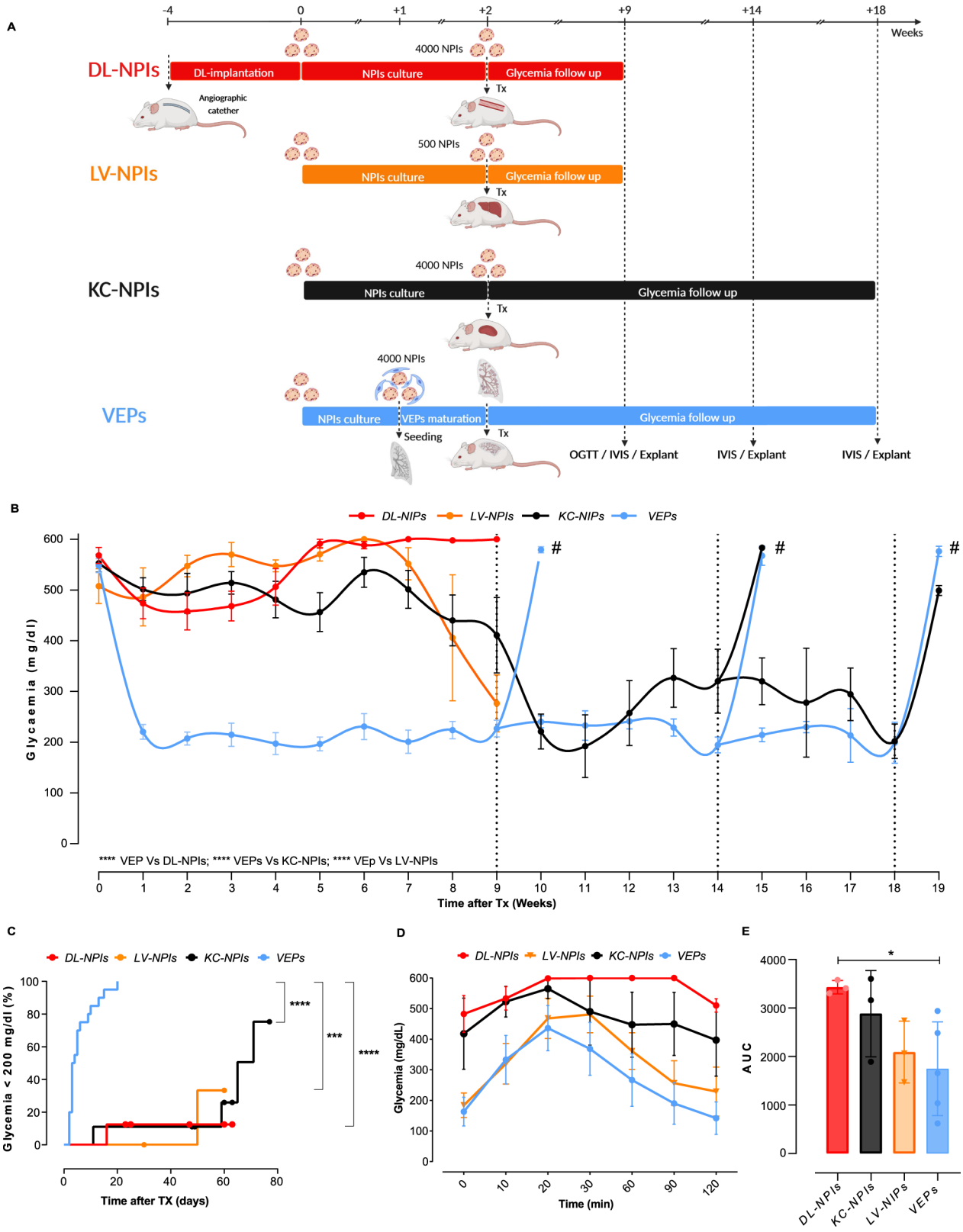

A
-4
0
+1
+2
+9
+14
+18
Weeks
DL-NPIs
DL-implantation
NPIs culture
Glycemia follow up
4000 NPIs
Tx
Angiographic catether
LV-NPIs
500 NPIs
NPIs culture
Glycemia follow up
Tx
KC-NPIs
4000 NPIs
NPIs culture
Glycemia follow up
Tx
VEPs
4000 NPIs
NPIs culture
VEPs maturation
Glycemia follow up
Seeding
Tx
OGTT / IVIS / Explant
IVIS / Explant
IVIS / Explant
B
DL-NIPs
LV-NPIs
KC-NIPs
VEPs
Glycaemia (mg/dl)
#
**** VEP Vs DL-NPIs; **** VEPs Vs KC-NPIs; **** VEp Vs LV-NPIs
Time after Tx (Weeks)
C
DL-NPIs
LV-NPIs
KC-NPIs
VEPs
Glycemia < 200 mg/dl (%)
****
***
****
Time after TX (days)
D
DL-NPIs
LV-NPIs
KC-NPIs
VEPs
Glycemia (mg/dL)
Time (min)
E
*
AUC
DL-NPIs
KC-NPIs
LV-NIPs
VEPs

Figure 24: Long-term in vivo performance of VEPs: A) *Schematic representation of in vivo experimental protocol;* ***B)*** *Weekly not fasting glycemia profile comparison between DL-NPIs (red, n = 8 implantations), LV-NPIs (yellow, n = 4 implantations), VEPs (blue, n = 20 implantations) and KC-NPIs (black, n = 10 implantations) for 9, 14, or 18 weeks follow up (# represents graft explants: 9 weeks VEP n = 4 explants; 14 weeks KC-NPIs=1 explants; VEPs n = 4 explants; 18 weeks KC-NPIs n = 3 explants, VEPs n = 2 explants). Values are presented as Mean ± SEM. general linear model for repeated measures corrected by Bonferroni;* ***C)*** *Kaplan Mayer analysis of the percentage of mice reaching normoglycaemia (≤200 mg/dl). Differences between VEPs, DL-NPIs, KC-NPIs, and LV-NPIs were estimated by the Log Rank test adjusted for multiple comparisons with the Benjamini & Hochberg method;* ***D)*** *VEPs (n = 5 mice), DL-NPIs (n = 3 mice), KC-NPIs (n = 3 mice) and LV-NPIs (n = 3 mice) OGTT performance 9 weeks after transplantation. Values presented as mean ± SEM;* ***E)*** *OGTT AUC over 120 min at 9 weeks after implantation (n = 5 in VEPs mice, n = 3 in DL-NPIs mice, n = 3 in KC- NPIs mice and n = 3 LV-NPIs mice); one-way Anova for multiple comparisons corrected for Dunn's. Values are presented as mean ± SD.*

The harvested VEPs showed that the engineered structure was fully integrated into the subcutaneous space (Fig. 25A, B). The VEP structure was clearly identifiable, with blood-perfused vascular structures of various sizes found within its architecture (Fig. 25A, white arrows). We conducted an analysis of vascular density in explanted VEPs at 1 (n = 2 explants), 2 (n = 6 explants), 4 (n = 6 explants), 9 (n = 6 explants), 14 (n = 7 explants), and 18 (n = 3 explants) weeks. Capillaries and vessel nodes were tracked and measured using the unbiased ANGIO TOOL 64 version 0.6a software(Zudaire *et al*, 2011) (Fig. 25B, C). The results indicated a significant increase in vascularization over time, with a surface vessel density of 12.53 ± 3.58% at 2/4 weeks compared to 32.26 ± 5.78 and 36.37 ± 2.37 at 14 weeks ($p < 0.0001$) and 18 weeks ($p < 0.0001$), respectively (ANOVA for multiple comparisons). Furthermore, IF analysis of VEPs at 9 weeks revealed the presence of both human and murine endothelium within the implanted organ's vascular architecture (Fig.25D).

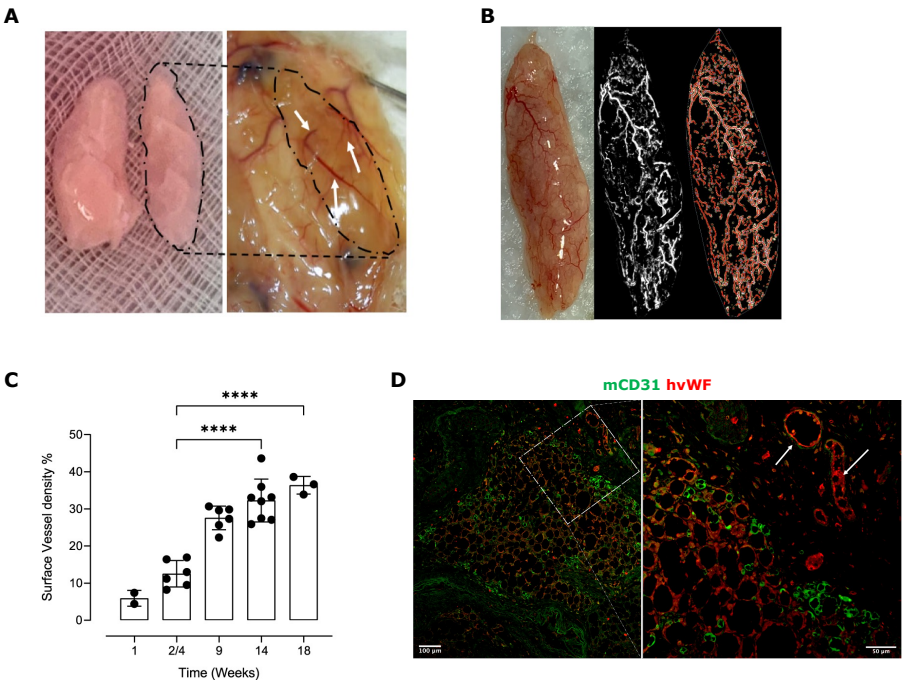


Figure 25: Long-term in vivo analysis of VEPs grafts: A) *Image of VEPs pre-transplant and gross pathology 9 weeks after transplantation;* ***B, C)*** *Vascular density analysis:* ***B)*** *gross pathology of 9 weeks VEP explants and its computational software analysis of vascular VEP surface;* ***C)*** *percentage of VEP surface vessel density 1, 2/4, 9, 14 and 18 weeks after implantation. Values are summarized as mean ± SD. One way ANOVA for multiple comparisons corrected by Tukey;* ***D)*** *IF 9 weeks after implantation, vascular structure was stained for human (hvWF- red) and murine (mCD31- green) endothelial cells.*

5.8. VEP as a model to study in endocrine niche leucocyte trafficking: evaluation of T cell-mediated β-cell damage

Baes on the VEP *in vivo* results, we preliminary start to move a step forward in the clinical application. We decided to investigate if the platform is able to reveal a possible xeno-reaction in an *ex vivo* setting. This will help, from a bioengineering perspective, in tuning the platform to escape possible immune recognition and generate a more immune-protected device. As a first step, we evaluate the possible xeno-reaction against NPIs in the presence of human PBMCs syngeneic with BOEC but pre-activated with pig splenocytes, syngeneic with the islet, via co-culture; then, we added the pre-activated PBMCs to the NPIs islets labeled with Vybrant DiO-488.

Before starting the analysis, we add Propidium Iodide (PI) to detect the NPI's death (see paragraph 7.18 in material and methods for technical details).
Using the Incucyte Basic analyzer tool, we detected the percentage of death in the fluorescent area of the islets in yellow (NPIs in green + PI in red) on the percentage of the fluorescent area of the islets in green. The assay ends after 4 days.
We compared the death of NPIs without PBMCs (as control_ n=1) to that of NPIs with PBMCs (n=3), and our results show a positive trend in the death of NPIs in co-culture with pre-activated PBMCs compared to the control after 24 hours from the start of the assay up to 96 hours (Fig.26A).
The Area Under the Curve (AUC) analysis revealed that the NPIs + PBMCs group exhibited an average AUC of 495 ± 44, while the control group showed an AUC of 191 ± 0. This suggests that the AUC for PBMCs + NPIs is more than double that of the control, highlighting a rising trend in NPI death (Fig.26B).
We measured miR-375 exclusively at the 48-hour mark. The control group (n=1) exhibited 20% β-cell death, while the NPIs + PBMCs group (n=2) exhibited 40% β-cell death (Fig. 26C). At this time point, the death trend indicated by the AUC is confirmed.
Once the Incucyte assay was completed, we performed an IF, and as shown in Figure 26 D, the control does not present the leukocyte infiltrate. In contrast, in Figure 26E, we can see how the CD3 cells surround the islet, inducing the destruction of the latter, which is also confirmed by the insulin staining, which is no longer inside the islet (Fig. 26D) but dispersed around it (Fig.26E).

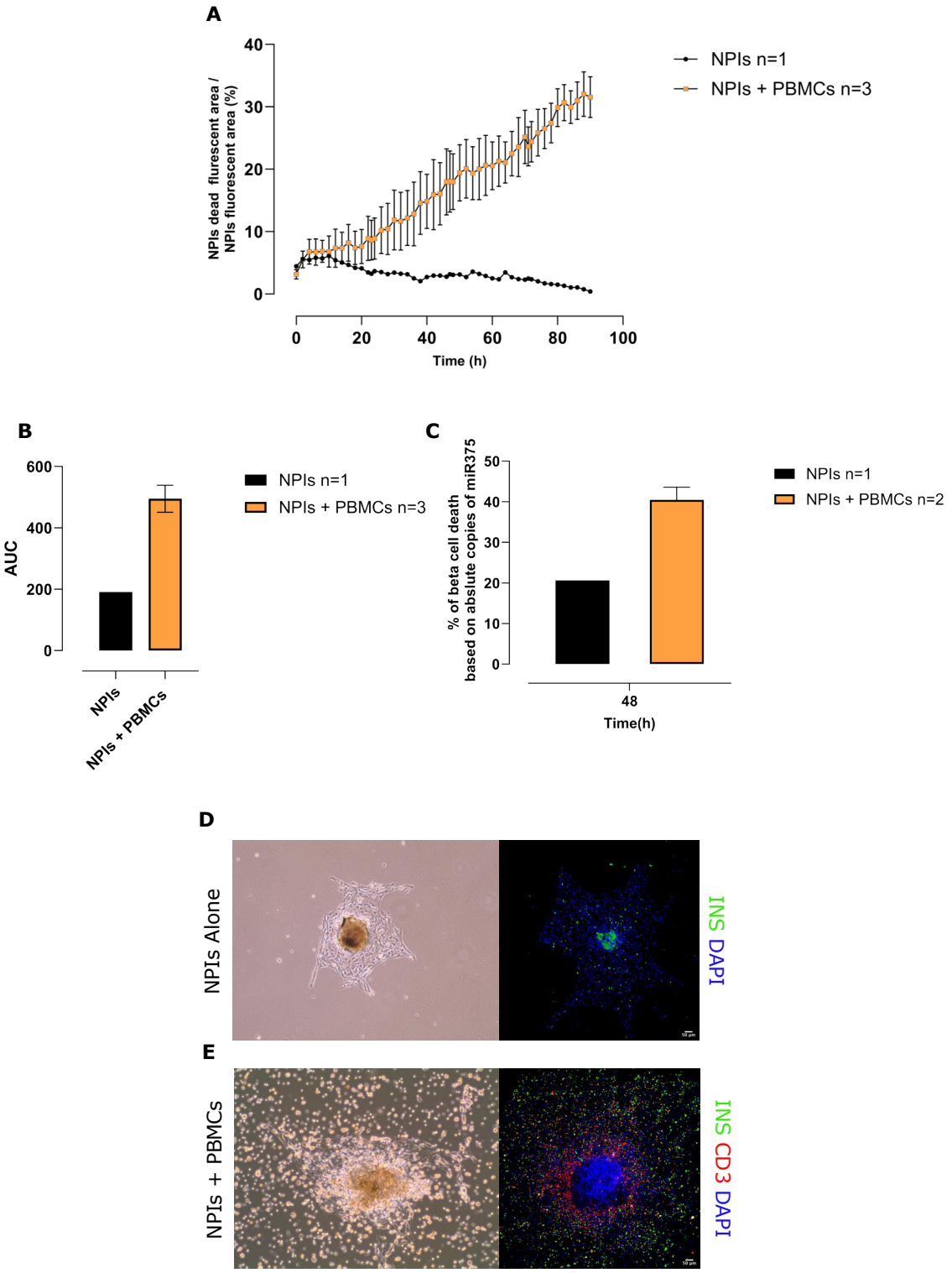


Figure 26: Leukocyte trafficking in an in vitro model: A) *Incucyte Basic analyzer tool to detect the NPIs dead fluorescent area/NPIs fluorescent area (%) (NPIs CTRL n=1, NPIs + PBMCs n=3);* ***B)*** *Quantification of miR-375 by Digital PCR at 48 hours of Incucyte Basic assay;* ***C)*** *Incucyte Basic analyzer AUC (n = 1 in NPIs, n = 3 in NPIs + PBMCs);* ***D)*** *Image of NPIs Alone after 96 hours of Incucyte Basic assay (bright-field image on the right and IF image on the left);* ***E)*** *Image of NPIs + PBMCs after 96 hours of Incucyte Basic assay (bright-field image on the right and IF image on the left.*

Based on the *in vitro* preliminary results as control of the reaction, we conducted a preliminary test on activated PBMCs, syngeneic to BOEC, and xenogeneic vs NPIs within the VEP. In this setting, we intentionally used PBMCs syngeneic to the endothelial compartment to avoid immune recognition against VEP cell components mimicking the transplantation setting where the transplant recipient may serve as a BOEC donor. Thus, the only immunologically reactive VEP compartment may be represented by the NPIs. PBMCs, stimulated against pig cells and labeled with CFSE, were perfused through the PA and circulated throughout the VEP structure. The miR-375 profile helps in monitoring the xeno-reaction. As expected from previous results, after the engraftment process, no miR-375 copies were found in the VEP after 7 days of culture. Accordingly, on day 7, we perfused $5x10^6$ pre-activated PBMCs through the PA to observe the potential β cell death (n=2; Fig. 27A). These initial experiments aimed to track both i) leukocyte trafficking and ii) the timing of β cell death in the VEP architecture with the presence of WT NPIs. As detailed below, VEP structures were observed for 7.5 days. A notable increase in miR-375 levels was detected within the first 12 hours after seeding the pre-activated PBMCs (Fig. 27B). Preliminary histological assessments of leukocyte interactions with VEP compartments showed $CFSE^+$ cells within the vascular network and in intra-/peri-NPI regions (Fig. 27C).

Based on this positive preliminary experiment, we plan further examinations of the VEP over extended time points to assess the overall infiltration window in our model.

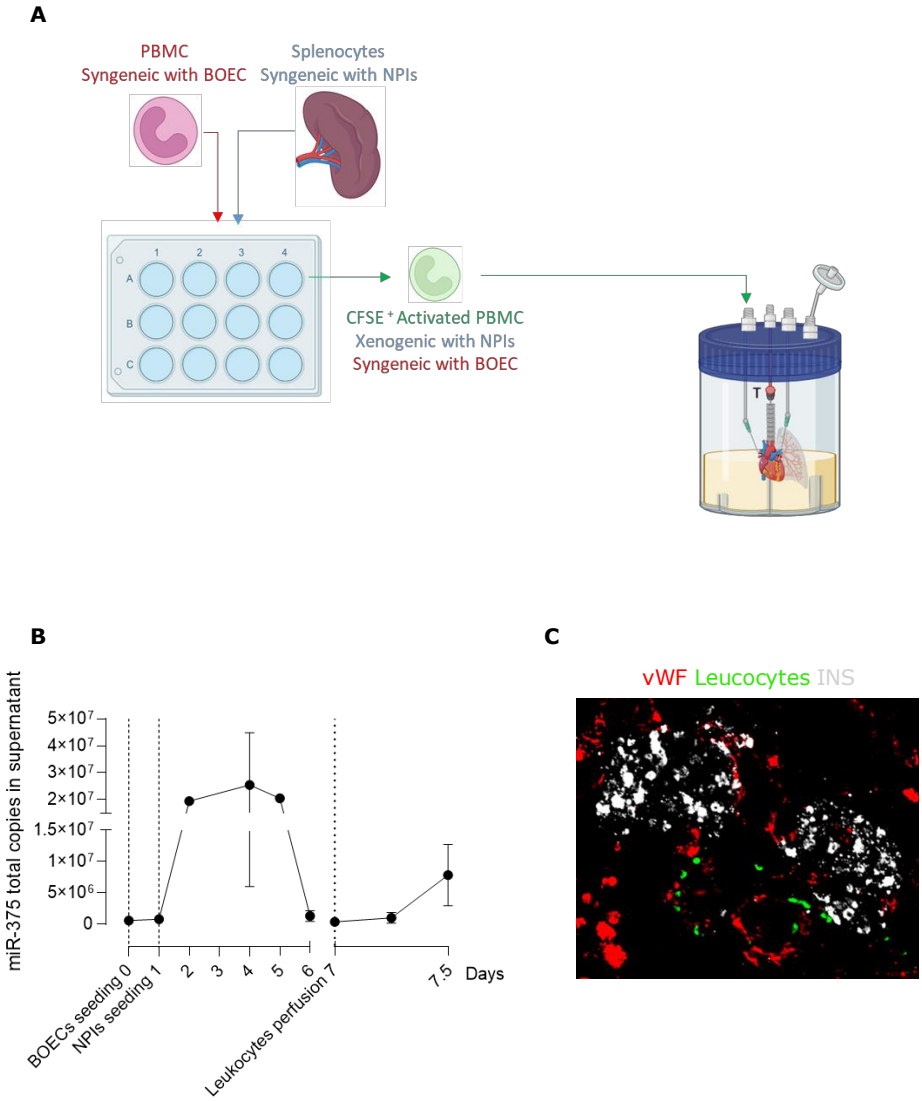


Figure 27: Leukocyte trafficking in VEP: A) A representative scheme of VEP xenogeneic immune response experimental flow; **B)** miR-375 kinetics within VEP maturation (7 days) and after leukocytes infusion; **C)** Representative IF of 7 days VEP with mature NPIs (INS-white), BOEC vascular structure (hVWF - red) perfused with activated leucocytes CFSE⁺ (green).

6. DISCUSSION

One of the major goals in diabetes bioengineering is the possibility to create innovative technology with a dual identity: i) to study *in vitro* and ii) to treat *in vivo* diseases. In the last few years, the endocrine pancreas has been used as an organ template to model technologies for studying or treating different disorders. Recent advances in the field of human endocrine disorders *in vitro* have been limited by the fact that the human pancreas is an organ that is not easily accessible for studying the effectiveness of real-time treatments, as well as the metabolic and immunological features. Currently, research on humans is limited to evaluating changes in biomarkers in peripheral blood and examining post-mortem tissue slices or pancreatic islets. This limited access makes it challenging to directly observe the molecular mechanisms involved in the progression of endocrine disorders. Although murine models such as NOD and Lep/r$^{ob/ob}$ are available, they do not fully replicate humans' metabolic and immunological features, restricting the clinical application of preclinical discoveries. Most *ex vivo* studies on pancreatic endocrine (dys)function involve evaluating the endocrine response of healthy isolated islets cultured in a petri dish with different molecules or stimuli (Henquin, 2021). However, under these conditions, islets rapidly lose their viability and function (i.e., secretion kinetics and magnitude) (Milojević *et al*, 2021),(Misler, 2010). The causes of this loss of functionality are widely recognized as related to their primary phenotype and lack of the native pancreatic environment composed by ECM and vascular network. This network is defined in terms of hierarchical distribution and caliber, providing physiological perfusion, as well as the lack of proper biochemical and mechanical ECM cues (Llacua *et al*, 2018). Additionally, the absence of vasculature prevents the preservation of the native inter-islet communication network, failing to replicate the physiological control over islets' secretory activity (d Oliveira *et al*, 2014). Therefore, an ideal engineered platform to study pancreatic endocrine disorders, with direct relevance in an *in vivo* setting, should allow whole islets to be seeded into a space that maximizes their interaction with proper ECM cues and a dense vascular network, promoting physiological-like perfusion and inter-islet communication (Citro *et al*, 2019a). This will allow the generation of an *ex vivo* perfusable endocrine device and possibly reduce the *in vivo* engraftment time.

The tissue engineering field has attempted to address this need by developing 3D bio-printed scaffolds (such as double-layered 3D bio-printed scaffolds to combine more cell types) (Abadpour *et al*, 2023) and OOC devices (such as human pancreas-on-a-chip technology) (Abadpour *et al*, 2020). However, these systems either lack a

native hierarchical organ vascular network and/or the proper physical/biochemical cues of the native organ ECM (Rogal *et al*, 2019),(Gurlin *et al*, 2021). Recent evidence has shown that ECM single components or ECM-derived hydrogels improve islets' function over long-term cultures, emphasizing the relevance of ECM cues in preserving pancreatic islets' functionality *ex vivo* (Henquin, 2019). In this context, whole organ decellularization supports the native tissue framework for endocrine regeneration by protecting the organs' ECM proteasome (He & Callanan, 2013), architecture, and vascular basement membrane (Ott *et al*, 2010). Various studies have demonstrated that decellularized organs can be repopulated with specialized cells to improve their function. This is achieved by utilizing suitable ECM cues and direct organ perfusion in a customized bioreactor. In 2019, our group successfully repurposed decellularized rat lung-left lobes into the endocrine pancreas using VIO technology. We utilized the decellularized rat lung left lobe as a template to re-engineer the endocrine side of the pancreas, taking advantage of its composition and architecture resembling the endocrine niche. By seeding endothelial cells and murine islets, we were able to reconstitute vascularized islet niches within the lung structure. This work demonstrated the successful integration of pancreatic islets into the bioengineered vasculature, improving β cell survival and function both *ex vivo* and *in vivo*. It has been extensively proven that appropriate ECM support combined with physiological perfusion positively impacts islets viability and functionality (Rogal *et al*, 2019),(Abadpour *et al*, 2020).

This project aims to advance the VIO technology by creating a human version called hVIO. This technology is based on human subjects' endothelial cells and pancreatic-isolated islets. Our goal is to develop a reliable and easily accessible *ex vivo* extracorporeal platform for studying endocrine disorders. To create an effective model for studying endocrine (dys)function, we carefully selected the cellular components for engineering the hVIO compartments based on their clinical relevance for future investigations. We utilized BOECs for the vascular compartment. The efficiency of isolation can be affected by the donor's colony formation capacity, but BOECs have several advantages over other sources of endothelial cells. They can be easily isolated from healthy and diabetic patients (Coppens *et al*, 2013),(Olgasi *et al*, 2021),(Mathur *et al*, 2019). Additionally, BOECs have a high proliferative capacity and can promote the formation of new blood vessels in immunodeficient mice (Hoshi *et al*, 2013), indicating their direct involvement in vessel formation. They have also been suggested for treating hemophilia in gene therapy approaches (Olgasi *et al*, 2021; Lin *et al*, 2002).

Furthermore, BOECs can be modified to express specific factors, making them an attractive option in a GMP setting (Olgasi *et al*, 2021). Lastly, BOECs can release therapeutic agents directly into the bloodstream due to their direct connection to the vascular system (Mathur *et al*, 2021). Incorporating these cells into hVIOs will enhance the compatibility of the scaffold, as the vascular compartment can comprise the patient's endothelial cells.

For the endocrine compartment, we adopted two different clinically relevant sources of endocrine cells: i) human islet for the *ex vivo* model and ii) NPIs for the *in vivo* application. In both cases, the platform has been validated and matured for 7 days *ex vivo* in a bioreactor and tested *in vitro* or *in vivo* according to the endocrine cells used. The use of alternative endocrine cells in our platform is linked to the scarcity of human pancreas and the possibility to validate the plasticity of our technology in the presence of different endocrine cells.

However, we have opted HIs for the *in vitro* model as the best clinical option to mimic the human endocrine pancreas structure *in vitro*. Human pancreatic islets are widely recognized as the gold standard for *ex vivo* evaluation in diabetes, making them the optimal endocrine source to assess hVIO performance during the *ex vivo* engineering process (Henquin, 2021). Recently, the field of bioengineering β cell replacement is moving in using alternative cell sources to the human islet (i.e., stem cells or pig islet) to overcome the classical limitation of the scarcity of the organ donation. However, to effectively create an *ex vivo* model that accurately represents the endocrine part of the pancreas, we need a cellular source that closely mimics human pancreatic islets. Stem cells reprogrammed into β cells replicate only the insulin-secreting cells, and neonatal pig islets lack the maturity to reflect HIs. These limitations prevent us from utilizing this model, for instance, in testing drugs for T2D. Therefore, we choose the optimal available option using the HIs for the *in vitro* component of creating a study model.

In the *in vivo* aspect, aligning with the recent clinical applications of genetically engineered pig organs, hVIO translational research has been confirmed through alternative endocrine sources like NPIs. These are an invaluable and abundant source of insulin-producing cells, showing promise for future clinical use if isolated from genetically modified pigs designed to prevent transplant rejection.

Regarding the use of hVIO as an *ex vivo* model, our first milestone, was to assess the platform's ability to support the viability and functionality of islets during long-term culture. We established a specific timeline for evaluating the structure and function of hVIO. Our results showed that a 7-day dynamic culture is necessary for

the structural and functional maturation of hVIO's endocrine and vascular compartments. This maturation remains stable for an additional 7 days. At the end of the maturation phase (d1-d7), hVIOs exhibited significantly improved endocrine survival and function compared to batch-matched HIs in early time points.

Furthermore, the hVIOs' endocrine performance improved progressively over the culture period, demonstrating a more stable second phase of insulin secretion at day 14 compared to day 7. These findings align with previous literature and demonstrate that combining the endocrine niche's three independent building blocks (ECM, vasculature, endocrine mass) and dynamic perfusion via the native organ vasculature preserves islet viability and function. This is a significant achievement as primary HIs have typically been tested for short time points immediately after isolation. We have shown that having a specific environment can greatly decrease the β cells death and maintain the function of islets for 14 days. As another achievement, we have demonstrated that endothelial cells derived from the peripheral blood of healthy donors can re-line the vasculature of a decellularized rat lung left lobe within 7 days, forming a stable, functional endothelial layer lasting at least 7 more days. Overall, our platform not only facilitates the spatial integration of the vascular and endocrine compartments during the last 7 days of culture but also enhances their function.

As a preliminary analysis, spatial transcriptomics provided interesting data. Regarding the endothelial component, the canonical endothelial genes, such as CDHR5, VEGFC, VEGFD, KDR, and VEFGA are expressed throughout the culture period. Additionally, five genes associated with pro-angiogenic activity (CTSS (Xu *et al*, 2023), PUM1 (Dai *et al*, 2022), TARS1 (Barai & Chen, 2024), LOXL1 (Xie *et al*, 2017), and PTBP1 (Liu *et al*, 2023)) showed increased expression on both day 7 and day 14, using day 1 as a reference (gene expression was measured by fold change). Another noteworthy gene, GJA1 (Behrens *et al*, 2010), also exhibited higher expression levels on days 7 and 14 compared to day 1, suggesting endothelial stability in the system. The KLC1 (Cyrus & Muller, 2016) gene rises during inflammation; specifically, in hVIO, KLC1 levels increase during islet engraftment and, consequently, during MP. Conversely, during TP, the expression of this gene declines. CLECL1 (Thebault *et al*, 2009) is vital for immunity and homeostasis as these proteins can identify pathogens and self-antigens. Our findings reveal an uptick in the expression of this gene during MP, suggesting that the endothelium initiates a protective response against allogeneic pancreatic islets.

We have become particularly interested in the PTGIS (Wang *et al*, 2020) gene. This gene is expressed by pulmonary endothelial cells; in hVIO, its levels rise during MP before declining in TP. This observation may suggest that at an organotypic level,

our endothelium leans more towards pulmonary than pancreatic characteristics. While this preliminary data it is not enough to confirm the hypothesis, we plan to explore this further through additional analyses, as it would be fascinating to understand how hVIO guides BOEC towards a specific phenotype.

Regarding the endocrine component, the canonical islet genes, such as GCG, SST, INS, MAFA, and NEUROD1, are expressed throughout the culture period. Interestingly, RGS2 (Dong *et al*, 2017), a gene implicated in islet survival, and TFAM (Mulder, 2017), a gene involved in islet mitochondrial activity, showed increased expression during the MP and the TP. In conclusion, the islets were positive for IL-8 receptors (CXCR1/2). This is not an overexpression, but this data confirms that the islets within the hVIO express CXCR1/2, as we have also seen from the IFs.

As preliminary consideration, hVIO, in respect to other competitor technologies for *in vitro* study of endocrine function (i.e. OOC and 3D bio-printing) represents a more complex platform based on dedicated form factor able to combine fine tune perfused vasculature in an organ-based 3D fashion. On the other hand, the use of native decellularized large organs requires a consistent amount of cells for both vascular and endocrine compartments, leading to a high complexity of the device handling, assembling and sterility. We can conclude that hVIO could be a valuable tool to test various compounds and investigate endocrine disorders under specific conditions.

We began testing the flexibility of hVIO as an extracorporeal model of the endocrine pancreas. Our first goal was to evaluate hVIO in the presence of an inflammatory stimulus. To do this, we aimed to identify an inflammatory pathway common to both BOECs and HIs.

Recently, the IL-8-CXCR1/2 pathway has been suggested to play a role in the pathophysiology of diabetes as a significant contributor to the disease (Citro *et al*, 2015a),(Citro *et al*, 2012). Our research group has found that IL-8 is the most abundant chemokine released from HIs in culture when isolated. Upon transplantation, its role is to reduce islet function and survival (Citro *et al*, 2012).

Additionally, the IL-8 pathway regulates the endothelium's permeability, viability, and proliferative potential. Before exposing hVIO to IL-8, we checked for CXCR1 and CXCR2 expression in both compartments. We found that BOECs do not express CXCR1/2, while we observed heterogeneous expression of CXCR2 on pancreatic islets. Among the $CXCR2^+$ islets population, the receptor was expressed alone or with insulin, glucagon, or somatostatin, indicating its heterogeneous expression by α, β, and δ cells.

Moreover, the number of $CXCR2^+$ α, β, and δ cells varied among different islet preparations. The biological relevance of this observation has not been clarified yet.

We aim to enhance qualitative immunofluorescence analysis of CXCR1/2 expression with quantitative assessments like Real-Time PCR. Additionally, excluding the inter-donor variability as an experimental artifact, the reduced number of HIs analyzed may not represent the entire islet population (Henquin, 2021). After testing freshly isolated human islet function using a dynamic IST, we found that IL-8 does not negatively affect insulin release during 20-minute high glucose stimulation. The secretion curve of islets treated with IL-8 was similar to islets not exposed to the inflammatory stimulus.

To rule out bias regarding whether IL-8 affects freshly isolated human islets without a native vascularized ECM environment, we used preliminary spatial transcriptomic data and immunofluorescence results showing CXCR1/2 presence on human islets within hVIO. We then tested hVIO with IL-8 stimuli to assess its potential impact on the perfused endocrine niche. Specifically, hVIOs were exposed to a chronic concentration of IL-8 (100 ng/ml) or vehicle during the TP. At the end of the treatment, firstly, we don't observe any β cells death in either control hVIOs or in hVIOs treated with IL-8, suggesting that eventually IL-8 in the absence of immune system (neutrophils expressing CXCR1/2 at high levels), or during the engraftment process, is not affecting β cells death. Regarding the function of hVIOs treated, the results showed an increased trend in insulin secretion during the first phase-peak of insulin release, indicating a possible impact of IL-8 on hVIO's insulin secretion capability. Further research is needed to comprehend the impact of IL-8 on islet insulin secretion as a potential inducer in inflamed conditions.

The observed increase in insulin secretion may result from chemokines' active modification of the insulin secretion process. This is supported by the lack of significant changes in the endocrine compartment, as observed in the immunofluorescence and miRNA-375 analysis. However, further research is necessary to validate these findings. These results are different from the effects of other inflammatory molecules (such as IL-1β, TNF-α, and INF-γ), which, after chronic exposure (less than 36 hours), have been shown to impair insulin secretion and promote apoptosis in β cells (Papaccio *et al*, 2005),(Wang *et al*, 2010).

However, we can conclude that IL-8 plays a role in a specific microenvironment, as its absence of ECM and vascular network does not affect the secretory function of the islets.

Concerning the vascular compartment, we did not observe any alteration regarding permeability and structural integrity. This was expected because BOECs, as Endothelial Colony-forming Cells, do not express the receptors that respond to IL-8 (Blandinières *et al*, 2021).

Once we validated the technology as a model of long-term culture perfusable vascularized islet organ, we decided to test its potential *in vivo* to confirm a possible dual application. As anticipated for this aim, we used neonatal pig islets as relevant alternative endocrine sources in the field of β cell replacement.

Indeed, pigs have embryonic development, anatomy, and physiological blood glucose levels similar to humans. These similarities, along with the feasibility of pig genome engineering and the demonstration that NPIs transplantation can reverse diabetes in adult pigs and non-human primates (Ludwig *et al*, 2017),(King & Bowe, 2016) make NPIs an intriguing endocrine cell source in β cell replacement.

Notably, after isolation, NPIs are not able to functionally produce insulin and require a dedicated culture protocol and/or *in vivo* step to mature into glucose-sensing endocrine-producing cells (Hassouna *et al*, 2018), as evidenced by the late reversal of hyperglycemia after transplantation in preclinical models of T1D (Salama *et al*, 2020),(Wolf-van Buerck *et al*, 2015). For this reason, we tested our technology with an immature source of unlimited endocrine cells to evaluate the ability of the VEP platform to allow not only the vascular engraftment of NPIs within BOECs architecture but also the ability of the technology in improving their functional maturation. To confirm the endocrine maturation, we first investigated the expression of insulin, glucagon, and somatostatin at protein levels. Higher insulin and glucagon fluorescence levels were evident in NPIs seeded in VEP compared to batch-matched NPIs in standard cultures at days 1 and 7. We confirmed that immature NPIs may improve their functional insulin-secreting status over time. Indeed, more interestingly, we discovered that the vascularized ECM significantly boosted NPIs' endocrine maturation within the VEP compared to batch-matched control NPIs, confirming the ability of the vascularized ECM not only in improving the NPIs endocrine status profile but also their functional secreting activity. Indeed, we used a dynamic IST to challenge mature VEP and batch-matched NPIs. We found improved insulin production and mature physiological insulin secretion kinetics at 7 and 14 days of VEP maturation.

Once the platform was engineered in the presence of BOEC and NPIs, we moved *in vivo*. We assessed VEP function in immunodeficient NSG diabetic mice. We compared the performance of NPIs implanted within VEP with NPIs transplanted in other standard sites such as the avascular kidney capsule, the pre-vascularized subcutaneous space (device-less), and the well-vascularized liver. The results showed that VEPs performed significantly better, demonstrating immediate function after subcutaneous implantation and maintaining normoglycemic function throughout the follow-up period (up to 18 weeks). In contrast, NPIs transplanted using the pre-

vascularized subcutaneous space approach failed to reverse diabetes in NSG diabetic mice, possibly due to the high metabolic activity required for functional maturation of the NPIs, which typically takes 6–12 weeks (Kemter *et al*, 2018) *in vivo* and the low oxygenation of the subcutaneous site. The failure of the device-less strategy stresses out the value of VEP, which achieve early function upon transplantation in the subcutaneous site.

As previous reported (Korbutt *et al*, 1996),(Otonkoski *et al*, 1999), the transplantation of NPIs under the kidney capsule successfully reversed diabetes within 8 weeks after implantation, which is a significant delay compared to VEP. In this study, we are also reporting the transplantation of NPIs into the liver for the first time. We encountered a limitation with the NPI implantable mass, which was significantly reduced compared to the other sites. The liver site showed a trend in restoring normoglycemia like the kidney capsule, even when using eight times lower NPIs dose. This confirms that the timing of β cell function after implantation mainly depends on the generation of vascular connection and is partially independent of the implanted mass. These results confirmed that once matured, *ex vivo* vascularized engrafted NPIs may perform faster and better than batch-matched clusters, both matured or not, implanted in different sites even without a pre-vascularized strategy. We also stressed the significance of the vascular connection between the host and implanted graft. Therefore, we evaluated the degree of vascular integration of implanted VEPs during the follow-up. We noted a substantial enhancement in the vascularization of the VEP surface after the implantation, marked by a gradual integration of the vascular structure from the host to the recipient. We noted a substantial enhancement in the vascularization of the VEP surface after the implantation, marked by a gradual integration of the vascular structure from the host to the recipient.

Thus, the VEP platform has been shown to be flexible and capable of being engineered not only with primary mature islets but also with immature endocrine clusters. It has the ability to enhance the endocrine maturation and secretory function of these clusters, both *in vitro* and *in vivo*. This results in immediate functional upon transplantation compared to the control groups.

In conclusion, our system has limitations for clinical use, including the presence of rat ECM and the scaffold's limited size. Therefore, enhancing our system's suitability to leverage its scalability is essential.

A common need of *ex vivo* and *in vivo* systems is their ability to predict the immune activation of the adaptive immune system. For this reason, we used the VEP platform to *ex vivo* trace leukocyte trafficking as a model to predict immune rejection of the

graft *in vivo*. Initially, we established a system to assess the capacity of PBMCs, which were syngeneic with BOECs, to attack NPIs. We cocultured PBMCs, with splenocytes syngeneic with NPIs, to pre-activate the PBMCs against pig antigens. After completing the activation, we conducted a coculture with the PBMCs and NPIs, and through live imaging acquisition, we monitored the death rate. Our observations indicated that the death rate of islets in coculture with PBMCs was doubled respect to control group (NPIs alone), a finding further corroborated by the quantification of miR-375. Additionally, through IF, we noted that CD3 cells performed a peri-insular infiltration contributing to the destruction of islets.

Following the establishment of the lymphocyte activation system, we performed a preliminary experiment by perfusing the pre-activated PBMCs into the VEP via PA. The kinetics of miR-375 allowed us to assess the activity of PBMCs, revealing a peak in islet death 12 hours post-infusion. Immunofluorescence analysis validated the interaction between leukocytes and both compartments of the VEP, including the vascular network and intra-/peri-NPI regions. We will plan experiments to clarify if BOECs also get killed by pre-activated PBMCs with pig splenocytes.

We will extend VEP observation time to evaluate the overall infiltration window and deeply study immune recognition interactions in an *ex vivo* model. Our platform allows us to evaluate leukocyte trafficking by monitoring the progression of the leukocyte infiltrate over time. To date, one way to study T1D is to use pancreatic slices (nPOD) to address immunological issues indirectly.

This will allow us to forecast and prevent *in vivo* immune rejection of the graft.

7. MATERIALS AND METHODS

7.1. EXPERIMENTAL ANIMALS

Experiments involving rats and mice were performed under protocols approved and monitored by the Animal Care and Use Committee of San Raffaele Scientific Institute. 6-8 weeks-old male Lewis rats (175–200 g; Charles River Laboratories) were used as scaffold donors. 6-8 weeks-old NSG female immune-compromised mice (22–25 g; Charles River Laboratories, Calco, Italy) were used as transplant recipients (Citro *et al*, 2023).

7.2. DECELLULARIZATION AND PREPARATION OF LUNG LEFT LOBE SCAFFOLD

Cadaveric rat lungs were removed and perfused for decellularization (Ott *et al*, 2010),(Song *et al*, 2013). After systemic heparinization, the lungs were obtained from male Lewis rats (175–200g, Charles River Laboratories). The procedure involved cannulating the pulmonary artery (PA) with an 18 G cannula (McMaster-Carr), cannulating the pulmonary veins (PV) through the left atrial appendage using a miniball cannula with a tip basket (1.9 mm ID) (Harvard Apparatus), and ligating the aorta. The trachea was cannulated with a 16 G cannula (McMaster-Carr), and the right main bronchus was ligated. After that, the right upper, middle, and lower lobes were tied off and removed (Fig.28)

The cannulated scaffold was placed in a custom-made decellularization chamber by connecting the PA's cannula to the chamber's inlet access using a male luer-lock (Fig.29).

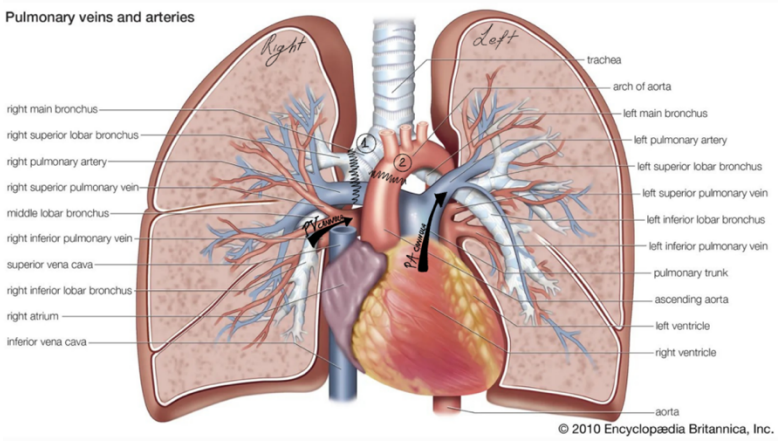


Figure 28: Representation of the lung anatomy: *1 and 2 indicate the previous ligation points for right lobe resection; the black arrows indicate the entry points of the PV and PA cannulas.*

To start the procedure:

1. Connect the inlet and side drain accesses of the decellularization chamber to two tubing lines to create a perfusion circuit from the chamber to a phosphate-buffered saline (PBS) 1x reservoir in the following way:

   a. Connect a perfusion line with incorporated pump tubing and a three-way stopcock.

   b. Connect a return line from the chamber's side drain port to the PBS 1x reservoir.

The three-way stopcock, placed after the pump tubing, allows alternating perfusion of detergent solutions for decellularization and of PBS 1x for washing steps.

2. Secure the perfusion line pump tubing into the peristaltic pump to ensure a closed loop.

3. To prime the system, start the pump to remove all air from the tubing and prefill the organ chamber with PBS 1x.

4. Double-check to ensure luer-lock connections are secured to avoid leaking fluid.

5. Attach an autoclaved modified bottle screw cap to the detergent solution reservoir in a sterile condition, and then attach an intravenous kit to the modified bottle cap.

6. Connect the entire system to the three-way stopcock of the perfusion line.

The process of decellularization involved perfusing the PA (at a constant pressure of 40 mm Hg) with heparinized PBS for 10 minutes, followed by perfusion with 0.1% sodium dodecyl sulfate (SDS) in deionized water for 2 hours, then with deionized water for 20 minutes, and finally with 1% Triton X-100 in deionized water for 20 minutes (Citro *et al*, 2019a) (Fig.30).

The solution reservoirs were connected to a tube extending from the inlet access using a three-way PVDF stopcock with two luer-locks. This setup allowed the inner

inlet to be connected to either the decellularization detergent reservoirs or to form a closed circuit for the final washing step (Fig.29). To remove residual detergent and cellular debris and maintain an aseptic environment, the decellularized scaffolds were washed with PBS 1x supplemented with 1% antibiotics and antimycotics for 72 hours. This perfusion was performed using a peristaltic pump set at a 1 ml/min rate. The perfused PBS was collected for recirculation through the side-drain outlet (Fig.29). All reagents were obtained from Sigma-Aldrich. We excluded scaffolds exhibiting signs of infection, vascular air trapping, or vascular leakage from the study.

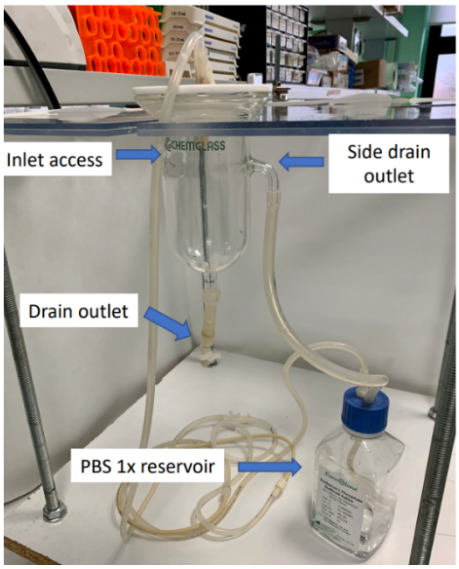


Figure 29: Decellularization chamber and washing circuit.

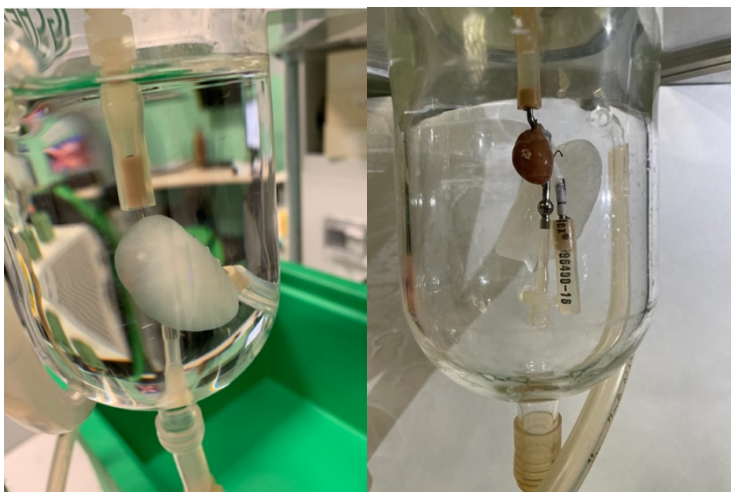


Figure 30: Decellularized rat lung left lobe scaffold

7.3. CELL SOURCES USED FOR hVIO GENERATION

The study used BOECs and isolated pancreatic islets to engineer hVIO's vascular and endocrine compartments.

1) *Vascular compartment:* Blood samples were collected from healthy donors or T1D patients using venipuncture, starting with 40 ml of peripheral blood collected in sodium citrate vacutainer plastic tubes (Olgasi *et al*, 2021),(Ormiston *et al*, 2015). The monocyte fraction was separated through density gradient centrifugation at 300g at room temperature for 20 minutes and then washed twice in PBS. The isolated cells were cultured on CELLCOAT Collagen Type 1-coated tissue culture flasks using MCDB 131 medium containing proprietary supplements (BOEC culture medium – BCM). To reduce expansion time and increase the final cell yield, a cell passaging step was introduced 7 days after the initial isolation of the peripheral blood mononuclear cells (Kolbe *et al*, 2010). The BOEC medium was changed every 2 days, and the cells were monitored until the appearance of the first colonies around day 14-28.

   Once the cells reach confluency, you can detach the BOECs using trypsin, replant them on CELLCOAT, and culture them in MCDB 131 medium, changing the medium every other day to promote colony expansion. BOECs between passages 3 and 8 should be detached with trypsin (TRIPLE express, Gibco) and immediately used for generating hVIO (20×10^6 cells) and for 2D *in vitro* experiments involving CXCL8.

2) *Endocrine compartment:* The Human Pancreas Isolation GMP Islets facility Unit at the Diabetes Research Institute of San Raffaele Hospital isolated human pancreatic islets from the cadaveric pancreas. To ensure consistency among our samples, we only used islet preparations with high purity (>70%) for hVIO generation.

7.4. CHARACTERIZATION OF BOECS' PHENOTYPIC AND FUNCTIONAL QUALITIES

7.4.1. Flow cytometry

Before seeding, BOECs are phenotypically characterized by flow cytometry to confirm the expression of specific endothelial markers and investigate additional markers (e.g., CXCR1/2).

Cells were detached from the cell culture support using trypsin, counted with Trypan Blue dye, and then divided into FACS tubes based on their number.

BOECs were stained for 30 min at 4°C in a dark place with Live Dead Pacific Blue dye (Life Technologies) using 1 µL of dye every 1 × 10^6 cells resuspended in 1 mL of PBS. Live Dead dye can stain selectively dead cells to select a living cell population. Cells are stained for 30 min with primary antibodies in dark at 4 +°C: anti-CD31-APC (1:100, Immunotools, 21270316), anti-CD34-PE (1:100, Immunotools, 21270344), anti-KDR-PE (VEGFR-2) (1:100, Miltenyi Biotech, 130-098- 905), anti-TIE-2-APC (1:100, Miltenyi Biotech, 130-101-606), and anti-VE-Chaderin-PE (1:100, Miltenyi Biotech, 130-100-716). Finally, samples are fixed with 200µL cytofix/cytoperm buffer (ThermoFisher) for 20min. Before every step, samples were washed with FACS Buffer (0,2 % BSA in PBS 1x) and centrifugated at 1500 rpm for 5 min. Samples were acquired on a CytoFLEX S, and the data were analyzed using FlowJo 10.6.2.

7.4.2. Tube formation assay

BOECs' proangiogenic assets were evaluated using the tube formation assay per the manufacturer's protocols for Corning® Matrigel® Matrix.

In short, Matrigel was thawed overnight at 4°C and then mixed with VEGF at a concentration of 200 ng/ml. Subsequently, 250 µL of the prepared matrix was added to each well of 24-well plates. Following a 1-hour incubation period at 37°C, cells at a concentration of 10×10^5 were seeded onto the Matrigel. The formation of BOEC tubes was observed for 16 hours in the presence of BCM containing proprietary supplements. The experiment used angiogenic medium (AM), modified stabilization medium (MSM), and the hVIO two-phase culture media protocol, which consists of 11.5 hours of angiogenic medium (AM) (70% of the culture time) and 4.5 hours of modified stabilization medium (MSM) (30% of the culture time) (Citro *et al*, 2019a). To mimic the two-phase culture media protocol, all groups were initially exposed to the same medium for 11.5 hours, followed by exposure to another medium for 4.5 hours. The cells were rinsed with each media change. Analyses were conducted at the end of the experiment using an inverted phase-contrast microscope (Evos

m7000) to observe tube formation. ImageJ Angiogenesis software was utilized to quantify the mesh size.

7.4.3. Proliferation WST-1 assay

WST-1 assays were conducted on BOECs seeded into 96-well plates at a density of 1×10^3 cells per well. The cells were cultured in either MCDB 131 medium or hVIO two-phase culture media protocol, with 70% of the culture time in AM and 30% in MSM. They were then adapted for either 24 or 48 hours. After 24 or 48 hours, the cells were treated with either BOEC control medium (BCM) or hVIO media protocol. Following this, the media was removed, and the cells were exposed to the WST-1 reagent for 30 minutes. Absorbance was measured at 450 nm using an ELISA plate reader.

7.5. ISLETS EQUIVALENT COUNT

The preparations of isolated islets are highly heterogeneous, containing islets with varying volumes. Therefore, the absolute count of HIs is not a reliable measure of the actual endocrine mass present in the preparation.
As documented in the literature (Henquin, 2019), we standardized the total mass in Islet equivalent (IEQ) present in the preparation and allocated the same IEQ amount to all experimental conditions to address this issue.
The volume of each islet was calculated based on its diameter and then converted to IEQ individually. One IEQ has the volume of a spherical islet with a 150 µm diameter, which typically contains approximately 1000 cells, including 40-60% β cells(Ramachandran *et al*, 2015).
To determine the IEQ, we incubated 50 ul of each isolated islet preparation with 50 ul of Dithizone (DTZ) in a 1:1 ratio. The DTZ solution was prepared at a 0.1 mg/ml concentration in 10% FBS and 10% DMSO in PBS. This allowed us to stain the zinc granules, distinguishing the endocrine mass from any exocrine contaminants present after the isolation process. We then captured images of the stained islets using a 4x magnification on an inverted phase-contrast microscope (Evos m7000) (see Fig.31). Subsequently, we counted the HIs. We referred to the overall mass as the absolute islet mass.

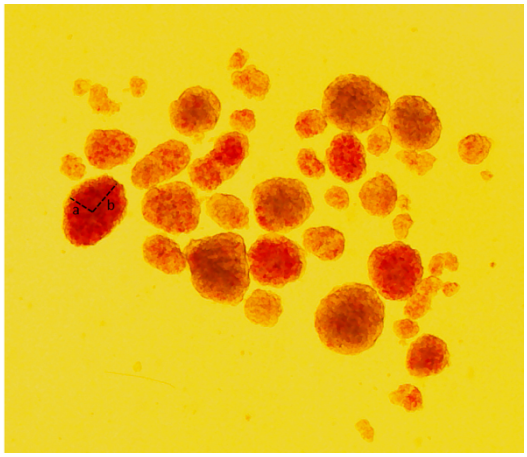


Figure 31: Schematic representation of isolated pancreatic islets stained with DTZ: *"a" and "b" are the calculation factors used to determine the ellipsoid volume.*

To convert the absolute number of islet clusters into IEQ, we approximated the volume of each islet to that of an ellipsoid with equal dimensions for the major and minor axes (see Fig.32). Using the acquired images, we calculated the values for the axes 'a' and 'b' using the Fiji software, as illustrated in Fig.31. This enabled us to determine the volume of each islet by applying the equation for the volume of an ellipsoid:

$$V = \frac{4}{3\pi 2a * b}$$

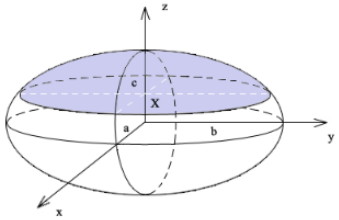


Figure 32: Schematic representation of an ellipsoid

The average volume of the sample is compared to the volume of an ideal sphere with a diameter of 150 µm (V_{sphere}), representing the volume of one IEQ. This comparison allows us to calculate an isolation index (I_{index}) that needs to be multiplied by the total number of clusters ($N_{cluster}$) in the analyzed sample to determine the total IEQ (N_{IEQ}). The resulting number can then be divided by the volume of the analyzed sample to determine the concentration of IEQ (C_{IEQ}), using these equations:

$$I_{index} = {V_{mean}}/{V_{sphere}}$$

$$N_{IEQ} = I_{index} \times N_{cluster}$$

$$[C_{IEQ}] = \frac{N_{IEQ}}{100ul}$$

7.6. BIOREACTOR CUSTOMIZATION AND ASSEMBLY

The bioreactor used in all the experiments is a custom-made and optimized closed system designed to isolate the organ engineered from the outside world, creating a stand-alone system. The bioreactor also enables constant and dynamic organ perfusion by using a peristaltic pump to mimic the physiological peristalsis of the heart, pumping culture media.

The bioreactor is composed of two main parts (Fig.33):

- the body is a glass chamber that serves as a medium reservoir and will contain the engineered scaffold
- The head has five inlet and outlet accesses: 1. Pulmonary artery (PA) and pulmonary vein accesses (PV); 2. Trachea access (T); 3. Filter access; 4. Draft access. Each inlet and outlet have a corresponding perfusion line above and luer-locks below, which will securely connect to the cannulas of the lung scaffold.

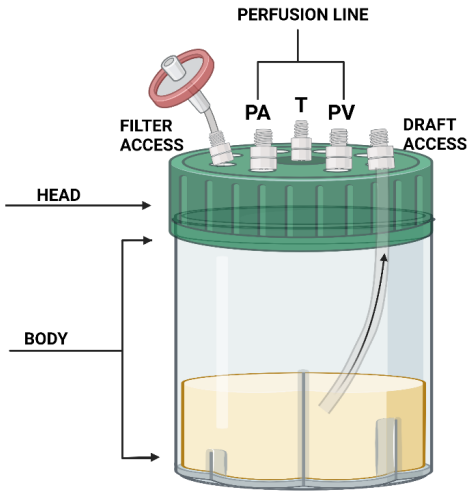


Figure 33:Schematic representation of the bioreactor composition

Assemble procedure:

1. Attach an oxygenating tube to the draft and incorporate a Y-connector to split this line into two separate perfusion routes (corresponding to PA and PV lines). Then, add pump tubing (using Masterflex L/S® Precision Pump Tubing, L/S 14) downstream at each end of the Y-connector and attach a three-way stopcock luer at the end of each line.
2. Connect a bubble-trapping tube to the three-way stopcock of each perfusion line to prevent bubbles from entering the organ. Attach another three-way stopcock to the other end of the bubble trap and connect it to the PA and PV inlet/outlet. During perfusion, insert the pump tubing downstream of the Y-connector into a peristaltic pump to allow media to flow through the PA, the PV, or both at a constant rate.
3. Mount a three-way stopcock at the end of the tracheal inlet/outlet and close all the open paths with a valve for the tracheal line.
4. Mount the HepaVent filter into the dedicated access to ensure guaranteed air filtration.
5. The decellularized lung must be connected after sterilizing the entire system with an autoclave.

7.7. *IN VITRO* SEEDING AND CULTURE OF hVIOs

The left lung lobes were decellularized and then placed in a custom-made bioreactor. A PA cannula and a PV cannula were connected to separate perfusion circuits. In contrast, the trachea cannula was connected to a reservoir positioned about 25cm (20 mmHg) above the level of the PA (Citro *et al*, 2019a). The trachea was kept open to the inside of bioreactor and closed to the reservoir through a three-way valve positioned 5 cm above the level of the PA.

To deliver endothelial cells through the PA and PV, $15x10^5$ of BOECs were re-suspended in two separate seeding chambers, with $7.5x10^5$ cells in each chamber, in 80 ml of AM culture media (Fig.34A). The cells were simultaneously seeded through the PA and PV under a gravity of 30 mmHg. The organ was then cultured under static conditions for two hours. Perfusion was initiated at 0.5 mL/min from both the PA and PV. The process involved releasing the PV cannula, opening the trachea to the reservoir, and then closing it to the chamber on day 1 of culture. 2000 IEQ HIs were mixed with $5x10^5$ BOECs and divided into 4 falcon tubes. These tubes contained different concentrations of cells: the 1st tube had 50% cell suspension, the 2nd and 3rd tubes had 25% each, and the 4th tube had 0% cells, containing only medium for

washing. The cells were seeded from the tracheal reservoir (Fig.34B). This was followed by adding 200 ml AM. Static culture for 2 hours was completed for airway seeding before initiating perfusion. The trachea was opened to the chamber to restart perfusion, and flow was set to 1 mL/min from the PA.

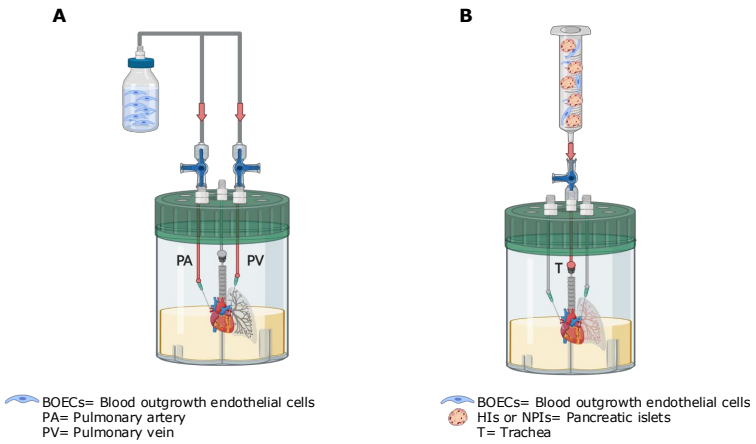


Figure 34: Representation of cell seeding: A) *Schematic representation of the BOECs seeding procedure through the PA and PV, and* ***B)*** *Schematic representation of isolated pancreatic islets (HI) and neonatal pig islets (NPIs) and BOECs seeding.*

hVIOs were cultured for 14 days, following a two-phase culturing protocol. The first phase, known as the maturation phase (MP), spanned the first 7 days, while the second phase, termed the testing phase (TP), covered the remaining 7 days. To moderate the endothelial permeability induced by angiogenic factors, hVIOs were cultured in AM for the first 12 days of each phase (Citro *et al*, 2019a), which has high serum and angiogenic growth factors to promote BOECs survival, migration, and vascular remodeling. In the remaining 2 days of cultures, AM was switched to MSM (Citro *et al*, 2019a) , which has lower serum and growth factor concentrations. Media was changed every other day.

The same culture protocol was used to seed VEP with 4000 clusters of NPIs and after MP was transplanted into diabetic mice (see figure 8B).

During the project, we used the TP to test the effects of different compounds on hVIO's vascular and endocrine compartments. During the TP, the media were supplemented with IL-8 (100 ng/ml) or vehicle (CTRL) at every media change (Fig.35A). Additionally, PBMCs were added during the TP to establish an *ex vivo* model of leukocyte trafficking in VEP's vascular architecture (Fig.35B). This allowed us to study (xeno) T cell responses to pancreatic islets.

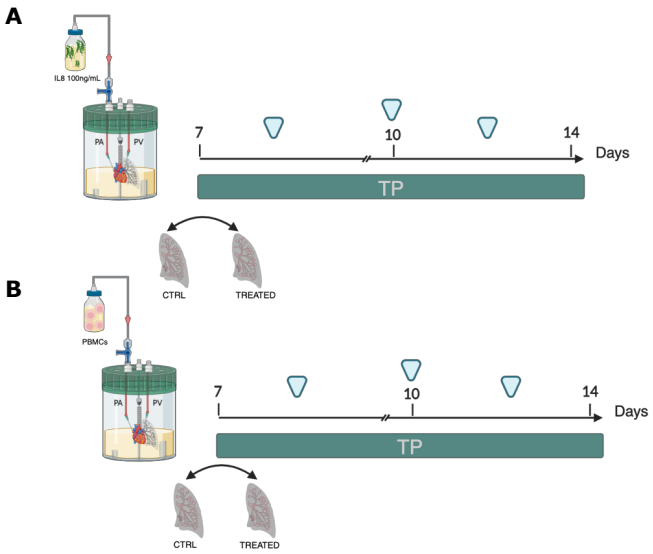


Figure 35: Graphic summary of hVIOs TP protocol of culture: A) *Schematic representation of IL-8 treatment;* ***B)*** *Schematic representation of PBMCs treatment.*

7.8. CULTURE PROTOCOLS OF ISOLATED ISLETS BATCH-MATCH AS AN INTERNAL CONTROL

The isolated pancreatic islets were cultured in a petri dish under suspension (Thermo Scientific Nunclon Delta Surface) for 14 days in complete Final Wash Medium (cFWM). cFWM is based on Final Wash Medium (Corning®, 99-785-CV) supplemented with 10% FBS, 1% Penicillin/Streptomycin (Sigma-Aldrich), 1% L-glutamine, Nitinamide (0.6105 mg/ml), DNAse, and ROCK inhibitor (100 U/mL and 5 uM, respectively). During the last 7 days of culture, cFWM was supplemented with IL-8 (100 ng/ml) or vehicle (Fig.36B). The medium was changed every two days during the first 7 days of culture and every other day during the last 7 days.

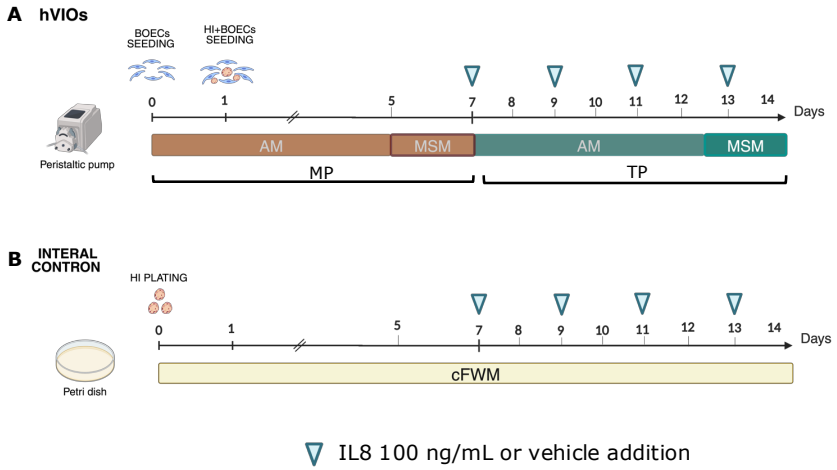


Figure 36: Graphic summary of IL-8 treatment: A) *hVIOs' protocol of culture;* ***B)*** *Internal controls' protocol of culture*

7.9. ISOLATION OF NEONATAL PANCREATIC ISLETS

Neonatal pancreatic islets (NPIs) were isolated from WT piglets aged 1 to 7 days (66% males and 34% females). The piglets were housed in a farrowing pen with their mother and provided with a heated nest. These procedures were approved by the district governments of Upper Bavaria, Germany, and were conducted by the German Animal Welfare Act (Citro *et al*, 2023).

The pancreas was cut into 1 mm pieces, digested using collagenase-V (Sigma-Aldrich), sieved through a 500µm mesh, and washed twice. The isolates were then cultured for 3 days in a recovery medium (Ham's F12/M199 with protease inhibitors, antioxidants, and additional nutrients). Complete media changes were carried out on day 1 and day 3 post-isolation to remove degenerated exocrine cells. Subsequently, NPIs were maintained in a maturation medium (Ham's F10, 10mmol/L glucose, 50 µmol/L 3-isobutyl-1- methylxanthine, 0.5% [wt/vol] BSA, 2 mmol/L L-glutamine, 10 mmol/L nicotinamide, and 1% [vol/vol] penicillin/streptomycin stock, 1,6 mM CaCl2) until they were used in VEP or insulin secretion tests. Half of the medium was replaced every other day (Citro *et al*, 2023).

7.10. FLUORESCENCE MICROANGIOGRAPHY

To study the function of the vascular network, we conducted the fluorescence microangiography assay. This assay aims to confirm the integrity of the newly formed vascular network and determine whether the network architecture allows direct perfusion of the hVIOs structure (Yuan *et al*, 2021).

Fluorescence microangiography was conducted after 14 days of culturing hVIOs without the islets ($hVIOs^{-islets}$) submerged in PBS at 37 °C.

A manual injection of 5 mL of 1% low melting point agarose (Invitrogen) in PBS, containing 1:10 diluted blue FluoSpheres (0.2 µm, 365/415 Invitrogen), was performed into the PA at a rate of about 5 mL/min (Fig.37). The PA perfusion pressure was maintained below 20 mmHg using the Pressure MAT Single-Use Sensor. Immediately following microangiography, the $hVIOs^{-islets}$ were transferred to the ice to facilitate the solidification of the agarose (Citro *et al*, 2019a),(Ren *et al*, 2015).

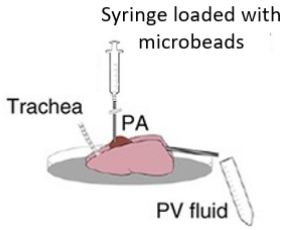


Figure 37: Schematic representation of microbeads infusion procedure(Ren *et al*, 2015)***.***

7.11. DEXTRAN PERMEABILITY ASSAY

A fluorescence dextran permeability assay was performed on mature $hVIO^{-islets}$ using 20 kDa or 150 kDa FITC-conjugated dextran. This test aimed to assess whether the engineered vasculature of hVIO retained physiological-like permeability (van Duinen *et al*, 2017). The $hVIO^{-islets}$ were mounted on the custom-built *ex vivo* perfusion device as follows: the hVIO was placed on a platform in a prone position with the PA cannula connected to a perfusion line. The PV cannula was left open to the level of the PA to allow for the collection of venous drainage, and the trachea was open 5 cm above the PA (Citro *et al*, 2019a). The $hVIO^{-islets}$ were perfused with PBS from the PA at a constant speed of 1 ml/min for 15 minutes. During the 3rd minute of perfusion, the PBS was replaced with a solution containing either 1mg/ml of 20 kDa or 150 kDa FITC-conjugated dextran, perfusing the scaffold at the

same speed. After 1 minute, the solution was switched back to PBS, which perfused the scaffold for another 11 minutes. PV drainage was collected at each minute of the experiment and analyzed using a spectrophotometer to quantify dextran release per minute (excitation laser 480/520).

7.12. miRNAs QUANTIFICATION

MiRNA-375 (miR-375) is the most abundant miRNA in pancreatic islets, with an essential role in maintaining the normal β cell mass (Poy *et al*, 2004),(Poy *et al*, 2009). Given the stability of miRNAs in the blood and the availability of susceptible technologies like droplet digital PCR (ddPCR) for their measurement (Marzinotto *et al*, 2017), miR-375 has been considered a promising biomarker for tracking β cell death in pre-diabetes and predicting endocrine dysfunction (Erener *et al*, 2013),(Latreille *et al*, 2015). Here, we measured the miR-375 release and quantified the β cell loss during the hVIO maturation. To account for any biases related to the miRNA contribution of BOECs, we also quantified miR-375 in a hVIO seeded with BOECs only. To do this, we collected supernatants from 100 mL of hVIOs culture media in DNA/RNA LoBind microcentrifuge tubes (Eppendorf®, Hamburg, Germany), stored them at −80 °C, and then extracted them using the NucleoSpin miRNA Plasma kit (Macherey-Nagel, Düren, Germany) following the manufacturer's instructions. We pelleted 100 HIs and $10x10^5$ BOECs, stored them at −80 °C, lysed them in ML lysis buffer from the Nucleospin miRNA kit (Macherey-Nagel, Düren, Germany), and used this for the subsequent extraction of small and large RNAs. The RNA extracted from cells was measured using the Epoch Microplate Spectrophotometer (BioTek Instruments, Inc., located in Winooski, VT, USA). For the reverse transcription process, 5 µL of extracted RNA from supernatants or 10 ng of RNA from cells miRNA was used. The TaqMan® MicroRNA Reverse Transcription kit (Applied Biosystems in Foster City, USA) was used to obtain the cDNA. A mixture of diluted reverse-transcription primers specific to human miR-375 (hsa-miR-375: assay ID 000564 Life Technologies, Carlsbad, USA) and miR-16 sequences (hsa-miR-16: assay ID 000391) was used as a 5× reverse transcription primer, following the manufacturer's protocol. The quantification of miR-375 and miR-16 (as a quality control) was done using droplet digital PCR (ddPCR) on the QX100 ddPCR system from Bio-Rad in Hercules, USA, as previously described (Marzinotto *et al*, 2017). The recommended amount of cDNA for each ddPCR

was previously determined as 5 µl and 2 µl of cDNA from supernatants and 0.5 ng and 1 ng of cDNA from cells for miR-375 and miR-16, respectively. The concentration of target miRNA copies in the supernatant was calculated by adjusting for the initial volume and the fraction of extracted RNA and cDNA used in each reaction. Target miRNA copies per cell were calculated by adjusting for the ng of RNA input, the total amount of extracted RNA, and the number of cells in the original sample. Using the estimated number of miR-375 copies per cell and the miR-375 copies measured in the hVIO supernatants at each time-point, we calculated the percentage of β cells lost during the hVIO maturation process.

7.13. HISTOLOGY AND IMMUNOFLUORESCENCE STAINING ON CELL AND TISSUE SAMPLES

Adhesion cell samples: The cells were plated on a culture slide with four separate removable chambers at 10x10^5 cells/cm^2 density. After adhesion, the cells were fixed with 4% PFA and stored at 4°C until staining. Immunofluorescence (IF) staining was carried out to confirm the endothelial phenotype of the cells for use in hVIO generation.

Tissue and Islets samples: Tissue samples and isolated pancreatic islets were fixed with 4% paraformaldehyde in PBS (PFA). After fixation, the tissue samples (hVIOs) were embedded in paraffin, while the isolated pancreatic islets and neonatal pig islets (NPIs) cultured in a petri dish were embedded in O.C.T. (Tissue-Tek). Paraffin-embedded samples, after overnight fixation in 4% PFA, were moved to a 70% EtOH solution overnight and then included in paraffin. On the other hand, isolated pancreatic islets were equilibrated in O.C.T. at 4°C for 20 minutes and then placed in a mold where they were included using dry ice and Dehyoil to facilitate O.C.T. freezing. Sections 5-10 µm from both paraffin-embedded and O.C.T.-embedded samples were used for IF staining. Before staining, paraffin sections were deparaffinized, rehydrated, and subjected to heat-induced antigen retrieval, while O.C.T. sections were rehydrated with PBS 1x. The staining process involved the following steps for both cell and paraffin/O.C.T. samples. First, we incubated the samples with a blocking solution (2% bovine serum albumin (BSA), 5% fetal bovine serum (FBS), 0.1% TRITON X-100 in PBS) to block non-specific binding sites. Then, the samples were exposed to primary antibodies for 1 hour at room temperature (RT)

or overnight at 4°C, diluted in the blocking solution. After that, the samples were washed three times with PBS 1x and incubated with secondary antibodies for 1 hour at RT. Finally, we applied DAPI (4'6-diamidino-2-phenylindole dye) for 5 minutes at RT. The secondary antibodies are designed to bind to the primary antibodies and are labeled with specific fluorescent markers. DAPI (1:500) is a fluorescent dye that binds to DNA segments rich in A and T, enabling us to stain the nuclei. We mounted the glass slides with a coverslip and stored them at 4°C until image acquisition.
All the antibodies used are summarized in the table below:

Cell Marker	Ab species	Ab reactivity	Dilution	Company
vWF	Rabbit	Human	1:200	DAKO
CD31	Mouse	Human	1:40	DAKO
Glucagon	Mouse	Human/Pig	1:200	Invitrogen
Somatostatin	Rabbit	Human	1:200	Abcam
Insulin	Guina Pig	Human/Pig	Ready to use	Dako
Chromogranin A	Mouse	Pig	1:200	Abcam
Somatostatin (H-11)	Mouse	Pig	1.100	Santa Cruz Biotechnology
CD181 (CXCR1)	Mouse	Human	1:100	BD Pharmingen
CD182 (CXCR2)	Mouse	Human	1:200	BD Pharmingen

Fluorophore	Ab species	Ab reactivity	Dilution for cells and tissues	Company
Alexa 488	Goat	Anti-rabbit / mouse	1:500	Invitrogen
Alexa 546	Goat	Anti-rabbit / mouse	1:500	Invitrogen
Alexa 647	Goat	Anti-g-pig	1:500	Invitrogen

After completing the IF staining, the glass slides were examined using widefield Zeiss AXIO Z1 Observer microscopy or Olympus fluoVIEW FV3000RS confocal microscopy. Images were captured at 4x, 10x, 20x, 30x, or 60x magnification using the appropriate acquisition software. The images were exported from the acquisition software as single-channel images and then analyzed using Fiji software.
NPIs' islets were subjected to immuno-fluorescence intensity quantification of insulin, glucagon, and somatostatin using Fiji software.

CXCR2+, CXCR2+/INS+, CXCR2+/GCG+, CXCR2+/SST+ islets quantification

A total of 87 HIs (average of 21 +/- 9 islets) from 4 different human islet preparations were stained to detect the presence of CXCR2, insulin, and glucagon or somatostatin. In each batch, we determined the percentage of islets that tested positive for CXCR2, considering an islet CXCR2+ if at least one cell showed positive for the receptor. Also, we calculated the percentage of CXCR2+ islets that had at least one cell co-expressing CXCR2+ with either insulin, glucagon, or somatostatin for each batch.

7.14. DYNAMIC INSULIN SECRETION TEST (IST) OF hVIOs

We tested the insulin secretion performance of hVIOs at day 1 and the end of both the MP and the TP, on the 7th and 14th day of culture, respectively. hVIOs were mounted on a custom-built *ex-vivo* perfusion device. The hVIO was positioned on a platform while lying down with the PA cannula connected to a perfusion line. The PV cannula was left open to the level of the PA, which allowed for the collection of venous drainage. Additionally, the trachea was left open 5cm above the PA. Insulin secretion of hVIOs was measured using a modified IST protocol (Citro *et al*, 2019a). Insulin secretion of hVIOs was measured using the following procedure. First, hVIOs were perfused sequentially with the following solutions:

1) Glucose-free KREBS HEPES-buffer solution (125 mM NaCl, 5.9 mM KCl, 2.56 mM CaCl2, 1 mM 54 MGCG2, 25 mM HEPES, 0.1% BSA, pH 7.4) as an acclimatization step to eliminate any residual insulin released during culture.

2) Low glucose KREBS HEPES-buffered solution (containing 2 mM glucose).

3) High glucose KREBS HEPES-buffered solution (containing 20 mM glucose).

The steps were as follows:

1) Acclimatization step: hVIOs were perfused with glucose-free KREBS HEPES-buffered solution for 40 minutes at a 1 ml/min rate to eliminate the stored insulin from the previous 7 or 14 days of culture.

2) Equilibration step: hVIOs were then perfused with low glucose (2mM) KREBS HEPES-buffered solution for 20 minutes at a 1 ml/min rate.

3) Stimulation step: hVIOs were further perfused with high glucose (20 mM) KREBS HEPES-buffered solution for 20 minutes at a 1 ml/min rate.

4) Recovery basal stimulation step: Finally, hVIOs were perfused with low glucose (2 mM) KREBS HEPES-buffered solution for 20 minutes at a 1 ml/min rate.

The same protocol for IST was performed for the VEP after 7 and 14 days of culture.

7.15. DYNAMIC INSULIN SECRETION TEST (IST) OF BATCH MATCH HUMAN ISLETS AS CONTROLS

To assess insulin secretion following the in vitro culture of HIs in a petri dish, a dynamic insulin secretion test (IST) was conducted on days 1, 7, and 14 of the culture. The Biorep perfusion system (BioRep® Perfusion V2.0.0) was used for this dynamic insulin secretion test (Fig.38A).

It is a high-capacity automated system that allows the stimulation of various samples with several stimuli solutions for a specific time according to an experimental plan. It also collects the eluate for subsequent quantification of a specific parameter (e.g., insulin, cytokines).

The system preserves live and viable cells at 37°C. The test's dynamicity is provided by a peristaltic pump, which ensures the automatic pumping of solutions within the cell loading chamber (see Figure 38B). The perfused solution is then retrieved from the outlet access and made available for subsequent evaluations.

The perfusion experimental plan is subdivided into 5 steps:

1. Acclimatation steps: A peristaltic pump with a low pulse rate was used to push KREBS HEPES-buffered solution with 2 mM glucose through the samples for 80 minutes. The flow rate was set to 0.03 ml/min for 60 minutes and then increased to 0.1 ml/min for the remaining 20 minutes.
2. Stimulation step: The islets are first stimulated with a high-glucose, insulin-free perfusion buffer (KREBS HEPES-buffered and supplemented with 20 mM glucose). In specific experiments, this solution was supplemented with either IL-8 (at concentrations of 100, 50, or 10 ng/ml) or a vehicle. Regardless of the supplement, the solution was perfused at a rate of 0.1 ml/min for 20 minutes.
3. 1st recovery basal stimulation step: Samples are perfused again with the low-glucose insulin-free perfusion buffer at 0.1 ml per ml for 20 minutes.
4. Aspecific stimulation step: The samples are stimulated with KREBS HEPES-buffered solution containing 30 mM KCl at a rate of 0.1 ml per minute for 20 minutes. The KCl solution causes significant depolarization of the β-cell membrane, leading to an influx of Ca^{2+} ions, which triggers the release of all insulin granules in the β-cell.

5. 2nd recovery basal stimulation step: samples are perfused again with the low-glucose, insulin-free perfusion buffer at 0.1 ml/ml for 20 minutes.

The same protocol for IST was performed for the NPIs after 7 days of culture.
Drainage perfusate was collected at representative time points for each phase of the experiments. All samples were frozen at -80°C. The most representative points for each phase were then assayed for insulin content using the Insulin ELISA Kit (Mercodia).
All samples were frozen at -20°C until assayed for insulin content using the Mercodia immunological ELISA kit assay. The ELISA samples were read at 450 nm using an Elisa Reader spectrophotometer (Model 680 Bio-Rad).

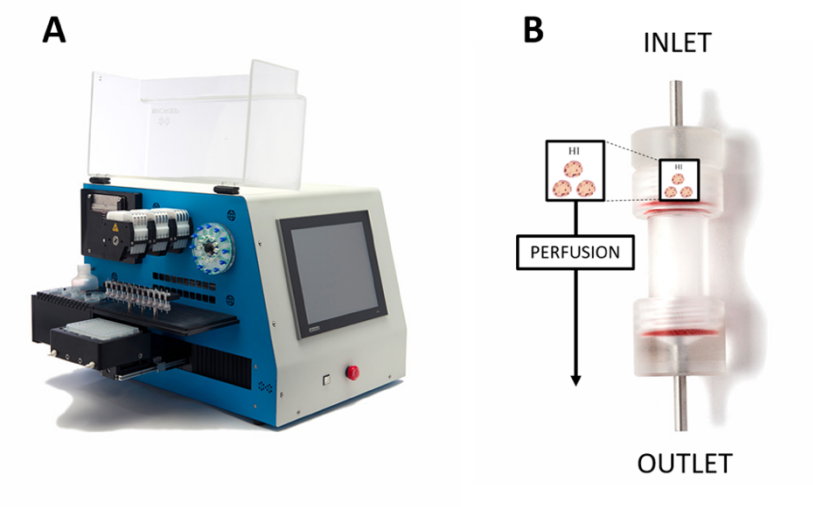


Figure 38: Schematic representation of the perfusion machine: A) *BioRep® Perfusion V2.0.0;* ***B)*** *perfusion chamber.*

7.16. SPATIAL TRANSCRIPTOMICS ANALYSES

We decided to perform spatial transcriptomic analyses to understand the trajectory of endothelial cells in our re-cellularized lung scaffold. We used 3 slides showing 3 different time points of hVIOs (days 1, 7, and 14).
The preparation of the experiment is subdivided into 9 steps (Fig.39) and was performed according to the manufacturer's protocol (Nanostring Technologies MAN-10150-02):

1) Pre-processing:

- Deparaffination and rehydration: Bake the slides at 60°C for an overnight (O/N) incubation. After that, we washed the slides in Xylene (VWR cat. nr. 28975.360) three times, 100% EtOH two times, 95% EtOH once, and finally, PBS 1x (BioNordika cat. nr. BN-53100).
- Target Retrieval: Dip the slides into nuclease-free water (BioNordika cat. nr. BN-51100) at 99°C for 10 seconds, then transfer them quickly to Tris-EDTA 1x (Invitrogen, eBioscience cat. nr. 00-4956-58), for 20 minutes. Finally, move the slides immediately to PBS 1x for 5 minutes.
- Expose RNA Targets: Incubate slides in a Proteinase K (0.1 µg/mL, ThermoFisher, AM2546) solution at 37°C for 15 min, and then wash slides in PBS 1x for 5 min.

2) Postfix to preserve tissue morphology:
   - Wash slides in 10% neutral buffered formalin (NBF, (Sigma-Alrich cat. nr. HT501128) for 5 min and then stop the fixation by washing the slides twice in NBF Stop buffer containing 2,42 g Tris-base (Sigma-Aldrich cat. nr. T1503), 1,5 g Glycine (Sigma-Aldrich cat. nr. G7126), and 200 mL nuclease-free water (BioNordika cat. nr. BN-51100), 5 min each.
   - Wash slides in PBS 1x for 5 min.
3) In situ hybridization:
   - Make a hybridization solution using 200 µL of Buffer R (GeoMx RNA Slide Prep Kit for FFPE, Nanostring Technologies cat. nr. 121300313) for each slide, 25 µl DSP RNA whole transcriptome detection probes for each slide (GeoMx NGS RNA WTA Hs, Nanostring Technologies cat. nr. 121401102), and 25 µL of nuclease-free water (BioNordika cat. nr. BN-51100). The GeoMx RNA Slide Prep Kit (GeoMx RNA Slide Prep Kit for FFPE, Nanostring Technologies cat. nr. 121300313) contains all the reagents.
   - Add 200 µL of hybridization solution to each slide and incubate overnight at 37 °C.
4) Perform stringent washes:
   - Perform 2 washes in Stringent Wash (equal parts SSC 4x (Rockland Immunochemicals cat. nr. ROCKMB-045)) and 100% formamide (APPLICHEM cat. nr. 11237117) at 37°C for 25 min each.
   - Perform two washes in SSC 2x for 2 min each.
5) IF:

- The samples were incubated at room temperature for 30 min with a blocking solution (Buffer W, GeoMx RNA Slide Prep Kit for FFPE, Nanostring Technologies cat. nr. 121300313) to block non-specific binding sites.
- The samples were exposed to primary antibodies (anti-human vWF (1:200, DAKO, A0082, polyclonal), anti-human glucagon (1:200 Invitrogen, PA5-83353, polyclonal) and anti-human Insulin (RTU; DAKO, A0564, polyclonal) for 1 hour at room temperature and diluted in the blocking solution.
- The samples were washed 3 times withSSC 2x for 5 min each.
- The samples were incubated with secondary antibodies (A546-, A488- or A647-labelled secondary antibodies, 1:500, Invitrogen) and Syto 13(a fluorescent dye that binds to DNA segments rich in A and T, enabling us to stain the nuclei (GeoMx Nuclear Stain Morp Kit, Nanostring Technologies cat. nr. 121300303)) for 1 hour at RT.
- The samples were washed 2 times with SSC 2x for 5 min each.

6) <u>ROI selection and AOI collection:</u>
    - The samples were scanned using the GeoMx Digital Spatial Profiler (Nanostring), ROIs were selected, and AOIs were defined using fluorescent thresholding and the instrument software. TheAOIs were then collected using the GeoMx Digital Spatial Profiler (Nanostring) and transferred to a 96-well collection plate.
7) <u>Library preparation and sequencing using the Illumina platform</u>
    Library preparation was carried out according to the manufacturer's protocol (Nanostring Technologies MAN-10153-03):

    - Add 2 µL of GeoMx NGS Master Mix to each well of a PCR plate and cover with aluminum film.
    - Transfer 4 µL of primer from a Seq Code Plate to the corresponding wells of the PCR plate.
    - Add 4 µL of DSP aspirate to the PCR plate and mix by pipetting up and down 10 times.
    - Seal the PCR plate with a sticker and pulse the centrifuge at 1000g.
    - Incubate the PCR plate in a thermocycler for 1h 30min.
    - After PCR, pulse the centrifuge at 1000g. Pool PCR products as follows:
        - Pool 4µL of each PCR product, including the NTC but excluding any PCR Positive Control, into one 1.5 mL tube. This is the Sample Pool.

- Pipette the remainder of the NTC PCR product into its own 1.5 mL tube.
- Pipette 10µL PCR Positive Control to its own 1.5 mL tube.

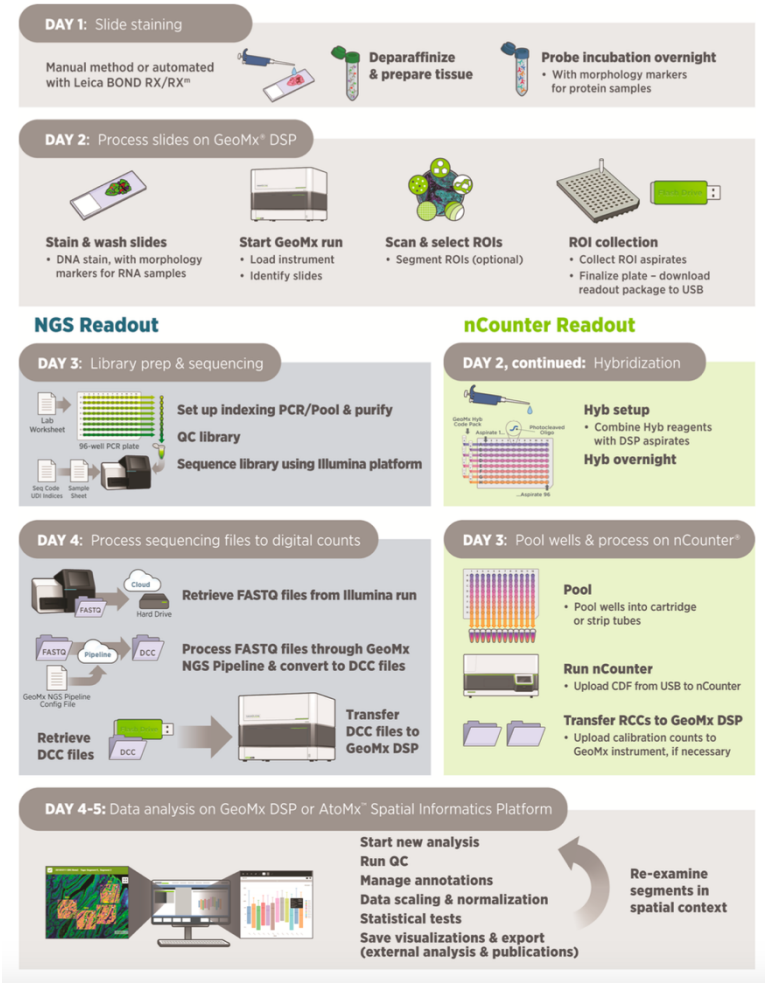


Figure 39: GeoMx DSP workflow summary (GeoMx® DSP NGS Readout User Manual).

Here are the simplified steps for the AMPure cleanup protocol (Fig.40):

- Measure the volume in each tube.
- Add 1.2x AMPure beads to the PCR products, mix, centrifuge, and incubate.
- Pellet the beads, remove the supernatant, and wash with 80% ethanol.
- Resuspend in Elution Buffer, incubate, and extract supernatant.
- Repeat the process with 60 uL AMPure beads.
- Transfer the supernatant to a new tube.

8) Assessing library quality and quantity
9) Sequencing with Illumina sequencer and Pipeline Processing

Heatmaps were generated using the "pheatmap" function from the pheatmap package in R (version 2024.09.0+375).

The input data consisted of a numeric matrix containing the fold-change expression data of the selected genes (log-transformed) calculated in each sample comparison. Hierarchical clustering with Euclidean distance was used to customize the heatmaps and to highlight potential patterns within the data.

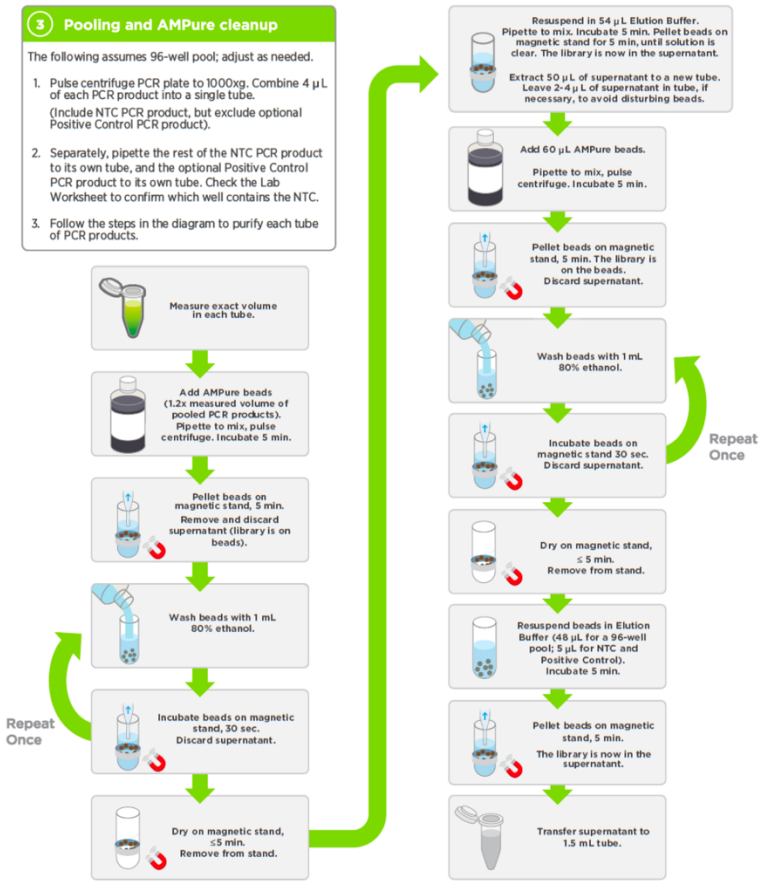


Figure 40: AMPure purification (GeoMx® DSP NGS Readout User Manual).

7.17. *IN VIVO* SYSTEM

7.17.1. Diabetes induction and metabolic monitoring

The female NSG mice, aged 6-8 weeks and weighing 22-25 grams, were made diabetic by injecting alloxan (72 mg/kg i.p., Sigma-Aldrich) two days before the transplantations (Citro *et al*, 2019a),(Gvazava *et al*, 2018),(Leiter & Schile, 2013),(Pepper *et al*, 2017). Mice with non-fasting glucose levels below 450 mg/dl before the transplantations were not considered diabetic and were excluded from the study. The reversal of diabetes was confirmed by two consecutive blood glucose measurements of 200 mg/dL or less, which had to be maintained until the end of the study. After the islet transplantation, the function of the graft was assessed daily by measuring non-fasting blood glucose levels using a portable glucometer (OneTouch Ultra, Bayer). Mice that died due to surgical complications within the first week were not included in the Kaplan-Meier analysis. Subcutaneous insulin therapy (LinBit pellet; Lin-Shin) was given peri-transplant to maintain a healthy status. The day after the transplantation, diabetic recipients with non-fasting blood glucose levels exceeding 250 mg/dL were implanted with two suboptimal insulin pellets. Animals with sustained graft function and non-fasting blood glucose levels below or equal to 250 mg/dL did not receive any pellets. One pellet was removed ten days after the transplantation, and the second pellet was removed twenty days after the transplantation (Citro *et al*, 2023).

7.17.2. Device-less (DL), Kidney capsule (KC), and Liver (LV) NPIs transplantation

Female NSG mice aged 6-8 weeks and weighing 22-25 grams were anesthetized using Avertin (tribromoethanol) with an intraperitoneal injection at a dose of 0.75mg/g (Sigma). To create the device-less (DL) site for islet transplantation, a 2-cm segment of 5-French (Fr.) textured nylon radiopaque angiographic catheter (Cook Medical, Indiana, USA) was implanted subcutaneously into the lower left quadrant of the recipient NSG mice 3 to 6 weeks before the transplantation (Pepper *et al*, 2015). During the

transplantation, a small (4 mm) incision was made to access the catheter, and the tissue matrix surrounding the superior margin of the catheter was cut to remove the catheter. A total of 4000 NPIs were placed into polyethylene (PE-50) tubing and infused within the DL space using a micro syringe (Hamilton). The incision was closed with a surgical silk suture (Ethicon, New Jersey, USA).

Additionally, a subset of diabetic animals was transplanted with 4000 NPIs per recipient either under the kidney capsule (KC) or into the liver (LV) via the portal vein, which are the standard sites for rodent islet transplantation (Citro *et al*, 2019b),(Marzorati *et al*, 2014). Due to surgical limitations, the liver accepted only 800 NPIs for each NSG diabetic recipient. For all experiments, NPIs were pooled, batched, and transplanted to either the DL, KC, or LV sites. Mice transplanted with NPIs in the DL and liver were followed for 9 weeks, while those transplanted in the kidney capsule were followed for 14 or 18 weeks after the implantation.

7.17.3. VEPs implantations in diabetic recipient mice

Female NSG mice, aged 6–8 weeks and weighing 22–25 grams, were anesthetized with Avertin. Prior to implantation, VEPs and VEPs–BOEC were flushed with 250 mL of ice-cold DMEM (GIBCO- 5.5 mM glucose) from the pulmonary artery (PA). The heart and trachea were carefully dissected, and the pulmonary artery (PA) was divided into two segments with a sagittal incision. The VEPs segments were then implanted into two separate subcutaneous pockets created on the dorsal left and right areas. A single pocket was created by making two 10-mm lateral transverse incisions, limiting a 2 cm tunneled area. An adequate void (1 cm by 2 cm) was created. Once the VEPs were placed in the dedicated space, the implant was secured under the skin with two prolene sutures (Ethicon, New Jersey, USA) on the sides, and the skin incision was closed with a surgical silk suture (Ethicon, New Jersey, USA). The transplanted mice were monitored for 9, 14, or 18 weeks after implantation (Citro *et al*, 2023).

7.18. ACTIVATION AND EVALUATION OF PBMCS' ABILITY TO KILL NPIS

To study an immune rejection, it is necessary to pre-activate the PBMCs against the target.

We use two different modes:

Aspecific activation: PBMCs were cultured at $2x10^5$ cells/well in 96-well plates in 5.5mM glucose medium: RPMI 1640 containing 50% RPMI 1640 without glucose (Gibco, Thermofisher Scientific) supplemented with 6.5% FBS, 100U/mL penicillin, and 100U/mL streptomycin. Cells were stimulated with Dynabeads™ Human T-Activator CD3/CD28 (Gibco) for 3 or 6 days. WZB117 (Merck) was used at a concentration of 10uM in all the experiments.

Specific activation against the xeno-islets: To activate the PBMCs, we used splenocytes isolated from the spleen of the same pig from which we obtained the NPIs. The activation process is as follows: we plated $3x10^6$ pig splenocytes in a 6-well plate in RPMI 1640 without supplements and allowed them to adhere for 2 hours. Then, we washed the cells twice with PBS 1x. Subsequently, we initiated the activation process by adding $5x10^6$ PBMCs to each well to expose them to xeno-antigens using RPMI 1640 without glucose (Gibco, Thermofisher Scientific) supplemented with 10% FBS, 100U/mL penicillin, and 100U/mL streptomycin. The activation typically takes around 14 days, with a weekly medium change and fresh medium added every two days. Successful activation results in the formation of PBMC clusters.

After the activation process, we recovered the NPIs, washed them twice in PBS 1x, and labeled them with Vybrant DiO-488 (Invitrogen, Cat: V22889, Lot: 617391_ used 5 µL in 1 mL of PBS 1x) for 20 min at 37°C. After the incubation, two washes followed in PBS 1x, and 50 CA of NPIs per well were plated in a 96-well plate. We recovered $10×10^5$ PBMCs activated with splenocytes and added them to the well containing the 50 CA of NPIs. The medium used for coculture is Angiogenic Medium, and Propidium Iodide (PI-546_BD Pharmingen Cat: 51-66211E, Lot: 4153746) was added (1.5 µL in 150 µL of medium). The analysis was carried out at Incucyte using the basic analyzer tool, which detects the area of yellow fluorescence, indicating the % death

of NPIs and the green fluorescence, indicating the % of NPIs detected. The test ended after 4 days.

7.19. STATISTICAL ANALYSIS

Values are presented as mean ± SD (or SEM) or median based on their distribution. Statistical analysis included Mann-Whitney U tests and two-tailed Student's t-tests. Statistically significant differences were considered when $p<0.05$, and the p-value is shown in each graph. The number of samples (n) for each graph can be found in the corresponding figure legend. The statistical analysis was conducted using Microsoft Excel 2024 version 16.88 (Microsoft Corporation, https://www.microsoft.com) and GraphPad Prism v10 version 10.3.1 (GraphPad Software, http://www.graphpad.com).

8. REFERENCES

Abadpour S, Aizenshtadt A, Olsen PA, Shoji K, Wilson SR, Krauss S & Scholz H (2020) Pancreas-on-a-Chip Technology for Transplantation Applications. *Curr Diab Rep* 20: 72

Abadpour S, Niemi EM, Orrhult LS, Hermanns C, de Vries R, Nogueira LP, Haugen HJ, Josefsen D, Krauss S, Gatenholm P, *et al* (2023) Adipose-Derived Stromal Cells Preserve Pancreatic Islet Function in a Transplantable 3D Bioprinted Scaffold. *Adv Healthc Mater* 12: e2300640

Abualhassan N, Sapozhnikov L, Pawlick RL, Kahana M, Pepper AR, Bruni A, Gala-Lopez B, Kin T, Mitrani E & Shapiro AMJ (2016) Lung-derived microscaffolds facilitate diabetes reversal after mouse and human intraperitoneal islet transplantation. *PLoS One* 11

Ahrén B (2012) Islet nerves in focus--defining their neurobiological and clinical role. *Diabetologia* 55: 3152–3154

Akiyama SK (1996) Integrins in cell adhesion and signaling. *Hum Cell* 9: 181–186

Akkouch A, Yu Y & Ozbolat IT (2015) Microfabrication of scaffold-free tissue strands for three-dimensional tissue engineering. *Biofabrication* 7: 31002

Al-Awar A, Kupai K, Veszelka M, Szűcs G, Attieh Z, Murlasits Z, Török S, Pósa A & Varga C (2016) Experimental Diabetes Mellitus in Different Animal Models. *J Diabetes Res* 2016: 9051426

Alberts B (2015) Molecular Biology of the Cell (6th ed.) 6th ed. Norton & Company. (ed)

Andrali SS, Sampley ML, Vanderford NL & Özcan S (2008) Glucose regulation of insulin gene expression in pancreatic β-cells. *Biochem J* 415: 1–10

Arndt T, Jörns A, Weiss H, Tiedge M, Hedrich H-J, Lenzen S & Wedekind D (2013) A variable $CD3^+$ T-cell frequency in peripheral blood lymphocytes associated with type 1 diabetes mellitus development in the LEW.1AR1-iddm rat. *PLoS One* 8: e64305

Arutyunyan I, Elchaninov A, Sukhikh G & Fatkhudinov T (2022) Cryopreservation of Tissue-Engineered Scaffold-Based Constructs: from Concept to Reality. *Stem cell Rev reports* 18: 1234–1252

Atkinson MA, Campbell-Thompson M, Kusmartseva I & Kaestner KH (2020) Organisation of the human pancreas in health and in diabetes. *Diabetologia* 63: 1966–1973

Atkinson MA & Eisenbarth GS (2001) Type 1 diabetes: new perspectives on disease pathogenesis and treatment. *Lancet (London, England)* 358: 221–229

Badylak SF, Taylor D & Uygun K (2011) Whole-organ tissue engineering: Decellularization and recellularization of three-dimensional matrix scaffolds. *Annu Rev Biomed Eng* 13: 27–53

Baetens D, Malaisse-Lagae F, Perrelet A & Orci L (1979) Endocrine pancreas: three-dimensional reconstruction shows two types of islets of langerhans. *Science* 206: 1323–1325

Balak JRA, Juksar J, Carlotti F, Lo Nigro A & de Koning EJP (2019) Organoids from the Human Fetal and Adult Pancreas. *Curr Diab Rep* 19: 160

Ballinger WF & Lacy PE (1972) Transplantation of intact pancreatic islets in rats. *Surgery* 72: 175–186

Banting FG & Best CH (1990) Pancreatic extracts. 1922. *J Lab Clin Med* 115: 254–272

Baptista PM, Siddiqui MM, Lozier G, Rodriguez SR, Atala A & Soker S (2011) The use of whole organ decellularization for the generation of a vascularized liver organoid. *Hepatology* 53: 604–617

Barai P & Chen J (2024) Beyond protein synthesis: non-translational functions of

threonyl-tRNA synthetases. *Biochem Soc Trans* 52: 661–670
Barbieux C, Parnaud G, Lavallard V, Brioudes E, Meyer J, Alibashe Ahmed M, Berishvili E, Berney T & Bosco D (2016) Asymmetrical distribution of δ and PP cells in human pancreatic islets. *J Endocrinol* 229: 123–132
Barker TH (2011) The role of ECM proteins and protein fragments in guiding cell behavior in regenerative medicine. *Biomaterials* 32: 4211–4214
Barrett JC, Clayton DG, Concannon P, Akolkar B, Cooper JD, Erlich HA, Julier C, Morahan G, Nerup J, Nierras C, *et al* (2009) Genome-wide association study and meta-analysis find that over 40 loci affect risk of type 1 diabetes. *Nat Genet* 41: 703–707
Battaglia C, Mayer U, Aumailley M & Timpl R (1992) Basement-membrane heparan sulfate proteoglycan binds to laminin by its heparan sulfate chains and to nidogen by sites in the protein core. *Eur J Biochem* 208: 359–366
Behrens J, Kameritsch P, Wallner S, Pohl U & Pogoda K (2010) The carboxyl tail of Cx43 augments p38 mediated cell migration in a gap junction-independent manner. *Eur J Cell Biol* 89: 828–838
Bellin MD & Dunn TB (2020) Transplant strategies for type 1 diabetes: whole pancreas, islet and porcine beta cell therapies. *Diabetologia* 63: 2049–2056
Bender RHF, O'Donnell BT, Shergill B, Pham BQ, Tahmouresie S, Sanchez CN, Juat DJ, Hatch MMS, Shirure VS, Wortham M, *et al* (2024) A vascularized 3D model of the human pancreatic islet forex vivostudy of immune cell-islet interaction. *Biofabrication* 16
Bi H, Karanth SS, Ye K, Stein R & Jin S (2020) Decellularized Tissue Matrix Enhances Self-Assembly of Islet Organoids from Pluripotent Stem Cell Differentiation. *ACS Biomater Sci Eng* 6: 4155–4165
Bijonowski BM, Miller WM & Wertheim JA (2013) Bioreactor design for perfusion-based, highly-vascularized organ regeneration. *Curr Opin Chem Eng* 2: 32–40
Blandinières A, Hong X, Philippe A, Bièche I, Vacher S, Rossi E, Detriche G, Gendron N, Gaussem P, Guerin CL, *et al* (2021) Interleukin-8 Receptors CXCR1 and CXCR2 Are Not Expressed by Endothelial Colony-forming Cells. *Stem cell Rev reports* 17: 628–638
Bloem SJ & Roep BO (2017) The elusive role of B lymphocytes and islet autoantibodies in (human) type 1 diabetes. *Diabetologia* 60: 1185–1189 doi:10.1007/s00125-017-4284-5 [PREPRINT]
Bonifacio E, Beyerlein A, Hippich M, Winkler C, Vehik K, Weedon MN, Laimighofer M, Hattersley AT, Krumsiek J, Frohnert BI, *et al* (2018) Genetic scores to stratify risk of developing multiple islet autoantibodies and type 1 diabetes: A prospective study in children. *PLoS Med* 15: e1002548
Bonifacio E, Krumsiek J, Winkler C, Theis FJ & Ziegler A-G (2014) A strategy to find gene combinations that identify children who progress rapidly to type 1 diabetes after islet autoantibody seroconversion. *Acta Diabetol* 51: 403–411
Bonner-Weir S, Sullivan BA & Weir GC (2015) Human Islet Morphology Revisited: Human and Rodent Islets Are Not So Different After All. *J Histochem Cytochem* 63: 604–612
Bortell R & Yang C (2012) The BB rat as a model of human type 1 diabetes. *Methods Mol Biol* 933: 31–44
Bottazzo GF (1986) Lawrence lecture. Death of a beta cell: homicide or suicide? *Diabet Med* 3: 119–130
Bottazzo GF, Florin-Christensen A & Doniach D (1974) Islet-cell antibodies in diabetes mellitus with autoimmune polyendocrine deficiencies. *Lancet (London, England)* 2: 1279–1283
Bottino R, Knoll MF, Knoll CA, Bertera S & Trucco MM (2018) The future of islet transplantation is now. *Front Med* 5: 202
Bowers DT, Song W, Wang LH & Ma M (2019) Engineering the vasculature for islet transplantation. *Acta Biomater* 95: 131–151

Braun M, Ramracheya R, Bengtsson M, Zhang Q, Karanauskaite J, Partridge C, Johnson PR & Rorsman P (2008) Voltage-gated ion channels in human pancreatic beta-cells: electrophysiological characterization and role in insulin secretion. *Diabetes* 57: 1618–1628

Brissova M, Fowler M, Wiebe P, Shostak A, Shiota M, Radhika A, Lin PC, Gannon M & Powers AC (2004) Intraislet Endothelial Cells Contribute to Revascularization of Transplanted Pancreatic Islets. *Diabetes* 53: 1318–1325

Brissova M, Fowler MJ, Nicholson WE, Chu A, Hirshberg B, Harlan DM & Powers AC (2005) Assessment of human pancreatic islet architecture and composition by laser scanning confocal microscopy. *J Histochem Cytochem Off J Histochem Soc* 53: 1087–1097

Brusko TM, Russ HA & Stabler CL (2021) Strategies for durable β cell replacement in type 1 diabetes. *Science* 373: 516–522

Buchwald P, Cechin SR, Weaver JD & Stabler CL (2015) Experimental evaluation and computational modeling of the effects of encapsulation on the time-profile of glucose-stimulated insulin release of pancreatic islets. *Biomed Eng Online* 14: 28

Buchwald P, Tamayo-Garcia A, Manzoli V, Tomei AA & Stabler CL (2018) Glucose-stimulated insulin release: Parallel perifusion studies of free and hydrogel encapsulated human pancreatic islets. *Biotechnol Bioeng* 115: 232–245

Burganova G, Bridges C, Thorn P & Landsman L (2021) The Role of Vascular Cells in Pancreatic Beta-Cell Function. *Front Endocrinol (Lausanne)* 12: 1–9

Cabrera O, Jacques-Silva MC, Berman DM, Fachado A, Echeverri F, Poo R, Khan A, Kenyon NS, Ricordi C, Berggren P-O, *et al* (2008) Automated, high-throughput assays for evaluation of human pancreatic islet function. *Cell Transplant* 16: 1039–1048

Campbell-Thompson M, Wasserfall C, Montgomery EL, Atkinson MA & Kaddis JS (2012) Pancreas organ weight in individuals with disease-associated autoantibodies at risk for type 1 diabetes. *JAMA* 308: 2337–2339

Campbell-Thompson ML, Atkinson MA, Butler AE, Chapman NM, Frisk G, Gianani R, Giepmans BN, von Herrath MG, Hyöty H, Kay TW, *et al* (2013) The diagnosis of insulitis in human type 1 diabetes. *Diabetologia* 56: 2541–2543 doi:10.1007/s00125-013-3043-5 [PREPRINT]

Campo F, Neroni A, Pignatelli C, Bignard J, Berishvili E, Piemonti L & Citro A (2023) Bioengineered Vascularized Insulin Producing Endocrine Tissues BT - Pluripotent Stem Cell Therapy for Diabetes. In, Piemonti L Odorico J Kieffer TJ Sordi V & de Koning E (eds) pp 151–177. Cham: Springer International Publishing

Cao Z & Wang X (2014) The endocrine role between β cells and intra-islet endothelial cells. *Endocr J* 61: 647–654

Caumo A & Luzi L (2004) First-phase insulin secretion: does it exist in real life? Considerations on shape and function. *Am J Physiol Endocrinol Metab* 287: E371-85

Cayabyab F, Nih LR & Yoshihara E (2021) Advances in Pancreatic Islet Transplantation Sites for the Treatment of Diabetes. *Front Endocrinol (Lausanne)* 12

Cerasi E (1975) Mechanisms of glucose stimulated insulin secretion in health and in diabetes: some re-evaluations and proposals. *Diabetologia* 11: 1–13

Chen J & Gunton JE (2021) Beta-cell function and human islet transplantation: Can we improve? *J Endocrinol* 248: R99–R112

Chen Y, Zhao X & Wu H (2019) Metabolic Stress and Cardiovascular Disease in Diabetes Mellitus: The Role of Protein O-GlcNAc Modification. *Arterioscler Thromb Vasc Biol* 39: 1911–1924

Chua JS, Tran VM, Kalita M, Quintero M V, Antelope O, Muruganandam G, Saijoh Y & Kuberan B (2017) A glycan-based approach to therapeutic angiogenesis.

PLoS One 12: e0182301
Citro A, Cantarelli E, Maffi P, Nano R, Melzi R, Mercalli A, Dugnani E, Sordi V, Magistretti P, Daffonchio L, *et al* (2012) CXCR1/2 inhibition enhances pancreatic islet survival after transplantation. *J Clin Invest* 122: 3647–3651
Citro A, Cantarelli E & Piemonti L (2015a) The CXCR1/2 Pathway: Involvement in Diabetes Pathophysiology and Potential Target for T1D Interventions. *Curr Diab Rep* 15
Citro A, Moser PT, Dugnani E, Rajab TK, Ren X, Evangelista-Leite D, Charest JM, Peloso A, Podesser BK, Manenti F, *et al* (2019a) Biofabrication of a vascularized islet organ for type 1 diabetes. *Biomaterials* 199: 40–51
Citro A, Neroni A, Pignatelli C, Campo F, Policardi M, Monieri M, Pellegrini S, Dugnani E, Manenti F, Maffia MC, *et al* (2023) Directed self-assembly of a xenogeneic vascularized endocrine pancreas for type 1 diabetes. *Nat Commun* 14: 878
Citro A & Ott HC (2018) Can We Re-Engineer the Endocrine Pancreas? *Curr Diab Rep* 18: 122
Citro A, Pellegrini S, Dugnani E, Eulberg D, Klussmann S & Piemonti L (2019b) CCL2/MCP-1 and CXCL12/SDF-1 blockade by L-aptamers improve pancreatic islet engraftment and survival in mouse. *Am J Transplant Off J Am Soc Transplant Am Soc Transpl Surg* 19: 3131–3138
Citro A, Valle A, Cantarelli E, Mercalli A, Pellegrini S, Liberati D, Daffonchio L, Kastsiuchenka O, Ruffini PA, Battaglia M, *et al* (2015b) CXCR1/2 Inhibition Blocks and Reverses Type 1 Diabetes in Mice. *Diabetes* 64: 1329–1340
Clarke G, Harley P, Hubber E-L, Manea T, Manuelli L, Read E & Watt FM (2018) Bench to bedside: Current advances in regenerative medicine. *Curr Opin Cell Biol* 55: 59–66
Cohen O, Filetti S, Castañeda J, Maranghi M & Glandt M (2016) When Intensive Insulin Therapy (MDI) Fails in Patients With Type 2 Diabetes: Switching to GLP-1 Receptor Agonist Versus Insulin Pump. *Diabetes Care* 39 Suppl 2: S180-6
Collier JH & Segura T (2011) Evolving the use of peptides as components of biomaterials. *Biomaterials* 32: 4198–4204
Collins MN & Birkinshaw C (2013) Hyaluronic acid based scaffolds for tissue engineering--a review. *Carbohydr Polym* 92: 1262–1279
Coppens V, Heremans Y, Leuckx G, Suenens K, Jacobs-Tulleneers-Thevissen D, Verdonck K, Lahoutte T, Luttun A, Heimberg H & De Leu N (2013) Human blood outgrowth endothelial cells improve islet survival and function when co-transplanted in a mouse model of diabetes. *Diabetologia* 56: 382–390
Coppieters KT, Dotta F, Amirian N, Campbell PD, Kay TWH, Atkinson MA, Roep BO & von Herrath MG (2012) Demonstration of islet-autoreactive CD8 T cells in insulitic lesions from recent onset and long-term type 1 diabetes patients. *J Exp Med* 209: 51–60
Costa A, Naranjo JD, Londono R & Badylak SF (2017) Biologic scaffolds. *Cold Spring Harb Perspect Med* 7: 1–23
Craig ME, Kim KW, Isaacs SR, Penno MA, Hamilton-Williams EE, Couper JJ & Rawlinson WD (2019) Early-life factors contributing to type 1 diabetes. *Diabetologia* 62: 1823–1834
Crapo PM, Gilbert TW & Badylak SF (2011) An overview of tissue and whole organ decellularization processes. *Biomaterials* 32: 3233–3243
Culina S, Lalanne AI, Afonso G, Cerosaletti K, Pinto S, Sebastiani G, Kuranda K, Nigi L, Eugster A, Østerbye T, *et al* (2018) Islet-reactive CD8(+) T cell frequencies in the pancreas, but not in blood, distinguish type 1 diabetic patients from healthy donors. *Sci Immunol* 3
Cyrus BF & Muller WA (2016) A Unique Role for Endothelial Cell Kinesin Light Chain 1, Variant 1 in Leukocyte Transendothelial Migration. *Am J Pathol* 186: 1375–

1386
d Oliveira RB, Carvalho CP d F, Polo CC, Dorighello G d G, Boschero AC, d Oliveira HCF & Collares-Buzato CB (2014) Impaired compensatory beta-cell function and growth in response to high-fat diet in LDL receptor knockout mice. *Int J Exp Pathol* 95: 296–308
Dai H, Jiang Y, Liu Z, Su X, Yang Y & Chen Z (2022) Pumilio RNA-Binding Family Member 1 Plays a Promoting Role on Pancreatic Cancer Angiogenesis. *Can J Gastroenterol Hepatol* 2022: 9202531
Danke NA, Koelle DM, Yee C, Beheray S & Kwok WW (2004) Autoreactive T cells in healthy individuals. *J Immunol* 172: 5967–5972
Datta P, Ayan B & Ozbolat IT (2017) Bioprinting for vascular and vascularized tissue biofabrication. *Acta Biomater* 51: 1–20 doi:10.1016/j.actbio.2017.01.035 [PREPRINT]
Diagnosis and classification of diabetes mellitus. (2011) *Diabetes Care* 34 Suppl 1: S62-9
Diedisheim M, Mallone R, Boitard C & Larger E (2016) β-cell Mass in Nondiabetic Autoantibody-Positive Subjects: An Analysis Based on the Network for Pancreatic Organ Donors Database. *J Clin Endocrinol Metab* 101: 1390–1397
Doliba NM, Qin W, Najafi H, Liu C, Buettger CW, Sotiris J, Collins HW, Li C, Stanley CA, Wilson DF, *et al* (2012) Glucokinase activation repairs defective bioenergetics of islets of Langerhans isolated from type 2 diabetics. *Am J Physiol Endocrinol Metab* 302: E87–E102
Dong H, Zhang Y, Wang J, Kim DS, Wu H, Sjögren B, Gao W, Luttrell L & Wang H (2017) Regulator of G protein signaling 2 is a key regulator of pancreatic β-cell mass and function. *Cell Death Dis* 8: e2821
Dotta F, Censini S, van Halteren AGS, Marselli L, Masini M, Dionisi S, Mosca F, Boggi U, Muda AO, Del Prato S, *et al* (2007) Coxsackie B4 virus infection of beta cells and natural killer cell insulitis in recent-onset type 1 diabetic patients. *Proc Natl Acad Sci U S A* 104: 5115–5120
Driver JP, Chen Y-G & Mathews CE (2012) Comparative genetics: synergizing human and NOD mouse studies for identifying genetic causation of type 1 diabetes. *Rev Diabet Stud* 9: 169–187
Du W, Zhou M, Zhao W, Cheng D, Wang L, Lu J, Song E, Feng W, Xue Y, Xu P, *et al* (2016) HID-1 is required for homotypic fusion of immature secretory granules during maturation. *Elife* 5
van Duinen V, van den Heuvel A, Trietsch SJ, Lanz HL, van Gils JM, van Zonneveld AJ, Vulto P & Hankemeier T (2017) 96 perfusable blood vessels to study vascular permeability in vitro. *Sci Rep* 7: 18071
Eisenbarth GS (1986) Type I diabetes mellitus. A chronic autoimmune disease. *N Engl J Med* 314: 1360–1368
Eizirik DL, Colli ML & Ortis F (2009) The role of inflammation in insulitis and beta-cell loss in type 1 diabetes. *Nat Rev Endocrinol* 5: 219–226
Emami A, Talaei-Khozani T, Vojdani Z & Zarei Fard N (2021) Comparative assessment of the efficiency of various decellularization agents for bone tissue engineering. *J Biomed Mater Res B Appl Biomater* 109: 19–32
Enemchukwu NO, Cruz-Acuña R, Bongiorno T, Johnson CT, García JR, Sulchek T & García AJ (2016) Synthetic matrices reveal contributions of ECM biophysical and biochemical properties to epithelial morphogenesis. *J Cell Biol* 212: 113–124
Epshtein A, Rachi E, Sakhneny L, Mizrachi S, Baer D & Landsman L (2017) Neonatal pancreatic pericytes support β-cell proliferation. *Mol Metab* 6: 1330–1338
Erener S, Mojibian M, Fox JK, Denroche HC & Kieffer TJ (2013) Circulating miR-375 as a biomarker of β-cell death and diabetes in mice. *Endocrinology* 154: 603–608
Espona-Noguera A, Ciriza J, Cañibano-Hernández A, Orive G, Hernández RM, Del

Burgo LS & Pedraz JL (2019) Review of advanced hydrogel-based cell encapsulation systems for insulin delivery in type 1 diabetes mellitus. *Pharmaceutics* 11

Evans M, Schumm-Draeger PM, Vora J & King AB (2011) A review of modern insulin analogue pharmacokinetic and pharmacodynamic profiles in type 2 diabetes: improvements and limitations. *Diabetes Obes Metab* 13: 677–684

Fathi I, Imura T, Inagaki A, Nakamura Y, Nabawi A & Goto M (2021) Decellularized Whole-Organ Pre-vascularization: A Novel Approach for Organogenesis. *Front Bioeng Biotechnol* 9: 1–12

Fischer K & Schnieke A (2022) Xenotransplantation becoming reality. *Transgenic Res* 31: 391–398

Franek E, Haluzík M, Canecki Varžić S, Sargin M, Macura S, Zacho J & Christiansen JS (2016) Twice-daily insulin degludec/insulin aspart provides superior fasting plasma glucose control and a reduced rate of hypoglycaemia compared with biphasic insulin aspart 30 in insulin-naïve adults with Type 2 diabetes. *Diabet Med* 33: 497–505

Friedrich LH, Jungebluth P, Sjöqvist S, Lundin V, Haag JC, Lemon G, Gustafsson Y, Ajalloueian F, Sotnichenko A, Kielstein H, *et al* (2014) Preservation of aortic root architecture and properties using a detergent-enzymatic perfusion protocol. *Biomaterials* 35: 1907–1913

Frisch SM & Screaton RA (2001) Anoikis mechanisms. *Curr Opin Cell Biol* 13: 555–562

Gandasi NR, Yin P, Riz M, Chibalina M V, Cortese G, Lund P-E, Matveev V, Rorsman P, Sherman A, Pedersen MG, *et al* (2017) Ca2+ channel clustering with insulin-containing granules is disturbed in type 2 diabetes. *J Clin Invest* 127: 2353–2364

Gao T, McKenna B, Li C, Reichert M, Nguyen J, Singh T, Yang C, Pannikar A, Doliba N, Zhang T, *et al* (2014) Pdx1 maintains β cell identity and function by repressing an α cell program. *Cell Metab* 19: 259–271

Garcia-Contreras M, Tamayo-Garcia A, Pappan KL, Michelotti GA, Stabler CL, Ricordi C & Buchwald P (2017) Metabolomics Study of the Effects of Inflammation, Hypoxia, and High Glucose on Isolated Human Pancreatic Islets. *J Proteome Res* 16: 2294–2306

Ghasemi A, Akbari E & Imani R (2021) An Overview of Engineered Hydrogel-Based Biomaterials for Improved β-Cell Survival and Insulin Secretion. *Front Bioeng Biotechnol* 9: 686

Gibly RF, Graham JG, Luo X, Lowe WL, Hering BJ & Shea LD (2011) Advancing islet transplantation: From engraftment to the immune response. *Diabetologia* 54: 2494–2505

Gilpin A & Yang Y (2017) Decellularization Strategies for Regenerative Medicine: From Processing Techniques to Applications. *Biomed Res Int* 2017: 9831534

Gilpin SE, Guyette JP, Gonzalez G, Ren X, Asara JM, Mathisen DJ, Vacanti JP & Ott HC (2014) Perfusion decellularization of human and porcine lungs: bringing the matrix to clinical scale. *J Hear lung Transplant Off Publ Int Soc Hear Transplant* 33: 298–308

Glowacki J & Mizuno S (2008) Collagen scaffolds for tissue engineering. *Biopolymers* 89: 338–344

Goh SK, Bertera S, Olsen P, Candiello JE, Halfter W, Uechi G, Balasubramani M, Johnson SA, Sicari BM, Kollar E, *et al* (2013) Perfusion-decellularized pancreas as a natural 3D scaffold for pancreatic tissue and whole organ engineering. *Biomaterials* 34: 6760–6772

Gotfredsen CF, Buschard K & Frandsen EK (1985) Reduction of diabetes incidence of BB Wistar rats by early prophylactic insulin treatment of diabetes-prone animals. *Diabetologia* 28: 933–935

Grande Tovar CD, Castro JI, Valencia CH, Navia Porras DP, Mina Hernandez JH,

Valencia ME, Velásquez JD & Chaur MN (2019) Preparation of Chitosan/Poly(Vinyl Alcohol) Nanocomposite Films Incorporated with Oxidized Carbon Nano-Onions (Multi-Layer Fullerenes) for Tissue-Engineering Applications. *Biomolecules* 9 doi:10.3390/biom9110684 [PREPRINT]

Grigoryan B, Paulsen SJ, Corbett DC, Sazer DW, Fortin CL, Zaita AJ, Greenfield PT, Calafat NJ, Gounley JP, Ta AH, *et al* (2019) Multivascular networks and functional intravascular topologies within biocompatible hydrogels. *Science (80-)* 364: 458–464

Grodsky GM, Bennett LL, Smith DF & Schmid FG (1967) Effect of pulse administration of glucose or glucagon on insulin secretion in vitro. *Metabolism* 16: 222–233

Grodsky GM, Curry D, Landahl H & Bennett L (1969) [Further studies on the dynamic aspects of insulin release in vitro with evidence for a two-compartmental storage system]. *Acta Diabetol Lat* 6 Suppl 1: 554–578

Groen H, Klatter F, Pater J, Nieuwenhuis P & Rozing J (2003) Temporary, but essential requirement of CD8+ T cells early in the pathogenesis of diabetes in BB rats as revealed by thymectomy and CD8 depletion. *Clin Dev Immunol* 10: 141–151

Grossman EJ, Lee DD, Tao J, Wilson RA, Park S-Y, Bell GI & Chong AS (2010) Glycemic control promotes pancreatic beta-cell regeneration in streptozotocin-induced diabetic mice. *PLoS One* 5: e8749

Gumerson JD & Michele DE (2011) The dystrophin-glycoprotein complex in the prevention of muscle damage. *J Biomed Biotechnol* 2011: 210797

Guo E, Wu J, Lu H, Wang L & Chen Q (2022) Tissue-engineered bones with adipose-derived stem cells - composite polymer for repair of bone defects. *Regen Med* 17: 643–657

Gurlin RE, Giraldo JA & Latres E (2021) 3D Bioprinting and Translation of Beta Cell Replacement Therapies for Type 1 Diabetes. *Tissue Eng - Part B Rev* 27: 238–252

Guruswamy Damodaran R & Vermette P (2018) Decellularized pancreas as a native extracellular matrix scaffold for pancreatic islet seeding and culture. *J Tissue Eng Regen Med* 12: 1230–1237

Guvendiren M & Burdick JA (2013) Engineering synthetic hydrogel microenvironments to instruct stem cells. *Curr Opin Biotechnol* 24: 841–846

Gvazava IG, Rogovaya OS, Borisov MA, Vorotelyak EA & Vasiliev A V (2018) Pathogenesis of Type 1 Diabetes Mellitus and Rodent Experimental Models. *Acta Naturae* 10: 24–33

Hassouna T, Seeberger KL, Salama B & Korbutt GS (2018) Functional Maturation and In Vitro Differentiation of Neonatal Porcine Islet Grafts. *Transplantation* 102: e413–e423

Hayashi K, Kojima R & Ito M (2006) Strain differences in the diabetogenic activity of streptozotocin in mice. *Biol Pharm Bull* 29: 1110–1119

He M & Callanan A (2013) Comparison of methods for whole-organ decellularization in tissue engineering of bioartificial organs. *Tissue Eng Part B Rev* 19: 194–208

Henquin J-C (2019) The challenge of correctly reporting hormones content and secretion in isolated human islets. *Mol Metab* 30: 230–239

Henquin J-C (2021) Glucose-induced insulin secretion in isolated human islets: Does it truly reflect β-cell function in vivo? *Mol Metab* 48: 101212

Henquin JC, Nenquin M, Ravier MA & Szollosi A (2009) Shortcomings of current models of glucose-induced insulin secretion. *Diabetes Obes Metab* 11 Suppl 4: 168–179

Herold KC, Gitelman SE, Ehlers MR, Gottlieb PA, Greenbaum CJ, Hagopian W, Boyle KD, Keyes-Elstein L, Aggarwal S, Phippard D, *et al* (2013) Teplizumab (anti-CD3 mAb) treatment preserves C-peptide responses in patients with new-

onset type 1 diabetes in a randomized controlled trial: metabolic and immunologic features at baseline identify a subgroup of responders. *Diabetes* 62: 3766–3774
Hillebrandt KH, Everwien H, Haep N, Keshi E, Pratschke J & Sauer IM (2019) Strategies based on organ decellularization and recellularization. *Transpl Int Off J Eur Soc Organ Transplant* 32: 571–585
Hober D & Sauter P (2010) Pathogenesis of type 1 diabetes mellitus: interplay between enterovirus and host. *Nat Rev Endocrinol* 6: 279–289
Hogrebe NJ, Augsornworawat P, Maxwell KG, Velazco-Cruz L & Millman JR (2020) Targeting the cytoskeleton to direct pancreatic differentiation of human pluripotent stem cells. *Nat Biotechnol*
Hölzl K, Lin S, Tytgat L, Van Vlierberghe S, Gu L & Ovsianikov A (2016) Bioink properties before, during and after 3D bioprinting. *Biofabrication* 8
Hoshi RA, Van Lith R, Jen MC, Allen JB, Lapidos KA & Ameer G (2013) The blood and vascular cell compatibility of heparin-modified ePTFE vascular grafts. *Biomaterials* 34: 30–41
Houtz J, Borden P, Ceasrine A, Minichiello L & Kuruvilla R (2016) Neurotrophin Signaling Is Required for Glucose-Induced Insulin Secretion. *Dev Cell* 39: 329–345
Huang YB, Mei J, Yu Y, Ding Y, Xia W, Yue T, Chen W, Zhou MT & Yang YJ (2019) Comparative Decellularization and Recellularization of Normal Versus Streptozotocin-Induced Diabetes Mellitus Rat Pancreas. *Artif Organs* 43: 399–412
Huh D, Hamilton GA & Ingber DE (2011) From 3D cell culture to organs-on-chips. *Trends Cell Biol* 21: 745–754
Huleihel L, Hussey GS, Naranjo JD, Zhang L, Dziki JL, Turner NJ, Stolz DB & Badylak SF (2016) Matrix-bound nanovesicles within ECM bioscaffolds. *Sci Adv* 2: e1600502
Hunckler MD & García AJ (2020) Engineered Biomaterials for Enhanced Function of Insulin-Secreting β-Cell Organoids. *Adv Funct Mater* 30: 2000134
Hutton JC (1994) Insulin secretory granule biogenesis and the proinsulin-processing endopeptidases. *Diabetologia* 37 Suppl 2: S48-56
Idaszek J, Volpi M, Paradiso A, Nguyen Quoc M, Górecka Ż, Klak M, Tymicki G, Berman A, Wierzbicki M, Jaworski S, *et al* (2021) Alginate-based tissue-specific bioinks for multi-material 3D-bioprinting of pancreatic islets and blood vessels: A step towards vascularized pancreas grafts. *Bioprinting* 24
Ilonen J, Lempainen J & Veijola R (2019) x. *Nat Rev Endocrinol* 15: 635–650
In't Veld P (2014) Insulitis in human type 1 diabetes: a comparison between patients and animal models. *Semin Immunopathol* 36: 569–579
Insel RA, Dunne JL, Atkinson MA, Chiang JL, Dabelea D, Gottlieb PA, Greenbaum CJ, Herold KC, Krischer JP, Lernmark Å, *et al* (2015) Staging presymptomatic type 1 diabetes: a scientific statement of JDRF, the Endocrine Society, and the American Diabetes Association. *Diabetes Care* 38: 1964–1974
Inshaw JRJ, Walker NM, Wallace C, Bottolo L & Todd JA (2018) The chromosome 6q22.33 region is associated with age at diagnosis of type 1 diabetes and disease risk in those diagnosed under 5 years of age. *Diabetologia* 61: 147–157
Iorio V, Troughton LD & Hamill KJ (2015) Laminins: Roles and Utility in Wound Repair. *Adv wound care* 4: 250–263 doi:10.1089/wound.2014.0533 [PREPRINT]
Izumi T, Yokota-Hashimoto H, Zhao S, Wang J, Halban PA & Takeuchi T (2003) Dominant negative pathogenesis by mutant proinsulin in the Akita diabetic mouse. *Diabetes* 52: 409–416
Jacobson AM, Braffett BH, Cleary PA, Gubitosi-Klug RA & Larkin ME (2013) The long-term effects of type 1 diabetes treatment and complications on health-

related quality of life: a 23-year follow-up of the Diabetes Control and Complications/Epidemiology of Diabetes Interventions and Complications cohort. *Diabetes Care* 36: 3131–3138

Jain A, van der Meer AD, Papa A-L, Barrile R, Lai A, Schlechter BL, Otieno MA, Louden CS, Hamilton GA, Michelson AD, *et al* (2016) Assessment of whole blood thrombosis in a microfluidic device lined by fixed human endothelium. *Biomed Microdevices* 18: 73

Jayasimhan A, Mansour KP & Slattery RM (2014) Advances in our understanding of the pathophysiology of Type 1 diabetes: lessons from the NOD mouse. *Clin Sci (Lond)* 126: 1–18

Jenkins TL & Little D (2019) Synthetic scaffolds for musculoskeletal tissue engineering: cellular responses to fiber parameters. *NPJ Regen Med* 4: 15

Jiang K, Chaimov D, Patel SN, Liang JP, Wiggins SC, Samojlik MM, Rubiano A, Simmons CS & Stabler CL (2019) 3-D physiomimetic extracellular matrix hydrogels provide a supportive microenvironment for rodent and human islet culture. *Biomaterials* 198: 37–48

Jörns A, Günther A, Hedrich H-J, Wedekind D, Tiedge M & Lenzen S (2005) Immune cell infiltration, cytokine expression, and beta-cell apoptosis during the development of type 1 diabetes in the spontaneously diabetic LEW.1AR1/Ztm-iddm rat. *Diabetes* 54: 2041–2052

Jörns A, Kubat B, Tiedge M, Wedekind D, Hedrich H-J, Klöppel G & Lenzen S (2004) Pathology of the pancreas and other organs in the diabetic LEW.1AR1/Ztm-iddm rat, a new model of spontaneous insulin-dependent diabetes mellitus. *Virchows Arch* 444: 183–189

Jörns A, Rath KJ, Terbish T, Arndt T, Meyer Zu Vilsendorf A, Wedekind D, Hedrich H-J & Lenzen S (2010) Diabetes prevention by immunomodulatory FTY720 treatment in the LEW.1AR1-iddm rat despite immune cell activation. *Endocrinology* 151: 3555–3565

Kahn SE, D'Alessio DA, Schwartz MW, Fujimoto WY, Ensinck JW, Taborsky GJJ & Porte DJ (1990) Evidence of cosecretion of islet amyloid polypeptide and insulin by beta-cells. *Diabetes* 39: 634–638

Kanak MA, Takita M, Shahbazov R, Lawrence MC, Chung WY, Dennison AR, Levy MF & Naziruddin B (2015) Evaluation of MicroRNA375 as a Novel Biomarker for Graft Damage in Clinical Islet Transplantation. *Transplantation* 99: 1568–1573

Kang HW, Kengla C, Lee SJ, Yoo JJ & Atala A (2014) 3-D organ printing technologies for tissue engineering applications. *Rapid Prototyp Biomater Princ Appl*: 236–253

Katari RS, Peloso A & Orlando G (2014) Tissue engineering. *Adv Surg* 48: 137–154

Katsuki Y, Yagi H, Okitsu T, Kitago M, Tajima K, Kadota Y, Hibi T, Abe Y, Shinoda M, Itano O, *et al* (2016) Endocrine pancreas engineered using porcine islets and partial pancreatic scaffolds. *Pancreatol Off J Int Assoc Pancreatol . [et al]* 16: 922–930

Kawano K, Hirashima T, Mori S, Saitoh Y, Kurosumi M & Natori T (1991) New inbred strain of Long-Evans Tokushima lean rats with IDDM without lymphopenia. *Diabetes* 40: 1375–1381

Kayton NS, Poffenberger G, Henske J, Dai C, Thompson C, Aramandla R, Shostak A, Nicholson W, Brissova M, Bush WS, *et al* (2015) Human islet preparations distributed for research exhibit a variety of insulin-secretory profiles. *Am J Physiol Endocrinol Metab* 308: E592-602

Kebede MA, Oler AT, Gregg T, Balloon AJ, Johnson A, Mitok K, Rabaglia M, Schueler K, Stapleton D, Thorstenson C, *et al* (2014) SORCS1 is necessary for normal insulin secretory granule biogenesis in metabolically stressed β cells. *J Clin Invest* 124: 4240–4256

Kemp CB, Knight MJ, Scharp DW, Ballinger WF & Lacy PE (1973) Effect of transplantation site on the results of pancreatic islet isografts in diabetic rats.

Diabetologia 9: 486–491
Kemter E, Denner J & Wolf E (2018) Will Genetic Engineering Carry Xenotransplantation of Pig Islets to the Clinic? *Curr Diab Rep* 18: 103
Kemter E & Wolf E (2018) Recent progress in porcine islet isolation, culture and engraftment strategies for xenotransplantation. *Curr Opin Organ Transplant* 23: 633–641 doi:10.1097/MOT.0000000000000579 [PREPRINT]
Kennedy KM, Bhaw-Luximon A & Jhurry D (2017) Cell-matrix mechanical interaction in electrospun polymeric scaffolds for tissue engineering: Implications for scaffold design and performance. *Acta Biomater* 50: 41–55
Khalil AS, Jaenisch R & Mooney DJ (2020) Engineered tissues and strategies to overcome challenges in drug development. *Adv Drug Deliv Rev* 158: 116–139
Khan AA, Vishwakarma SK, Bardia A & Venkateshwarulu J (2014) Repopulation of decellularized whole organ scaffold using stem cells: an emerging technology for the development of neo-organ. *J Artif organs Off J Japanese Soc Artif Organs* 17: 291–300
Kieffer TJ, Heller RS, Unson CG, Weir GC & Habener JF (1996) Distribution of glucagon receptors on hormone-specific endocrine cells of rat pancreatic islets. *Endocrinology* 137: 5119–5125
Kilimnik G, Jo J, Periwal V, Zielinski MC & Hara M (2012) Quantification of islet size and architecture. *Islets* 4: 167–172
Kim BS, Baez CE & Atala A (2000) Biomaterials for tissue engineering. *World J Urol* 18: 2–9
Kim J, Shim IK, Hwang DG, Lee YN, Kim M, Kim H, Kim SW, Lee S, Kim SC, Cho DW, *et al* (2019) 3D cell printing of islet-laden pancreatic tissue-derived extracellular matrix bioink constructs for enhancing pancreatic functions. *J Mater Chem B* 7: 1773–1781
King A & Bowe J (2016) Animal models for diabetes: Understanding the pathogenesis and finding new treatments. *Biochem Pharmacol* 99: 1–10
King A, Lau J, Nordin A, Sandler S & Andersson A (2003) The effect of capsule composition in the reversal of hyperglycemia in diabetic mice transplanted with microencapsulated allogeneic islets. *Diabetes Technol Ther* 5: 653–663
Kirchmajer DM, Gorkin R & In Het Panhuis M (2015) An overview of the suitability of hydrogel-forming polymers for extrusion-based 3D-printing. *J Mater Chem B* 3: 4105–4117
Kolbe M, Dohle E, Katerla D, Kirkpatrick CJ & Fuchs S (2010) Enrichment of outgrowth endothelial cells in high and low colony-forming cultures from peripheral blood progenitors. *Tissue Eng Part C Methods* 16: 877–886
Komeda K, Noda M, Terao K, Kuzuya N, Kanazawa M & Kanazawa Y (1998) Establishment of two substrains, diabetes-prone and non-diabetic, from Long-Evans Tokushima Lean (LETL) rats. *Endocr J* 45: 737–744
Korbutt GS, Elliott JF, Ao Z, Smith DK, Warnock GL & Rajotte R V (1996) Large scale isolation, growth, and function of porcine neonatal islet cells. *J Clin Invest* 97: 2119–2129
Kort-Mascort J, Bao G, Elkashty O, Flores-Torres S, Munguia-Lopez JG, Jiang T, Ehrlicher AJ, Mongeau L, Tran SD & Kinsella JM (2021) Decellularized Extracellular Matrix Composite Hydrogel Bioinks for the Development of 3D Bioprinted Head and Neck in Vitro Tumor Models. *ACS Biomater Sci Eng* 7: 5288–5300
Kourtzelis I, Magnusson PU, Kotlabova K, Lambris JD & Chavakis T (2015) Regulation of Instant Blood Mediated Inflammatory Reaction (IBMIR) in Pancreatic Islet Xeno-Transplantation: Points for Therapeutic Interventions. *Adv Exp Med Biol* 865: 171–188
Kriegel MA, Rathinam C & Flavell RA (2012) Pancreatic islet expression of chemokine CCL2 suppresses autoimmune diabetes via tolerogenic CD11c+ CD11b+ dendritic cells. *Proc Natl Acad Sci U S A* 109: 3457–3462

Krischer JP, Liu X, Lernmark Å, Hagopian WA, Rewers MJ, She J-X, Toppari J, Ziegler A-G & Akolkar B (2017) The Influence of Type 1 Diabetes Genetic Susceptibility Regions, Age, Sex, and Family History on the Progression From Multiple Autoantibodies to Type 1 Diabetes: A TEDDY Study Report. *Diabetes* 66: 3122–3129

Krishnan R, Buder B, Alexander M, Foster CE 3rd & Lakey JR (2015) Juvenile porcine islets can restore euglycemia in diabetic athymic nude mice after xenotransplantation. *Transplantation* 99: 710–716

Krogvold L, Edwin B, Buanes T, Frisk G, Skog O, Anagandula M, Korsgren O, Undlien D, Eike MC, Richardson SJ, *et al* (2015) Detection of a low-grade enteroviral infection in the islets of langerhans of living patients newly diagnosed with type 1 diabetes. *Diabetes* 64: 1682–1687

Kuric E, Seiron P, Krogvold L, Edwin B, Buanes T, Hanssen KF, Skog O, Dahl-Jørgensen K & Korsgren O (2017) Demonstration of Tissue Resident Memory CD8 T Cells in Insulitic Lesions in Adult Patients with Recent-Onset Type 1 Diabetes. *Am J Pathol* 187: 581–588

Lammert E & Thorn P (2020) The Role of the Islet Niche on Beta Cell Structure and Function. *J Mol Biol* 432: 1407–1418 doi:10.1016/j.jmb.2019.10.032 [PREPRINT]

Langer R & Vacanti J (2016) Advances in tissue engineering. *J Pediatr Surg* 51: 8–12

Langer R & Vacanti JP (1993) Tissue engineering. *Science* 260: 920–6

Latreille M, Herrmanns K, Renwick N, Tuschl T, Malecki MT, McCarthy MI, Owen KR, Rülicke T & Stoffel M (2015) miR-375 gene dosage in pancreatic β-cells: implications for regulation of β-cell mass and biomarker development. *J Mol Med (Berl)* 93: 1159–1169

Leiter EH (1993) The NOD Mouse: A Model for Analyzing the Interplay Between Heredity and Environment in Development of Autoimmune Disease. *ILAR J* 35: 4–14

Leiter EH & Schile A (2013) Genetic and Pharmacologic Models for Type 1 Diabetes. *Curr Protoc Mouse Biol* 3: 9–19

Lemaire K, Ravier MA, Schraenen A, Creemers JWM, Van de Plas R, Granvik M, Van Lommel L, Waelkens E, Chimienti F, Rutter GA, *et al* (2009) Insulin crystallization depends on zinc transporter ZnT8 expression, but is not required for normal glucose homeostasis in mice. *Proc Natl Acad Sci U S A* 106: 14872–14877

Lenzen S, Tiedge M, Elsner M, Lortz S, Weiss H, Jörns A, Klöppel G, Wedekind D, Prokop CM & Hedrich HJ (2001) The LEW.1AR1/Ztm-iddm rat: a new model of spontaneous insulin-dependent diabetes mellitus. *Diabetologia* 44: 1189–1196

Li A, Dubey S, Varney ML, Dave BJ & Singh RK (2003) IL-8 directly enhanced endothelial cell survival, proliferation, and matrix metalloproteinases production and regulated angiogenesis. *J Immunol* 170: 3369–3376

Li W-C, Chen C-Y, Kao C-W, Huang P-C, Hsieh Y-T, Kuo T-Y, Chen T-Y, Chia H-Y & Juang J-H (2018) Porcine Neonatal Pancreatic Cell Clusters Maintain Their Multipotency in Culture and After Transplantation. *Sci Rep* 8: 8212

Like AA, Dirodi V, Thomas S, Guberski DL & Rossini AA (1984) Prevention of diabetes mellitus in the BB/W rat with Cyclosporin-A. *Am J Pathol* 117: 92–97

Like AA, Kislauskis E, Williams RR & Rossini AA (1982) Neonatal thymectomy prevents spontaneous diabetes mellitus in the BB/W rat. *Science* 216: 644–646

Like AA, Rossini AA, Guberski DL, Appel MC & Williams RM (1979) Spontaneous diabetes mellitus: reversal and prevention in the BB/W rat with antiserum to rat lymphocytes. *Science* 206: 1421–1423

Lin Y, Chang L, Solovey A, Healey JF, Lollar P & Hebbel RP (2002) Use of blood outgrowth endothelial cells for gene therapy for hemophilia A. *Blood* 99: 457–

462
Liu H, Duan R, He X, Qi J, Xing T, Wu Y, Zhou L, Wang L, Shao Y, Zhang F, *et al* (2023) Endothelial deletion of PTBP1 disrupts ventricular chamber development. *Nat Commun* 14: 1796
Liu X, Carter SSD, Renes MJ, Kim J, Rojas-Canales DM, Penko D, Angus C, Beirne S, Drogemuller CJ, Yue Z, *et al* (2019) Development of a Coaxial 3D Printing Platform for Biofabrication of Implantable Islet-Containing Constructs. *Adv Healthc Mater* 8
Llacua LA, de Haan BJ & de Vos P (2018) Laminin and collagen IV inclusion in immunoisolating microcapsules reduces cytokine-mediated cell death in human pancreatic islets. *J Tissue Eng Regen Med* 12: 460–467
Londono R & Badylak SF (2015) Biologic scaffolds for regenerative medicine: mechanisms of in vivo remodeling. *Ann Biomed Eng* 43: 577–592
Lorsch JR, Collins FS & Lippincott-Schwartz J (2014) Cell Biology. Fixing problems with cell lines. *Science* 346: 1452–1453
Loskill P & Wu JC (2019) Stem cell based human organ-on-a-chip models for drug discovery and development. *Adv Drug Deliv Rev* 140: 1–2 doi:10.1016/j.addr.2019.07.004 [PREPRINT]
Ludwig B, Ludwig S, Steffen A, Knauf Y, Zimerman B, Heinke S, Lehmann S, Schubert U, Schmid J, Bleyer M, *et al* (2017) Favorable outcome of experimental islet xenotransplantation without immunosuppression in a nonhuman primate model of diabetes. *Proc Natl Acad Sci U S A* 114: 11745–11750
van Lummel M, van Veelen PA, de Ru AH, Pool J, Nikolic T, Laban S, Joosten A, Drijfhout JW, Gómez-Touriño I, Arif S, *et al* (2016) Discovery of a Selective Islet Peptidome Presented by the Highest-Risk HLA-DQ8trans Molecule. *Diabetes* 65: 732–741
Makino S, Kunimoto K, Muraoka Y, Mizushima Y, Katagiri K & Tochino Y (1980) Breeding of a non-obese, diabetic strain of mice. *Jikken Dobutsu* 29: 1–13
Marchioli G, Van Gurp L, Van Krieken PP, Stamatialis D, Engelse M, Van Blitterswijk CA, Karperien MBJ, De Koning E, Alblas J, Moroni L, *et al* (2015) Fabrication of three-dimensional bioplotted hydrogel scaffolds for islets of Langerhans transplantation. *Biofabrication* 7: 25009
Marchioli G, Luca A Di, de Koning E, Engelse M, Van Blitterswijk CA, Karperien M, Van Apeldoorn AA & Moroni L (2016) Hybrid Polycaprolactone/Alginate Scaffolds Functionalized with VEGF to Promote de Novo Vessel Formation for the Transplantation of Islets of Langerhans. *Adv Healthc Mater* 5: 1606–1616
Marei I, Abu Samaan T, Al-Quradaghi MA, Farah AA, Mahmud SH, Ding H & Triggle CR (2022) 3D Tissue-Engineered Vascular Drug Screening Platforms: Promise and Considerations. *Front Cardiovasc Med* 9: 847554
Martin-Ramirez J, Hofman M, van den Biggelaar M, Hebbel RP & Voorberg J (2012) Establishment of outgrowth endothelial cells from peripheral blood. *Nat Protoc* 7: 1709–1715
Martin I, Wendt D & Heberer M (2004) The role of bioreactors in tissue engineering. *Trends Biotechnol* 22: 80–86
Marzinotto I, Pellegrini S, Brigatti C, Nano R, Melzi R, Mercalli A, Liberati D, Sordi V, Ferrari M, Falconi M, *et al* (2017) miR-204 is associated with an endocrine phenotype in human pancreatic islets but does not regulate the insulin mRNA through MAFA. *Sci Rep* 7: 14051
Marzorati S, Melzi R, Citro A, Cantarelli E, Mercalli A, Scavini M & Piemonti L (2014) Engraftment versus immunosuppression: cost-benefit analysis of immunosuppression after intrahepatic murine islet transplantation. *Transplantation* 97: 1019–1026
Mathews CE (2005) Utility of murine models for the study of spontaneous autoimmune type 1 diabetes. *Pediatr Diabetes* 6: 165–177

Mathieu C, Gillard P & Benhalima K (2017) Insulin analogues in type 1 diabetes mellitus: getting better all the time. *Nat Rev Endocrinol* 13: 385–399
Mathur T, Singh KA, R Pandian NK, Tsai S-H, Hein TW, Gaharwar AK, Flanagan JM & Jain A (2019) Organ-on-chips made of blood: endothelial progenitor cells from blood reconstitute vascular thromboinflammation in vessel-chips. *Lab Chip* 19: 2500–2511
Mathur T, Tronolone JJ & Jain A (2021) Comparative Analysis of Blood-Derived Endothelial Cells for Designing Next-Generation Personalized Organ-on-Chips. *J Am Heart Assoc* 10: e022795
Medina RJ, O'Neill CL, O'Doherty TM, Chambers SEJ, Guduric-Fuchs J, Neisen J, Waugh DJ, Simpson DA & Stitt AW (2013) Ex vivo expansion of human outgrowth endothelial cells leads to IL-8-mediated replicative senescence and impaired vasoreparative function. *Stem Cells* 31: 1657–1668
Meezan E, Hjelle JT, Brendel K & Carlson EC (1975) A simple, versatile, nondisruptive method for the isolation of morphologically and chemically pure basement membranes from several tissues. *Life Sci* 17: 1721–1732
Melloul D, Marshak S & Cerasi E (2002) Regulation of insulin gene transcription. *Diabetologia* 45: 309–326
Melton D (2021) The promise of stem cell-derived islet replacement therapy. *Diabetologia* 64: 1030–1036
Mendoza-Novelo B, Avila EE, Cauich-Rodríguez J V, Jorge-Herrero E, Rojo FJ, Guinea G V & Mata-Mata JL (2011) Decellularization of pericardial tissue and its impact on tensile viscoelasticity and glycosaminoglycan content. *Acta Biomater* 7: 1241–1248
Milojević M, Rožanc J, Vajda J, Činč Ćurić L, Paradiž E, Stožer A, Maver U & Vihar B (2021) In Vitro Disease Models of the Endocrine Pancreas. *Biomedicines* 9
Miri AK, Khalilpour A, Cecen B, Maharjan S, Shin SR & Khademhosseini A (2019) Multiscale bioprinting of vascularized models. *Biomaterials* 198: 204–216
Misler S (2010) The isolated pancreatic islet as a micro-organ and its transplantation to cure diabetes: celebrating the legacy of Paul Lacy. *Islets* 2: 210–224
Misler S, Barnett DW, Pressel DM, Gillis KD, Scharp DW & Falke LC (1992) Stimulus-secretion coupling in beta-cells of transplantable human islets of Langerhans. Evidence for a critical role for Ca2+ entry. *Diabetes* 41: 662–670
Moffat D, Ye K & Jin S (2022) Decellularization for the retention of tissue niches. *J Tissue Eng* 13: 20417314221101150
Mordes JP, Bortell R, Blankenhorn EP, Rossini AA & Greiner DL (2004) Rat models of type 1 diabetes: genetics, environment, and autoimmunity. *ILAR J* 45: 278–291
Mourad NI & Gianello P (2019) Long-term culture and in vitro maturation of macroencapsulated adult and neonatal porcine islets. *Xenotransplantation* 26: e12461
Mulder H (2017) Transcribing β-cell mitochondria in health and disease. *Mol Metab* 6: 1040–1051
Muller YD, Golshayan D, Ehirchiou D, Wyss JC, Giovannoni L, Meier R, Serre-Beinier V, Puga Yung G, Morel P, Bühler LH, *et al* (2011) Immunosuppressive effects of streptozotocin-induced diabetes result in absolute lymphopenia and a relative increase of T regulatory cells. *Diabetes* 60: 2331–2340
Murphy SV & Atala A (2013) Organ engineering--combining stem cells, biomaterials, and bioreactors to produce bioengineered organs for transplantation. *Bioessays* 35: 163–172
Nakhooda AF, Like AA, Chappel CI, Murray FT & Marliss EB (1977) The spontaneously diabetic Wistar rat. Metabolic and morphologic studies. *Diabetes* 26: 100–112
Nakrani MN, Wineland RH & Anjum F (2024) Physiology, Glucose Metabolism. In

Treasure Island (FL)
Nazari M, Kurdi M & Heerklotz H (2012) Classifying surfactants with respect to their effect on lipid membrane order. *Biophys J* 102: 498–506
Nepom GT, Ehlers M & Mandrup-Poulsen T (2013) Anti-cytokine therapies in T1D: Concepts and strategies. *Clin Immunol* 149: 279–285
Nerup J, Mandrup-Poulsen T, Helqvist S, Andersen HU, Pociot F, Reimers JI, Cuartero BG, Karlsen AE, Bjerre U & Lorenzen T (1994) On the pathogenesis of IDDM. *Diabetologia* 37 Suppl 2: S82-9
Nishimori I & Onishi S (2001) Carbonic anhydrase isozymes in the human pancreas. *Dig liver Dis Off J Ital Soc Gastroenterol Ital Assoc Study Liver* 33: 68–74
Nyman LR, Wells KS, Head WS, McCaughey M, Ford E, Brissova M, Piston DW & Powers AC (2008) Real-time, multidimensional in vivo imaging used to investigate blood flow in mouse pancreatic islets. *J Clin Invest* 118: 3790–3797
O'Brien FJ (2011) Biomaterials & scaffolds for tissue engineering. *Mater Today* 14: 88–95
Olgasi C, Borsotti C, Merlin S, Bergmann T, Bittorf P, Adewoye AB, Wragg N, Patterson K, Calabria A, Benedicenti F, *et al* (2021) Efficient and safe correction of hemophilia A by lentiviral vector-transduced BOECs in an implantable device. *Mol Ther Methods Clin Dev* 23: 551–566
Olsson R & Carlsson P-O (2006) The pancreatic islet endothelial cell: emerging roles in islet function and disease. *Int J Biochem Cell Biol* 38: 492–497
Olsson R, Olerud J, Pettersson U & Carlsson PO (2011) Increased numbers of low-oxygenated pancreatic islets after intraportal islet transplantation. *Diabetes* 60: 2350–2353
Oram RA, Patel K, Hill A, Shields B, McDonald TJ, Jones A, Hattersley AT & Weedon MN (2016) A Type 1 Diabetes Genetic Risk Score Can Aid Discrimination Between Type 1 and Type 2 Diabetes in Young Adults. *Diabetes Care* 39: 337–344
Orlando G, Baptista P, Birchall M, De Coppi P, Farney A, Guimaraes-Souza NK, Opara E, Rogers J, Seliktar D, Shapira-Schweitzer K, *et al* (2011) Regenerative medicine as applied to solid organ transplantation: current status and future challenges. *Transpl Int Off J Eur Soc Organ Transplant* 24: 223–232
Ormiston ML, Toshner MR, Kiskin FN, Huang CJZ, Groves E, Morrell NW & Rana AA (2015) Generation and Culture of Blood Outgrowth Endothelial Cells from Human Peripheral Blood. *J Vis Exp*: e53384
Otonkoski T, Ustinov J, Rasilainen S, Kallio E, Korsgren O & Häyry P (1999) Differentiation and maturation of porcine fetal islet cells in vitro and after transplantation. *Transplantation* 68: 1674–1683
Ott HC, Clippinger B, Conrad C, Schuetz C, Pomerantseva I, Ikonomou L, Kotton D & Vacanti JP (2010) Regeneration and orthotopic transplantation of a bioartificial lung. *Nat Med* 16: 927–933
Ott HC, Matthiesen TS, Goh SK, Black LD, Kren SM, Netoff TI & Taylor DA (2008) Perfusion-decellularized matrix: Using nature's platform to engineer a bioartificial heart. *Nat Med* 14: 213–221
Papaccio G, Graziano A, D'Aquino R, Valiante S & Naro F (2005) A biphasic role of nuclear transcription factor (NF)-kappaB in the islet beta-cell apoptosis induced by interleukin (IL)-1beta. *J Cell Physiol* 204: 124–130
Partington L, Mordan NJ, Mason C, Knowles JC, Kim H-W, Lowdell MW, Birchall MA & Wall IB (2013) Biochemical changes caused by decellularization may compromise mechanical integrity of tracheal scaffolds. *Acta Biomater* 9: 5251–5261
Patel KA, Oram RA, Flanagan SE, De Franco E, Colclough K, Shepherd M, Ellard S, Weedon MN & Hattersley AT (2016) Type 1 Diabetes Genetic Risk Score: A Novel Tool to Discriminate Monogenic and Type 1 Diabetes. *Diabetes* 65:

2094–2099
Pathak V, Pathak NM, O'Neill CL, Guduric-Fuchs J & Medina RJ (2019) Therapies for Type 1 Diabetes: Current Scenario and Future Perspectives. *Clin Med Insights Endocrinol Diabetes* 12: 1179551419844521
Pellegata AF, Tedeschi AM & De Coppi P (2018) Whole Organ Tissue Vascularization: Engineering the Tree to Develop the Fruits. *Front Bioeng Biotechnol* 6: 56
Pellegrini S (2019) Alternative transplantation sites for islet transplantation Elsevier Inc.
Pellegrini S, Cantarelli E, Sordi V, Nano R & Piemonti L (2016) The state of the art of islet transplantation and cell therapy in type 1 diabetes. *Acta Diabetol* 53: 683–691 doi:10.1007/s00592-016-0847-z [PREPRINT]
Peloso A, Citro A, Oldani G, Brambilla S, Piemonti L & Cobianchi L (2017) Bioengineering the Pancreas: Cell-on-Scaffold Technology. *Scaffolds Tissue Eng - Mater Technol Clin Appl*
Peloso A, Citro A, Zoro T, Cobianchi L, Kahler-Quesada A, Bianchi CM, Andres A, Berishvili E, Piemonti L, Berney T, *et al* (2018) Regenerative medicine and diabetes: Targeting the extracellular matrix beyond the stem cell approach and encapsulation technology. *Front Endocrinol (Lausanne)* 9
Peloso A, Urbani L, Cravedi P, Katari R, Maghsoudlou P, Fallas MEA, Sordi V, Citro A, Purroy C, Niu G, *et al* (2016) The Human Pancreas as a Source of Protolerogenic Extracellular Matrix Scaffold for a New-generation Bioartificial Endocrine Pancreas. *Ann Surg* 264: 169–179
Pepper AR, Gala-Lopez B, Pawlick R, Merani S, Kin T & Shapiro AMJ (2015) A prevascularized subcutaneous device-less site for islet and cellular transplantation. *Nat Biotechnol 2015 335* 33: 518–523
Pepper AR, Pawlick R, Bruni A, Wink J, Rafiei Y, O'Gorman D, Yan-Do R, Gala-Lopez B, Kin T, MacDonald PE, *et al* (2017) Transplantation of Human Pancreatic Endoderm Cells Reverses Diabetes Post Transplantation in a Prevascularized Subcutaneous Site. *Stem cell reports* 8: 1689–1700
Phillips B, Trucco M & Giannoukakis N (2011) Current state of type 1 diabetes immunotherapy: incremental advances, huge leaps, or more of the same? *Clin Dev Immunol* 2011: 432016
Piccoli M, Urbani L, Alvarez-Fallas ME, Franzin C, Dedja A, Bertin E, Zuccolotto G, Rosato A, Pavan P, Elvassore N, *et al* (2016) Improvement of diaphragmatic performance through orthotopic application of decellularized extracellular matrix patch. *Biomaterials* 74: 245–255
Piemonti L & Pileggi A (2013) 25 YEARS OF THE RICORDI AUTOMATED METHOD FOR ISLET ISOLATION. *CellR4-- repair, Replace Regen reprogramming* 1
Pignatelli C, Campo F, Neroni A, Piemonti L & Citro A (2022) Bioengineering the Vascularized Endocrine Pancreas: A Fine-Tuned Interplay Between Vascularization, Extracellular-Matrix-Based Scaffold Architecture, and Insulin-Producing Cells. *Transpl Int* 35: 168
Plow EF, Haas TA, Zhang L, Loftus J & Smith JW (2000) Ligand binding to integrins. *J Biol Chem* 275: 21785–21788
Pociot F, Akolkar B, Concannon P, Erlich HA, Julier C, Morahan G, Nierras CR, Todd JA, Rich SS & Nerup J (2010) Genetics of type 1 diabetes: what's next? *Diabetes* 59: 1561–1571
Popovic J, Kover KL & Moore W V (2004) The effect of immunomodulators on prevention of autoimmune diabetes is stage dependent: FTY720 prevents diabetes at three different stages in the diabetes-resistant biobreeding rat. *Pediatr Diabetes* 5: 3–9
Poy MN, Eliasson L, Krutzfeldt J, Kuwajima S, Ma X, Macdonald PE, Pfeffer S, Tuschl T, Rajewsky N, Rorsman P, *et al* (2004) A pancreatic islet-specific microRNA regulates insulin secretion. *Nature* 432: 226–230

Poy MN, Hausser J, Trajkovski M, Braun M, Collins S, Rorsman P, Zavolan M & Stoffel M (2009) miR-375 maintains normal pancreatic alpha- and beta-cell mass. *Proc Natl Acad Sci U S A* 106: 5813–5818
Pozzilli P, Signore A, Williams AJ & Beales PE (1993) NOD mouse colonies around the world--recent facts and figures. *Immunol Today* 14: 193–196
Quintard C, Tubbs E, Jonsson G, Jiao J, Wang J, Werschler N, Laporte C, Pitaval A, Bah T-S, Pomeranz G, *et al* (2024) A microfluidic platform integrating functional vascularized organoids-on-chip. *Nat Commun* 15: 1452
Rackham CL, Dhadda PK, Chagastelles PC, Simpson SJS, Dattani AA, Bowe JE, Jones PM & King AJF (2013) Pre-culturing islets with mesenchymal stromal cells using a direct contact configuration is beneficial for transplantation outcome in diabetic mice. *Cytotherapy* 15: 449–459
Rackham CL, Dhadda PK, Le Lay AM, King AJF & Jones PM (2014) Preculturing Islets With Adipose-Derived Mesenchymal Stromal Cells Is an Effective Strategy for Improving Transplantation Efficiency at the Clinically Preferred Intraportal Site. *Cell Med* 7: 37–47
Ramachandran K, Huang H-H & Stehno-Bittel L (2015) A Simple Method to Replace Islet Equivalents for Volume Quantification of Human Islets. *Cell Transplant* 24: 1183–1194
Ratner BD, Castner DG, Horbett TA, Lenk TJ, Lewis KB & Rapoza RJ (1990) Biomolecules and surfaces. *J Vac Sci Technol A Vacuum, Surfaces, Film* 8: 2306–2317
Redondo MJ, Geyer S, Steck AK, Sharp S, Wentworth JM, Weedon MN, Antinozzi P, Sosenko J, Atkinson M, Pugliese A, *et al* (2018) A Type 1 Diabetes Genetic Risk Score Predicts Progression of Islet Autoimmunity and Development of Type 1 Diabetes in Individuals at Risk. *Diabetes Care* 41: 1887–1894
Reed JC & Herold KC (2015) Thinking bedside at the bench: the NOD mouse model of T1DM. *Nat Rev Endocrinol* 11: 308–314
Reing JE, Zhang L, Myers-Irvin J, Cordero KE, Freytes DO, Heber-Katz E, Bedelbaeva K, McIntosh D, Dewilde A, Braunhut SJ, *et al* (2009) Degradation products of extracellular matrix affect cell migration and proliferation. *Tissue Eng Part A* 15: 605–614
Ren X, Moser PT, Gilpin SE, Okamoto T, Wu T, Tapias LF, Mercier FE, Xiong L, Ghawi R, Scadden DT, *et al* (2015) Engineering pulmonary vasculature in decellularized rat and human lungs. *Nat Biotechnol* 33: 1097–1102
Ricordi C, Lacy PE, Finke EH, Olack BJ & Scharp DW (1988) Automated method for isolation of human pancreatic islets. *Diabetes* 37: 413–420
Rieder E, Kasimir M-T, Silberhumer G, Seebacher G, Wolner E, Simon P & Weigel G (2004) Decellularization protocols of porcine heart valves differ importantly in efficiency of cell removal and susceptibility of the matrix to recellularization with human vascular cells. *J Thorac Cardiovasc Surg* 127: 399–405
Robertson RP (1999) Prevention of recurrent hypoglycemia in type 1 diabetes by pancreas transplantation. *Acta Diabetol* 36: 3–9
Rodriguez-Diaz R, Abdulreda MH, Formoso AL, Gans I, Ricordi C, Berggren P-O & Caicedo A (2011) Innervation patterns of autonomic axons in the human endocrine pancreas. *Cell Metab* 14: 45–54
Rodríguez-Vázquez M, Vega-Ruiz B, Ramos-Zúñiga R, Saldaña-Koppel DA & Quiñones-Olvera LF (2015) Chitosan and Its Potential Use as a Scaffold for Tissue Engineering in Regenerative Medicine. *Biomed Res Int* 2015: 821279
Roep BO, Kleijwegt FS, van Halteren AGS, Bonato V, Boggi U, Vendrame F, Marchetti P & Dotta F (2010) Islet inflammation and CXCL10 in recent-onset type 1 diabetes. *Clin Exp Immunol* 159: 338–343
Rogal J, Zbinden A, Schenke-Layland K & Loskill P (2019) Stem-cell based organ-on-a-chip models for diabetes research. *Adv Drug Deliv Rev* 140: 101–128
Rorsman P & Ashcroft FM (2018) Pancreatic β-Cell Electrical Activity and Insulin

Secretion: Of Mice and Men. *Physiol Rev* 98: 117–214
Rorsman P & Renström E (2003) Insulin granule dynamics in pancreatic beta cells. *Diabetologia* 46: 1029–1045
Rufaihah AJ, Huang NF, Jamé S, Lee JC, Nguyen HN, Byers B, De A, Okogbaa J, Rollins M, Reijo-Pera R, *et al* (2011) Endothelial cells derived from human iPSCS increase capillary density and improve perfusion in a mouse model of peripheral arterial disease. *Arterioscler Thromb Vasc Biol* 31: e72-9
Saba I, Jakubowska W, Bolduc S & Chabaud S (2018) Engineering Tissues without the Use of a Synthetic Scaffold: A Twenty-Year History of the Self-Assembly Method. *Biomed Res Int* 2018: 5684679
Sackett SD, Tremmel DM, Ma F, Feeney AK, Maguire RM, Brown ME, Zhou Y, Li X, O'Brien C, Li L, *et al* (2018) Extracellular matrix scaffold and hydrogel derived from decellularized and delipidized human pancreas. *Sci Rep* 8: 1–16
Saisho Y, Butler AE, Meier JJ, Monchamp T, Allen-Auerbach M, Rizza RA & Butler PC (2007) Pancreas volumes in humans from birth to age one hundred taking into account sex, obesity, and presence of type-2 diabetes. *Clin Anat* 20: 933–942
Sakhneny L, Epshtein A & Landsman L (2021) Pericytes contribute to the islet basement membranes to promote beta-cell gene expression. *Sci Rep* 11: 1–10
Sakhneny L, Rachi E, Epshtein A, Guez HC, Wald-Altman S, Lisnyansky M, Khalifa-Malka L, Hazan A, Baer D, Priel A, *et al* (2018) Pancreatic pericytes support β-cell function in a Tcf7l2-dependent manner. *Diabetes* 67: 437–447
Salama BF, Seeberger KL & Korbutt GS (2020) Fibrin supports subcutaneous neonatal porcine islet transplantation without the need for pre-vascularization. *Xenotransplantation* 27: e12575
Samojlik MM & Stabler CL (2021) Designing biomaterials for the modulation of allogeneic and autoimmune responses to cellular implants in Type 1 Diabetes. *Acta Biomater* 133: 87–101 doi:10.1016/j.actbio.2021.05.039 [PREPRINT]
Samuel R, Daheron L, Liao S, Vardam T, Kamoun WS, Batista A, Buecker C, Schäfer R, Han X, Au P, *et al* (2013) Generation of functionally competent and durable engineered blood vessels from human induced pluripotent stem cells. *Proc Natl Acad Sci U S A* 110: 12774–12779
Sandler S & Swenne I (1983) Streptozotocin, but not alloxan, induces DNA repair synthesis in mouse pancreatic islets in vitro. *Diabetologia* 25: 444–447
Saorin G, Caligiuri I & Rizzolio F (2023) Microfluidic organoids-on-a-chip: The future of human models. *Semin Cell Dev Biol* 144: 41–54
Sarker MD, Naghieh S, Sharma NK & Chen X (2018) 3D biofabrication of vascular networks for tissue regeneration: A report on recent advances. *J Pharm Anal* 8: 277–296
Savari O, Zielinski MC, Wang X, Misawa R, Millis JM, Witkowski P & Hara M (2013) Distinct function of the head region of human pancreas in the pathogenesis of diabetes. *Islets* 5: 226–228
Scarritt ME, Pashos NC & Bunnell BA (2015) A review of cellularization strategies for tissue engineering of whole organs. *Front Bioeng Biotechnol* 3: 43
Schwartz MW, Seeley RJ, Tschöp MH, Woods SC, Morton GJ, Myers MG & D'Alessio D (2013) Cooperation between brain and islet in glucose homeostasis and diabetes. *Nature* 503: 59–66
Scott FW, Cloutier HE, Kleemann R, Wöerz-Pagenstert U, Rowsell P, Modler HW & Kolb H (1997) Potential mechanisms by which certain foods promote or inhibit the development of spontaneous diabetes in BB rats: dose, timing, early effect on islet area, and switch in infiltrate from Th1 to Th2 cells. *Diabetes* 46: 589–598
Shapiro AMJ, Lakey JRT, Ryan EA, Korbutt GS, Toth E, Warnock GL, Kneteman NM & Rajotte R V. (2000) Islet Transplantation in Seven Patients with Type 1 Diabetes Mellitus Using a Glucocorticoid-Free Immunosuppressive Regimen. *N Engl J Med* 343: 230–238

Shapiro AMJ, Ricordi C, Hering BJ, Auchincloss H, Lindblad R, Robertson RP, Secchi A, Brendel MD, Berney T, Brennan DC, *et al* (2006) International Trial of the Edmonton Protocol for Islet Transplantation. *N Engl J Med* 355: 1318–1330

Skog O, Korsgren S, Melhus A & Korsgren O (2013) Revisiting the notion of type 1 diabetes being a T-cell-mediated autoimmune disease. *Curr Opin Endocrinol Diabetes Obes* 20: 118–123

Song JJ, Guyette JP, Gilpin SE, Gonzalez G, Vacanti JP & Ott HC (2013) Regeneration and experimental orthotopic transplantation of a bioengineered kidney. *Nat Med* 19: 646–651

Spicer CD (2020) Hydrogel scaffolds for tissue engineering: the importance of polymer choice. *Polym Chem* 11: 184–219

Srinivasan K & Ramarao P (2007) Animal models in type 2 diabetes research: an overview. *Indian J Med Res* 125: 451–472

Stock AA, Gonzalez GC, Pete SI, De Toni T, Berman DM, Rabassa A, Diaz W, Geary JCJ, Willman M, Jackson JM, *et al* (2022) Performance of islets of Langerhans conformally coated via an emulsion cross-linking method in diabetic rodents and nonhuman primates. *Sci Adv* 8: eabm3145

Stucker S, De Angelis J & Kusumbe AP (2021) Heterogeneity and Dynamics of Vasculature in the Endocrine System During Aging and Disease. *Front Physiol* 12 doi:10.3389/fphys.2021.624928 [PREPRINT]

Sullivan DC, Mirmalek-Sani S-H, Deegan DB, Baptista PM, Aboushwareb T, Atala A & Yoo JJ (2012) Decellularization methods of porcine kidneys for whole organ engineering using a high-throughput system. *Biomaterials* 33: 7756–7764

Syed O, Walters NJ, Day RM, Kim H-W & Knowles JC (2014) Evaluation of decellularization protocols for production of tubular small intestine submucosa scaffolds for use in oesophageal tissue engineering. *Acta Biomater* 10: 5043–5054

SYKES M, SACHS DH, NIENHUIS AW, PEARSON DA, MOULTON AD & BODINE DM (1993) Specific prolongation of skin graft survival following retroviral transduction of bone marrow with an allogeneic major histocompatibility complex gene. *Transplantation* 55: 197–202

Szkudelski T (2001) The mechanism of alloxan and streptozotocin action in B cells of the rat pancreas. *Physiol Res* 50: 537–546

Tao T, Wang Y, Chen W, Li Z, Su W, Guo Y, Deng P & Qin J (2019) Engineering human islet organoids from iPSCs using an organ-on-chip platform. *Lab Chip* 19: 948–958

Tapias LF & Ott HC (2014) Decellularized scaffolds as a platform for bioengineered organs. *Curr Opin Organ Transplant* 19: 145–152 doi:10.1097/MOT.0000000000000051 [PREPRINT]

Thebault P, Lhermite N, Tilly G, Le Texier L, Quillard T, Heslan M, Anegon I, Soulillou J-P, Brouard S, Charreau B, *et al* (2009) The C-type lectin-like receptor CLEC-1, expressed by myeloid cells and endothelial cells, is up-regulated by immunoregulatory mediators and moderates T cell activation. *J Immunol* 183: 3099–3108

Tokarz VL, MacDonald PE & Klip A (2018) The cell biology of systemic insulin function. *J Cell Biol* 217: 2273–2289

Tong J, Prigeon RL, Davis HW, Bidlingmaier M, Kahn SE, Cummings DE, Tschöp MH & D'Alessio D (2010) Ghrelin suppresses glucose-stimulated insulin secretion and deteriorates glucose tolerance in healthy humans. *Diabetes* 59: 2145–2151

Trevitt S, Simpson S & Wood A (2016) Artificial Pancreas Device Systems for the Closed-Loop Control of Type 1 Diabetes: What Systems Are in Development? *J Diabetes Sci Technol* 10: 714–723

Ueda H, Howson JMM, Esposito L, Heward J, Snook H, Chamberlain G, Rainbow DB, Hunter KMD, Smith AN, Di Genova G, *et al* (2003) Association of the T-cell

regulatory gene CTLA4 with susceptibility to autoimmune disease. *Nature* 423: 506–511
Veld PI & Smeets S (2015) Microscopic anatomy of the human islet of langerhans. In *Islets of Langerhans, Second Edition* pp 19–38.
Vishwakarma SK, Lakkireddy C, Bardia A, Raju N, Paspala SAB, Habeeb MA & Khan AA (2018) Molecular dynamics of pancreatic transcription factors in bioengineered humanized insulin producing neoorgan. *Gene* 675: 165–175
Wagner DE, Bonenfant NR, Parsons CS, Sokocevic D, Brooks EM, Borg ZD, Lathrop MJ, Wallis JD, Daly AB, Lam YW, *et al* (2014) Comparative decellularization and recellularization of normal versus emphysematous human lungs. *Biomaterials* 35: 3281–3297
Wang C, Guan Y & Yang J (2010) Cytokines in the Progression of Pancreatic β-Cell Dysfunction. *Int J Endocrinol* 2010: 515136
Wang X-J, Xu X-Q, Sun K, Liu K-Q, Li S-Q, Jiang X, Zhao Q-H, Wang L, Peng F-H, Ye J, *et al* (2020) Association of Rare PTGIS Variants With Susceptibility and Pulmonary Vascular Response in Patients With Idiopathic Pulmonary Arterial Hypertension. *JAMA Cardiol* 5: 677–684
Wang Z & Thurmond DC (2009) Mechanisms of biphasic insulin-granule exocytosis - roles of the cytoskeleton, small GTPases and SNARE proteins. *J Cell Sci* 122: 893–903
Warnock GL, Ellis D, Rajotte R V, Dawidson I, Baekkeskov S & Egebjerg J (1988) Studies of the isolation and viability of human islets of Langerhans. *Transplantation* 45: 957–963
Weber LM & Anseth KS (2008) Hydrogel encapsulation environments functionalized with extracellular matrix interactions increase islet insulin secretion. *Matrix Biol* 27: 667–673
Willenberg BJ, Oca-Cossio J, Cai Y, Brown AR, Clapp WL, Abrahamson DR, Terada N, Ellison GW, Mathews CE, Batich CD, *et al* (2015) Repurposed biological scaffolds: Kidney to pancreas. *Organogenesis* 11: 47–57
Williams DP, Shipley R, Ellis MJ, Webb S, Ward J, Gardner I & Creton S (2013) Novel in vitro and mathematical models for the prediction of chemical toxicity. *Toxicol Res (Camb)* 2: 40–59
Wolf-van Buerck L, Schuster M, Baehr A, Mayr T, Guethoff S, Abicht J, Reichart B, Nam-Apostolopoulos Y-C, Klymiuk N, Wolf E, *et al* (2015) Engraftment and reversal of diabetes after intramuscular transplantation of neonatal porcine islet-like clusters. *Xenotransplantation* 22: 443–450
Wu SM & Hochedlinger K (2011) Harnessing the potential of induced pluripotent stem cells for regenerative medicine. *Nat Cell Biol* 13: 497–505
Xie Q, Xie J, Tian T, Ma Q, Zhang Q, Zhu B & Cai X (2017) Hypoxia triggers angiogenesis by increasing expression of LOX genes in 3-D culture of ASCs and ECs. *Exp Cell Res* 352: 157–163
Xu S, Piao L, Wan Y, Huang Z, Meng X, Inoue A, Wang H, Yue X, Jin X, Shi G-P, *et al* (2023) CTSS Modulates Stress-Related Carotid Artery Thrombosis in a Mouse FeCl(3) Model. *Arterioscler Thromb Vasc Biol* 43: e238–e253
Yannas I V (1990) Biologically Active Analogues of the Extracellular Matrix: Artificial Skin and Nerves. *Angew Chemie Int Ed English* 29: 20–35
Yeh H-C, Brown TT, Maruthur N, Ranasinghe P, Berger Z, Suh YD, Wilson LM, Haberl EB, Brick J, Bass EB, *et al* (2012) Comparative effectiveness and safety of methods of insulin delivery and glucose monitoring for diabetes mellitus: a systematic review and meta-analysis. *Ann Intern Med* 157: 336–347
Yi B, Xu Q & Liu W (2022) An overview of substrate stiffness guided cellular response and its applications in tissue regeneration. *Bioact Mater* 15: 82–102
Yokoi N, Fujiwara Y, Wang H-Y, Kitao M, Hayashi C, Someya T, Kanamori M, Oiso Y, Tajima N, Yamada Y, *et al* (2008) Identification and functional analysis of CBLB mutations in type 1 diabetes. *Biochem Biophys Res Commun* 368: 37–42

Yokoi N, Hayashi C, Fujiwara Y, Wang H-Y & Seino S (2007) Genetic reconstitution of autoimmune type 1 diabetes with two major susceptibility genes in the rat. *Diabetes* 56: 506–512

Yokoi N, Hidaka S, Tanabe S, Ohya M, Ishima M, Takagi Y, Masui N & Seino S (2012) Role of major histocompatibility complex class II in the development of autoimmune type 1 diabetes and thyroiditis in rats. *Genes Immun* 13: 139–145

Yoon C-H, Hur J, Park K-W, Kim J-H, Lee C-S, Oh I-Y, Kim T-Y, Cho H-J, Kang H-J, Chae I-H, *et al* (2005) Synergistic neovascularization by mixed transplantation of early endothelial progenitor cells and late outgrowth endothelial cells: the role of angiogenic cytokines and matrix metalloproteinases. *Circulation* 112: 1618–1627

Youos JG (2011) The role of α-, δ- and F cells in insulin secretion and action. *Diabetes Res Clin Pract* 93 Suppl 1: S25-6

Yuan Y, Leiby KL, Greaney AM, Raredon MSB, Qian H, Schupp JC, Engler AJ, Baevova P, Adams TS, Kural MH, *et al* (2021) A Pulmonary Vascular Model From Endothelialized Whole Organ Scaffolds. *Front Bioeng Biotechnol* 9: 760309

Zbinden A, Urbanczyk M, Layland SL, Becker L, Marzi J, Bosch M, Loskill P, Duffy GP & Schenke-Layland K (2021) Collagen and Endothelial Cell Coculture Improves β-Cell Functionality and Rescues Pancreatic Extracellular Matrix. *Tissue Eng Part A* 27: 977–991

Zhang J, Hu ZQ, Turner NJ, Teng SF, Cheng WY, Zhou HY, Zhang L, Hu HW, Wang Q & Badylak SF (2016) Perfusion-decellularized skeletal muscle as a three-dimensional scaffold with a vascular network template. *Biomaterials* 89: 114–126

Zhang X, Ma Z, Song E & Xu T (2022) Islet organoid as a promising model for diabetes. *Protein Cell* 13: 239–257

Zhao W (2024) Pig organs in humans: a forum on xenotransplantation. *Natl Sci Rev* 11: nwae208

Zhou J, Fritze O, Schleicher M, Wendel H-P, Schenke-Layland K, Harasztosi C, Hu S & Stock UA (2010) Impact of heart valve decellularization on 3-D ultrastructure, immunogenicity and thrombogenicity. *Biomaterials* 31: 2549–2554

Zhou P, Guo Y, Huang Y, Zhu M, Fan X, Wang L, Wang Y, Zhu S, Xu T, Wu D, *et al* (2016) The dynamic three-dimensional culture of islet-like clusters in decellularized liver scaffolds. *Cell Tissue Res* 365: 157–171

Zudaire E, Gambardella L, Kurcz C & Vermeren S (2011) A computational tool for quantitative analysis of vascular networks. *PLoS One* 6: e27385

Alessia Nedoma